

**DEVELOPMENT OF EMBEDDED MULTIMATERIAL BIOPRINTING
PLATFORM FOR THE BIOFABRICATION OF VASCULAR TISSUES**

by
CANER DİKYOL

Submitted to the Graduate School of Engineering and Natural Sciences
in partial fulfilment of
the requirements for the degree of Master of Science

Sabancı University
September 2020

**DEVELOPMENT OF EMBEDDED MULTIMATERIAL BIOPRINTING
PLATFORM FOR THE BIOFABRICATION OF VASCULAR TISSUES**

Approved by:

Prof. Dr. Bahattin Koç
(Thesis Supervisor)



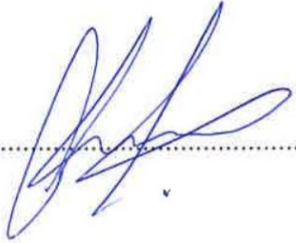
.....

Assoc. Prof. Dr. Bekir Dizman



.....

Assoc. Prof. Dr. Ozan Karaman



.....

Approval Date: September 1, 2020

Caner Dikyol, 2020 ©

All Rights Reserved

ABSTRACT

DEVELOPMENT OF EMBEDDED MULTIMATERIAL BIOPRINTING PLATFORM FOR THE BIOFABRICATION OF VASCULAR TISSUES

CANER DİKYOL

MATERIALS SCIENCE AND NANO ENGINEERING MSc. THESIS,
SEPTEMBER 2020

Thesis Supervisor: Prof. Bahattin Koç

Keywords: Multimaterial bioprinting, 3D bioprinting, tissue engineering, biofabrication,
vascular tissues, blood vessel

Cardiovascular diseases are one of the major causes of mortality throughout the world. Availability and suitability issues of the currently available autologous vessel and synthetic graft transplantations have created an immense need for the development of tissue engineered vascular tissue substitutes that could be benefited not only for therapeutic replacements of diseased blood vessels but also for fabrication of thick vascularized tissues and in vitro vascular disease modelling. The advent of bioprinting technology into the tissue engineering field has permitted the attainment of complex-shaped tissue constructs with spatiotemporal control, unprecedented degree of precision and reproducibility when compared with conventional methodologies. However, most of the bioprinted vascular tissue substitutes still lack either the zonally stratified multimaterial composition or hierarchical complexity of native blood vessels which have been residing as major challenges in vascular tissue engineering domain and are crucial on the biofabrication of anatomically and functionally correct vascular tissue analogs. Multimaterial bioprinting is a promising technology integrating multimaterial setups into bioprinting platforms for the fabrication of multicellular, heterogeneous and functional tissue constructs. In this thesis work, a multimaterial bioprinting platform incorporating multiple-channel microfluidic multimaterial printhead was combined with the embedded bioprinting technique for the fabrication of vascular-like constructs mimicking spatial heterogeneity, multicellular and multimaterial composition and hierarchical microarchitecture of native blood vessels. Three different bioink formulations were

sequentially extruded from the developed microfluidic multimaterial printhead into the prepared hydrogel-nanoclay support bath in a controlled manner, which allowed the generation of complex-shaped tubular constructs with three distinct concentric layers resembling the intimal, medial and adventitial layers of the natural vascular tissues.

ÖZET

VASKÜLER DOKULARIN BİYOFABRİKASYONU İÇİN GÖMÜLÜ ÇOK MALZEMELİ BİYOBASIM PLATFORMUNUN GELİŞTİRİLMESİ

CANER DİKYOL

MALZEME BİLİMİ VE NANO MÜHENDİSLİK YÜKSEK LİSANS TEZİ,
EYLÜL 2020

Tez Danışmanı: Prof. Dr. Bahattin Koç

Anahtar Kelimeler: Çok malzemeli biyobasım, 3B biyobasım, doku mühendisliği,
biyofabrikasyon, vasküler dokular, kan damarı

Kardiyovasküler hastalıklar, dünyada meydana gelen ölümlerin başlıca sebeplerindedir. Halihazırda uygulanmakta olan otolog damar ve sentetik greft transplantasyonlarında yaşanan mevcudiyet ve uygunluk sorunları, doku mühendisliği vasıtasıyla üretilmiş vasküler doku ikamelerinin geliştirilmesi için büyük bir ihtiyaç yaratmıştır ve geliştirilecek vasküler doku ikameleri sadece hastalıklı kan damarlarının tedavi amaçlı değişimi için değil, aynı zamanda kalın vaskülarize dokuların üretimi ve in vitro hastalık modellerinin geliştirilmesi için de yararlanılabilecektir. Biyobasım teknolojisinin doku mühendisliği alanına gelişi, kompleks geometride dokuların, geleneksel üretim yöntemleriyle kıyasla uzamsal-zamansal kontrollü, emsalsiz bir hassasiyette ve tekrarlanabilirlikte üretilmesine olanak sağlamıştır. Ancak, biyobasımla üretilen vasküler doku ikamelerinin çoğu, vasküler doku mühendisliği alanında büyük zorluklar olarak bulunan ve anatomik ve fonksiyonel vasküler doku analoglarının biyofabrikasyonu için kritik öneme sahip olan, kan damarlarının bölgesel olarak tabakalandırılmış çok malzemeli bileşimden veya hiyerarşik karmaşıklığından yoksundur. Çok malzemeli biyobasım, çok hücreli, heterojen ve fonksiyonel dokuların biyofabrikasyonu için çok malzemeli donanımların biyobasım platformlarına entegrasyonunu barındıran ve umut vadeden bir teknolojidir. Bu tez çalışmasında, kan damarının konumsal heterojenliğini, çok malzemeli kompozisyonunu ve hiyerarşik mikro-mimarisini taklit edebilen vasküler-benzeri yapıların biyofabrikasyonu için; çok kanallı mikroakışkan bir başlığa sahip çok

malzemeli biyobasım platformu ile gömülü biyobasım tekniđi birleřtirilmiřtir. Üç farklı biyomürekkep formülasyonu, geliřtirilen çok malzemeli mikroakıřkan yazıcı bařlıđından hidrojel-nanokil bazlı destek banyosuna kontrollü bir řekilde ekstrüde edilmiř ve bu sayede kan damarının intimal, medial ve adventif katmanlarına benzer eřmerkezli üç katmana sahip ve karmařık řekilli tübüler yapılar üretilmiřtir.

ACKNOWLEDGEMENTS

Although you only see my name written in the title page as an author, this thesis work would not have been completed without sincere and significant contribution of many people. To begin with, I would like to acknowledge the Technological Research Council of Turkey (2210-National Scholarship Programme for MSc Students) for the financial support. Some parts of this work related to the preparation and characterization of nanoclay-hydrogel composite support-bath for bioprinting of complex structures was partially supported by the TUBITAK (Grant number: 218S678).

I would like to express my deepest sense of gratitude to my thesis supervisor Prof. Bahattin Koc for his continuous guidance and encouragement throughout the course of this thesis. His advices have significantly enhanced my scientific perspective. I am also thankful to my jury members Prof. Bekir Dizman and Prof. Ozan Karaman for their interests and feedbacks about my thesis.

Every member of Koç Research Group had significant contribution in this thesis work and I am thankful to all of them; especially to Dr. Mine Altunbek for her never-ending support in almost every step of my research, to Seyedeh Ferdows Afghah for her will to transfer her knowledge, to Dr. Cigdem Bilici, Asena Gulenay Tatar and Efsun Senturk for their cheerful help throughout my experiments, to Anil Ahmet Acar and Dr. Ali Fallah for their valuable criticisms on my printhead design and scripting.

Finally, I take this opportunity to express the profound gratitude to my beloved family members and friends for their endless moral support throughout my stay in Sabanci University.

To my lovely family and friends

TABLE OF CONTENTS

LIST OF FIGURES	xiii
LIST OF ABBREVIATIONS.....	xx
1. INTRODUCTION.....	1
1.1. Bioprinting	2
1.1.1. Bioprinting Inside Support Bath: Embedded Bioprinting	5
1.2. Anatomy of Vascular Tissue.....	8
1.3. Multimaterial Bioprinting	10
1.3.1. Multi-Head Multimaterial Bioprinting	12
1.3.2. Coaxial Multimaterial Bioprinting.....	15
1.3.3. Microfluidic Multimaterial Bioprinting.....	18
1.3.4. Laser-Based Multimaterial Bioprinting	20
1.1.1. Scaffold-Based Multimaterial Bioprinting Approaches	23
1.1.2. Scaffold-Free Multimaterial Bioprinting Approaches	28
1.2. Multimaterial Bioprinting of Vascularized Tissues	31
2. EXPERIMENTAL	42
2.1. Design and Development of Embedded Multimaterial Bioprinting Platform ..	42
2.1.1. A General Overview on the Embedded Multimaterial Bioprinting Platform	42
2.1.2. Development of Multiple-Channel Microfluidic Multimaterial Printhead	43
2.1.2.1. CAD modelling and fabrication of multimaterial printhead backbone	43
2.1.2.2. Multi-barrel microcapillary pulling.....	45
2.1.2.3. Construction of Multiple-Channel Microfluidic Multimaterial Printhead And Assembly of Multimaterial Bioprinting Platform Components ..	46

2.2.	Preparation and Characterization of Nanoclay-Hydrogel Composite Support-Bath	47
2.2.1.	Preparation of PF-RDS Support-Bath and Characterization	47
2.2.2.	Rheological Measurements	48
2.2.3.	CAD Design of Complex Structures and 3D Printing Inside Support-Bath	49
2.2.4.	Bioprinting of Cell-Laden Alginate in PF-RDS Support-Bath	50
2.2.5.	Evaluation of In-Gel Bioprinting Biocompatibility	50
2.2.6.	Statistical Analysis	51
2.3.	Preparation and Characterization of Alginate-GelMA Blend Bioink	51
2.3.1.	Methacrylated Gelatin Synthesis	52
2.3.2.	Characterization of Synthesized Methacrylated Gelatin and Determination of Degree of Functionalization	53
2.3.3.	Preparation of Alginate-GelMA Blend Bioink	54
2.4.	CAD Modelling and Tool Path Planning for the Generation of Multilayered Vascular-Like Constructs	55
2.4.1.	Biomodelling of Vascular Constructs	56
2.4.2.	Tool Path Planning for Multimaterial Bioprinting	58
2.5.	Embedded Multimaterial Printing of Complex-Shaped Structures	61
2.6.	Embedded Multimaterial Bioprinting of Vascular Constructs	63
2.6.1.	Cell culture	63
2.6.2.	Preparation of Bioinks Encapsulated with Different Cells	64
2.6.3.	Multimaterial Bioprinting Inside Support Bath	64
2.7.	Investigation of Bioprinted Vascular Constructs	65
2.7.1.	Live / Dead Assay	65
2.7.2.	Cellular Labelling	66
3.	RESULTS AND DISCUSSIONS	67
3.1.	Preparation and Characterization of Nanoclay-Hydrogel Composite Support-Bath	67
3.1.1.	Rheological Characterization of the Support Bath	67
3.1.2.	Printability of Overhanging and Complex Structures in PF-RDS Support-Bath	72
3.1.3.	Bioprinting of Cell-Laden Alginate Hydrogel in Support-Bath	78

3.2.	Characterization of Synthesized GelMA for the Preparation of Alginate-GelMA Blend Bioink	79
3.3.	Embedded Multimaterial Printing of Complex-Shaped Structures	81
3.3.1.	Printing of Single-Material Multilayered Structures Inside Support Bath	81
3.3.2.	Investigation of Valve Interchangeability for Multimaterial Extrusion ...	83
3.3.3.	Multimaterial Printing of Complex-Shaped Structures Inside Support Bath	87
4.	CONCLUSIONS AND FUTURE WORK.....	93
	BIBLIOGRAPHY.....	97

LIST OF FIGURES

Figure 1.1 An illustration of multimaterial bioprinting platform with multi-head, microfluidic and coaxial dispensing units (from left to right). Development and implementations of different multimaterial bioprinting approaches have achieved several milestones on the biofabrication of vascular and vascularized tissues by patterning various types of material formulations in a spatially-controlled manner. Multimaterial bioprinting approaches demonstrates a potential for the reconstruction of vascular networks within the thick tissues and also generation of vascular tissues with zonally stratified, multicellular and concentric arrangement (Gantry model of the illustrated multimaterial bioprinting platform was obtained and modified from 3D ContentCentral service (<https://www.3dcontentcentral.com/parts/supplier/Aerotech-Inc.aspx>) with permission from Aerotech Inc. Digital models of human heart and brain were obtained and adapted from the BodyParts3D database (<http://lifesciencedb.jp/bp3d/>) (Mitsuhashi et al. 2008))..... 3

Figure 1.2 Different biofabrication platforms employing multi-head and coaxial multimaterial bioprinting approaches: **a)** ITOP system, which is a multi-head multimaterial bioprinting platform with the capability of dispensing multiple types of thermoplastic polymers and bioink formulations (left) and illustration, photograph and fluorescent image of a construct fabricated by ITOP system (right). Reproduced/adapted with permission from Ref. (H.-W. Kang et al. 2016). Copyright 2016, Nature America. **b)** Combination of multi-head multimaterial bioprinting approach with embedded bioprinting technique for the fabrication of cardiac ventricle model. Reproduced/adapted with permission from Ref. (A. Lee et al. 2019). Copyright 2019, AAAS. **c)** Coaxial printheads enable the simultaneous extrusion of several concentric layers of materials and the developed printheads may be integrated with different crosslinking techniques such as aerosol delivery. Reproduced/adapted with permission from Ref. (Yeo et al. 2016). Copyright 2016, American Chemical Society. **d)** Multi-arm bioprinter system

incorporating coaxial printhead and cell spheroid depositing secondary printhead for multimaterial patterning. Reproduced/adapted with permission from Ref. (Ozbolat, Chen, and Yu 2014). Copyright 2013, Elsevier. **e)** Handheld printer for *in situ* biofabrication of cartilage tissue by coaxial deposition of GelMA-HAMA hydrogels. Reproduced/adapted with permission from Ref. (Duchi et al. 2017). Copyright 2017, Springer Nature 17

Figure 1.3 Different biofabrication platforms employing microfluidic and laser-based multimaterial bioprinting approaches: **a)** Microfluidic printhead with on-the-fly multimaterial switching capability. Reproduced/adapted with permission from Ref. (Dickman et al. 2020). Copyright 2019, FASEB. **b)** Combination of coaxial needles with microfluidic chips, where bioink solutions are delivered from the microfluidic printhead and then crosslinked by CaCl₂ supplied from the coaxial needle. Reproduced/adapted with permission from Ref. (Maiullari et al. 2018). Copyright 2018, Springer Nature. **c)** Capillary-based microfluidic printhead, in which bioinks are flowed through separate capillaries without any contact with each other till the end of the nozzle. Reproduced/adapted with permission from Ref. (Zhou et al. 2018). Copyright 2018, American Chemical Society. **d)** Setup of DMD-based, microfluidics-enabled multimaterial bioprinting platform (up) and a skeletal muscle model fabricated with this platform (bottom). Reproduced/adapted with permission from Ref. (Miri et al. 2018). Copyright 2018, WILEY-VCH Verlag GmbH & Co. KGaA, Weinheim. **e)** LIFT setups also include multimaterial bioprinting capability. Reproduced/adapted with permission from Ref. (Koch et al. 2012). Copyright 2012, Wiley Periodicals 22

Figure 1.4 Scaffold-based multimaterial bioprinting approaches enable the fabrication of multilayered and concentric vascular tissue analogs with functionality by depositing cells within exogenous materials. **a)** Coaxial multimaterial bioprinting of vascular construct with endothelial and muscular layers by dispensing Pluronic F127 from inner channel (core), endothelial cell-laden bioink from middle channel and SMC-laden bioink from outer channel of triple coaxial nozzle. Following the *in vitro* remodeling process that include incubation, and static culture and pulsatile conditioning, fabricated vascular construct exhibited (i) intact monolayer formation in endothelial cell layer and (ii) circumferentially-oriented SMCs at muscular layer at day 18. Reproduced/adapted with permission from Ref. (G. Gao et al. 2019). Copyright 2019, AIP Publishing. **b)** Biofabrication of vascular construct with micro- and macro-channels by co-axially extruding SMC-laden and fibroblast-laden bioinks onto a rotating rod, followed by the delivery of endothelial cells into the lumen. (i) Longitudinal section of the fabricated

construct clearly demonstrates the presence of multi-level channels. (ii) Confocal imaging showed distribution of three different cell types and presence of apparent micro-channels within the vessel-like construct. Reproduced/adapted with permission from Ref. (Q. Gao et al. 2017). Copyright 2017, American Chemical Society. **c)** Multimaterial bioprinting of a multilayered vascular model by employing droplet-based printheads. Cell-laden gelatin was deposited to manufacture sacrificial rod, which was followed by deposition of SMC-laden fibrinogen and thrombin solutions from two droplet-based printheads onto the fabricated sacrificial rod. Further, a fibrinogen loaded bioink formulation was casted onto the printed structure. (i) Schematic cross section of the vascular model illustrating single layer of endothelial cells and a SMC layer. (ii) Fluorescence microscopy image after seven days dynamic cultivation, demonstrating the combination of endothelial layer and the muscular layer, where SMCs distributed close to the lumen. (iii) Cross-sectional fluorescence micrograph of multilayered vascular model after 4 days dynamic culture, exhibiting the localization of endothelial cells in the inner wall that was encircled by SMCs and fibroblasts. Reproduced/adapted with permission from Ref. (Schöneberg et al. 2018). Copyright 2018, Springer Nature 27

Figure 1.5 Scaffold-free multimaterial bioprinting approaches allow fabrication of vascular constructs by dispensing cells without encapsulating them within any exogenous material. **a)** Step-by-step illustration of scaffold-free multimaterial bioprinting, where agarose rods and multicellular aggregates extruded from different printheads are deposited layer-by-layer (up). Fabrication of multilayered vascular construct by assembling HUVSMC and HSF multicellular cylinders in pre-determined pattern. While HUVSMC cylinders form inner layer, HSF cylinders form outer layer of vascular construct which may also be identified in histological examinations (bottom). Reproduced/adapted with permission from Ref. (Norotte et al. 2009). Copyright 2009, Elsevier. **b)** Roadmap for scaffold-free multimaterial bioprinting of biomimetic and self-supporting macrovascular constructs by employing algorithmic model developed by Kucukgul et al. Reproduced/adapted with permission from Ref. (Kucukgul et al. 2015). Copyright 2014, Wiley Periodicals..... 30

Figure 1.6 Vascularized tissue biofabrication through coaxial multimaterial bioprinting. **a)** Schematic diagram of microfluidic co-axial nozzle system for monolayer (M), bilayer (B) and complex hollow tube bioprinting and representative views. **b)** Confocal images of bilayered hollow tube, **c)** complex hollow tube with monolayer and bilayer structures and **d)** their transitional region. Inner and outer shells were demonstrated with red and

green fluorescent beads embedded in the ink, respectively. Copyright 2019, with permission from Elsevier. Readapted from Ref. (N. K. Singh et al. 2020)	33
Figure 1.7 Printability of multiple materials in a support medium using multi-printheads. a) computer-aided design (CAD) model for human heart, b) printed heart within a support bath, c) after removal of support medium and d) after perfusion of red and blue dyes. Copyright 2019, The Authors. Published by WILEY-VCH Verlag GmbH & Co. KGaA, Weinheim. Reused from Ref. (Noor et al. 2019)	37
Figure 1.8 Dual bioprinting platform. Schematic diagram exhibiting step-by-step fabrication process using EBB and inkjet bioprinting technologies to generate full-thickness skin model. Copyright 2018, WILEY-VCH Verlag GmbH & Co. KGaA, Weinheim. Reused from Ref. (B. S. Kim et al. 2019)	39
Figure 1.9 Capillary based and preset extrusion-based multimaterial bioprinting systems for vascularized tissue biofabrication. a) Capillary (Copyright 2017, WILEY-VCH Verlag GmbH & Co. KGaA, Weinheim. Reused from Ref. (Byambaa et al. 2017)) and b) preset extrusion (Copyright 2020, WILEY-VCH Verlag GmbH & Co. KGaA, Weinheim. Reused from Ref. (D. Kang et al. 2020)) based multimaterial bioprinting to generate vascularized tissues	41
Figure 2.1 Top, front, right and perspective views of the modelled (left) and fabricated (right) multimaterial printhead backbone from top to bottom, respectively. Main part, supporting part and sliding part of the multimaterial printhead backbone were respectively illustrated in light gray, orange and blue colors in the designed CAD model.	44
Figure 2.2 Multi-barrel microcapillary pulling for the fabrication of multiple channel microfluidic nozzle. Microcapillary pulling device (left) and 4X magnified inverted microscope image of the pulled multi-barrel microcapillary (right)	45
Figure 2.3 Embedded multimaterial bioprinting platform (left) and microfluidic multiple-channel multimaterial printhead (middle and right).	47
Figure 2.4 Synthesis of GelMA by the addition of methacrylate groups to the gelatin. Reproduced under the terms of the Creative Commons CC-BY 4.0 License (https://creativecommons.org/licenses/by/4.0/) from Ref. (Yoon et al. 2016). Copyright 2016, Yoon et al.	52
Figure 2.5 Crosslinking of synthesized GelMA into hydrogel through exposure to UV light in the presence of Irgacure 2959. Reproduced under the terms of the Creative	

Commons CC-BY 4.0 License (https://creativecommons.org/licenses/by/4.0/) from Ref. (Yoon et al. 2016). Copyright 2016, Yoon et al.	55
Figure 2.6 Biomodelling of an aortic construct from a medical image. (a) Coronal, (b) axial, (c) sagittal and (d) 3D rendered views of the aorta segmentations. (e) Surface improvement on the segmented model.	57
Figure 2.7 Main steps of tool path planning for the generation of multilayered and concentric vascular-like constructs: (a) generation of BoundingBox, (b) intersection of plane with aorta model, (c) generation of first layer by offsetting through the center, (d) generation of second layer by offsetting through the wall, (e) repeating offsetting through inside and outside for the generation of a structure with a specified layer number. White arrows represent offsetting direction in the specified layer.	61
Figure 3.1 Time sweep measurement of the support-bath showing storage and loss moduli over time for different concentrations of PF. Laponite and CaCl ₂ concentrations were set to 3% and 1%, respectively. Storage (G') modulus (filled symbols) and loss (G'') modulus (open symbols).	68
Figure 3.2 Dynamic rheological characterization of the support-bath representing the effect of PF concentration on flow behavior and recoverability of the structure at 37 °C (Laponite-RDS and CaCl ₂ concentrations were constant at 3 and 1%, respectively except for control samples). Control 1 and control 2 included 10% PF, and 3%RDS, respectively at constant 1% CaCl ₂ (a) Strain amplitude sweep profiles of supporting mediums, (b) frequency sweep profiles within the linear viscoelastic range, (c) viscosity vs. shear rate plots revealing the shear thinning behavior of the support material, (d) cyclic strain measurements at high (50%) and low (0.6%) strains showing storage (G') moduli of the samples in 4 cycles. Storage (G') modulus (filled symbols) and loss (G'') modulus (open symbols).	70
Figure 3.3 Characterization of PF-RDS support-bath for printability of tubular structures in various angular configurations. Digital images of the printed tubular alginate structures using 25 gauge nozzle in the support-bath angled at (a) 90°, (b) 60° and (c) 45°, and (d) a conical structure with 60° angle with respect to the surface. Digital images of front and top views of (a1, a2) 90°, (b1, b2) 60° and (c1, c2) 45° bended tubular structures and (d1, d2) conical structure after removal from support-bath. Scale bars indicate 5 mm.	75
Figure 3.4 Fabrication of 3D complex constructs. CAD models of (a) star shape, (b) 0-90° grid pattern, (c) branched vascular structure, and (d) nose shape. Digital images of	

the fabricated structures (a1, b1, c1, d1) before and (a2, b2, c2, d2) after recovery from PF-RDS support-bath. Scale bars indicate 5 mm.	77
Figure 3.5 Fabrication of cell-laden alginate constructs using PF-RDS support-bath. (a) Image of harvested bioprinted tubular structure from support bath. (b) Confocal microscopy image of live/dead cells encapsulated in the alginate hydrogel in a complete 3D bioprinted hollow structure at Day 3 and the zoomed images of cells obtained on Day 1, Day 3 and Day 7. (c) Quantitative viability analysis of cells for Day 1, 3 and 7 after bioprinting. Two tail Students <i>t</i> -test was used to analyze the significant change in the cell-viability after bioprinting process. P-values $* < 0.05$ were considered as significant. Scale bars indicate 1 mm for (a) and (b) and 0.5 mm for the zoomed images.	79
Figure 3.6 NMR spectrums of gelatin and synthesized GelMA with different DoF percentages.	80
Figure 3.7 Embedded printing of a multilayered structure by microcapillary-based printhead. (a) CAD modelling of the multilayered structure with six concentric contours in each layer. Photographs of the four-layered structure (b) inside support bath and (c) after removal from the support bath. (d) Confocal image of one part of the structure. ...	83
Figure 3.8 Investigation of valve interchangeability between different valves. (a) Schematic of a code including transitions in between pressure-driven valves for simultaneous and sequential extrusion. (b) Tool path planning of the single layered construct where valve transition occurs in between each contour. (c) Photograph of a multimaterial structure with valve transitions inside support bath.	85
Figure 3.9 Investigation of transition regions. (a) Schematic of a code including transitions in between pressure-driven valves to evaluate hydrogel diffusion during transition. (b) Tool path planning of the continuous single stripe where transitions occur at 6 points. (c) Photograph of the continuous stripe that includes alternating extrusion of three different hydrogel solutions. (d) Confocal images of three parts of the continuous stripe where transitions occur between different fluorescent colors.	86
Figure 3.10 Embedded multimaterial printing of the initial letters of Sabanci University. (a) Tool path planning of the code which provides printing of structures with two different material combinations. Photography of the printed structures (b) inside support bath and (c) after removal from the support bath. (d) Confocal image of the one part of the Letter S.	87
Figure 3.11 Embedded multimaterial printing of the four layered circular construct which includes three different material compositions. (a) Tool path planning of the code which	

provides printing of structures with three material combinations in different contours of each layer. Photography of the printed structures (b) inside support bath and (c) after removal from the support bath. (d) Confocal images of the two parts of the circular and concentric multilayered structure..... 89

Figure 3.12 Embedded multimaterial bioprinting of three layers of the aortic construct incorporating six contours with bioink transitions in each layer. (a) Cross-sectional view of the artery. (b) Top view of the aortic construct CAD model which includes concentric six contours: one contour, three contours and two contours resembling tunica intima, tunica media and tunica adventitia of the native aorta, respectively. Three different cell types were encapsulated within distinct bioink solutions. Photography of the bioprinted aortic constructs (c) inside support bath and (d) after removal from the support bath. (e) Confocal microscopy image of live and dead cells encapsulated within the biomanufactured aortic construct at Day 4. (f) Quantitative viability analysis of cells for Day 1, 4 and 7 after bioprinting..... 90

Figure 3.13 Demonstration of zonally stratified arrangement of the multimaterial bioprinted vascular constructs (a) Tool path planning of the aortic construct where HUVECs and HSFs were stained with green fluorescent tracker and HASMCs were stained with red fluorescent tracker. (b) Image of the bioprinted aortic construct together with confocal microscopy images of several regions 91

LIST OF ABBREVIATIONS

2D	Two dimensional
3D	3D dimensional
ADSC	Adipose-derived stromal cell
CaCl₂	Calcium chloride
CAD	Computer-aided design
CM	Cardiomyocyte
CPF127	CaCl ₂ containing Pluronic F127
DBB	Droplet-based bioprinting
dECM	Decellularized extracellular matrices
DLP	Digital light processing
DMD	Digital micro-mirror device
DMEM	Dulbecco's Modified Eagle Medium
DMSO	Dimethyl sulfoxide
DoF	Degree of functionalization
DPBS	Dulbecco's phosphate-buffered saline
EBB	Extrusion-based bioprinting
ECM	Extracellular matrix
EMEM	Eagle's minimum essential medium
EPC	Endothelial progenitor cell
FBS	Fetal bovine serum
GAM	Glioblastoma-associated macrophage
GBM	Glioblastoma
GeIMA	Gelatin methacrylate
HAMA	Hyaluronic acid methacrylate
HASMC	Human aortic smooth muscle cell

HDF	Human dermal fibroblast
hiPSC	Human induced pluripotent stem cell
HSF	Human skin fibroblast
HUVEC	Human umbilical vein endothelial cell
HUVSMC	Human umbilical vein smooth muscle cell
iPSC	Induced pluripotent stem cell
Irgacure 2959	2-hydroxy-1-[4 (hydroxyethoxy)phenyl]-2-methyl-1-propanone
ITOP	Integrated tissue-organ printing
LBB	Laser-based bioprinting
LIFT	Laser-induced forward transfer
LVE	Linear viscoelastic
MA	Methacrylic anhydrite
MEF	Mouse embryonic fibroblast
MSC	Mesenchymal stem cell
NMR	Nuclear magnetic resonance
NURBS	Non-uniform rational basis spline
PBS	Phosphate buffered saline
PCL	Polycaprolactone
PDMS	Polydimethylsiloxane
PEGDA	Poly(ethylene glycol) diacrylate
PEUU	Polyester urethane urea
PEVA	Poly (ethylene/vinyl acetate)
PF	Pluronic F127
Pluronic F127	Poly(ethylene oxide)-poly(propylene oxide)-poly(ethylene oxide)
PTFE	Polytetrafluoroethylene
PU	Polyurethane
RGD	Arginine-glycine-aspartic acid
SLA	Stereolithography
SMC	Smooth muscle cell
TEVG	Tissue engineered vascular graft

Some parts of this thesis include information from the following published and unpublished papers:

[published] Afghah, F., Altunbek, M., Dikyol, C. et al. Preparation and characterization of nanoclay-hydrogel composite support-bath for bioprinting of complex structures. Sci Rep 10, 5257 (2020). <https://doi.org/10.1038/s41598-020-61606-x>

[under submission] Dikyol, C., Altunbek, M., Koc, B. Multimaterial Bioprinting Approaches and Their Implementations for Vascular and Vascularized Tissue Biofabrication

1. INTRODUCTION

Cardiovascular diseases are one of the major causes of mortality throughout the world (Nemeno-Guanzon et al. 2012). Diseased and malfunctional vascular tissues are mostly treated through the transplantation of autologous vessels and synthetic grafts, however availability and suitability issues of them hinder the treatment of vascular diseases (Pashneh-Tala, MacNeil, and Claeysens 2016). Besides therapeutic transplantation for diseased blood vessels, reconstruction of functional vascular networks within the created constructs also has a crucial role for the engineering of physiologically-relevant artificial tissues and organs (Hasan et al. 2015). Tissue engineering approaches alleviate these limitations and emerge as a promising strategy for the generation of living and physiologically appealing vascular tissue analogs.

Introduction of additive manufacturing technologies into tissue engineering field has permitted the attainment of tissue constructs with unprecedented degree of precision and reproducibility when compared with conventional methodologies (M. Singh and Jonnalagadda 2020). Among different technologies, bioprinting has gained considerable attention as living cells and biological materials are directly utilized as building blocks to pattern into complex-shaped constructs within spatiotemporal control. However, native tissues are intrinsically complex compositions, comprised of multiple types of cells,

various extracellular matrix (ECM) components and, with few exemptions, infiltrated vasculature in a hierarchical organization (Stock and Vacanti 2001; Rose and De Laporte 2018). Deposition of single bioink formulation from the single nozzle of traditional bioprinters cannot allow to reach the heterogeneous and complex structures of native tissues. In this regard, different multimaterial bioprinting technologies have been developed, which carried bioprinting applications a step forward on the engineering of functional, mechanically stable and anatomically-correct biological constructs by enabling the patterning of multiple materials and cell types simultaneously or sequentially with high precision (Figure 1.1). Especially, multimaterial bioprinting technology holds a great potential for addressing the major challenge in the field by the reconstruction of perfusable vascular networks within large engineered tissues necessary to obtain functional tissues and their transition into clinical applications (Miri et al. 2019; Holland et al. 2018; Tomasina et al. 2018). Multimaterial bioprinting approaches have showed great advancements with the feasible results for the biofabrication of vascular and vascularized tissues.

In this thesis work, microfluidic-based multimaterial bioprinting platform combined with embedded bioprinting technique was developed for the biofabrication of vascular tissues recapitulating both multimaterial and multilayered hierarchical arrangement and complex geometrical shape of native vascular tissues.

1.1. Bioprinting

Bioprinting is a cluster of additive manufacturing technologies focusing on the biofabrication of living tissues and organs by spatially patterning cells and other biomaterials in a layer-by-layer approach (Mota et al. 2020). A systematic workflow for bioprinting mostly starts with the data acquisition (e.g., magnetic resonance imaging, computerized tomography) and computer-aided modelling of the targeted tissue/organ, which continues through selection, preparation and controlled deposition of the bioinks and then post-bioprinting processes (Mandrycky et al. 2016). Depending on their working principles, bioprinting modalities are categorized into three: extrusion-based bioprinting (EBB), droplet-based bioprinting (DBB) and laser-based bioprinting (LBB).

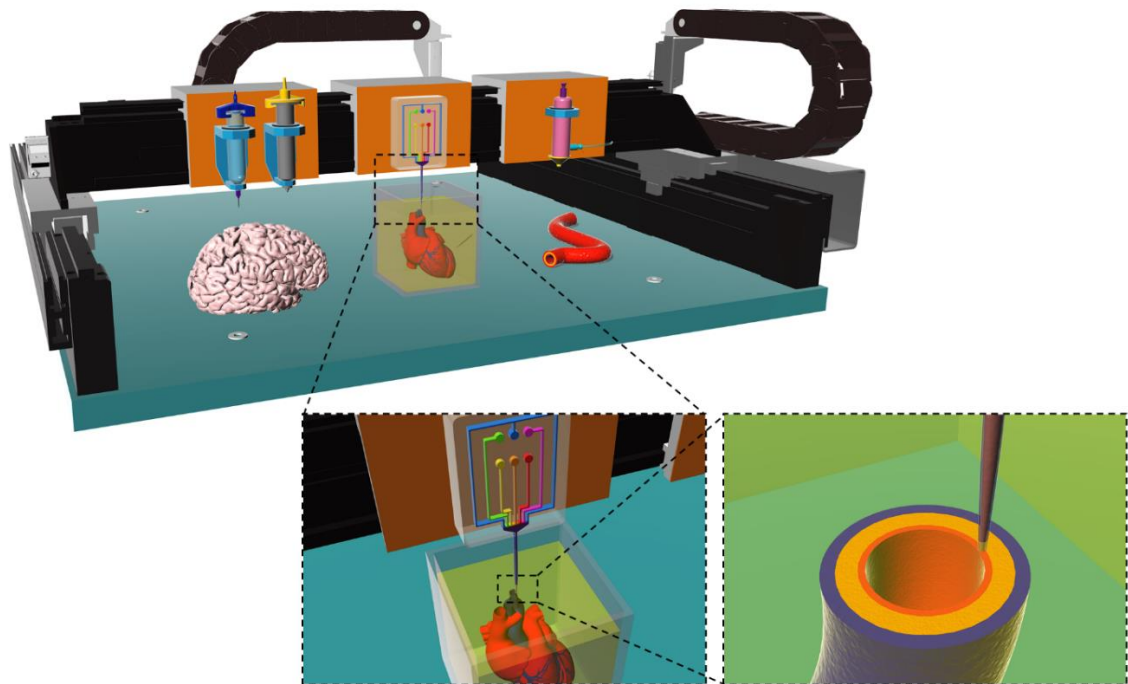


Figure 1.1 An illustration of multimaterial bioprinting platform with multi-head, microfluidic and coaxial dispensing units (from left to right). Development and implementations of different multimaterial bioprinting approaches have achieved several milestones on the biofabrication of vascular and vascularized tissues by patterning various types of material formulations in a spatially-controlled manner. Multimaterial bioprinting approaches demonstrates a potential for the reconstruction of vascular networks within the thick tissues and also generation of vascular tissues with zonally stratified, multicellular and concentric arrangement (Gantry model of the illustrated multimaterial bioprinting platform was obtained and modified from 3D ContentCentral service (<https://www.3dcontentcentral.com/parts/supplier/Aerotech-Inc.aspx>) with permission from Aerotech Inc. Digital models of human heart and brain were obtained and adapted from the BodyParts3D database (<http://lifesciencedb.jp/bp3d/>) (Mitsuhashi et al. 2008))

EBB is the most widespread bioprinting modality, in which a cell-laden bioink is continuously extruded from the nozzle in a layer-by-layer manner to biomanufacture a pre-designed three-dimensional (3D) construct. Extrusion of the continuous cell-laden cylindrical filaments is driven by pneumatic or mechanical (piston-based or screw-based) dispensing systems (Murphy and Atala 2014).

Natural and synthetic hydrogels have been utilized for the preparation of bioinks. Together with resembling the ECM of encapsulated cells, they also provide a supporting milieu for the cells throughout the bioprinting and cultivation processes (Hölzl et al. 2016). Hydrogels exhibiting shear-thinning behavior are preferred for EBB applications. These kind of bioinks maintain their rheological stability in the hydrogel reservoir throughout the bioprinting process. During extrusion, exerted external shear stress reduces the viscosity of the biopolymer and the material exhibits fluid-like behavior. Following the extrusion from the nozzle, bioink quickly recovers to its initial state (Leijten et al. 2017). For the maintenance of shape fidelity of the 3D construct, gelation is performed right after extrusion through physical or chemical crosslinking.

DBB, which is also named as inkjet bioprinting or drop-on-demand technique, generates droplets from bioinks via thermal, electrostatic or piezoelectric actuators and precisely deposits by employing non-contact bioprinting approach (Gudupati, Dey, and Ozbolat 2016). Droplet volume and density of cells per droplet are specified by adjusting parameters such as pressure, feeding rate and valve aperture time. Even though this bioprinting modality enables patterning in higher-resolution compared to EBB modality, biomanufacturing of large-scale 3D constructs is challenging.

LBB modality can be sub-categorized into two different technologies: cell-transfer technologies involving laser-induced forward transfer (LIFT) technology and photopolymerization technologies involving stereolithography (SLA). In LIFT technology, laser energy is directed to a donor slide (also called as target or ribbon) which has an energy-absorbing layer on the top and a bioink distributed layer on the bottom. Through focusing a laser pulse to a small region between energy-absorbing layer and bioink layer, formation of high-pressure bubble occurs, which cause detachment of bioink droplets from the donor slide and ejection to a receiving layer in non-contact mode (Duocastella et al. 2008). SLA technology relies on the photopolymerization principle. Through the scanning of pre-programmed path via ultra-fast laser beam, photosensitive bioink is selectively cured in a layer-by-layer manner (H. Kumar and Kim 2020).

1.1.1. Bioprinting Inside Support Bath: Embedded Bioprinting

3D bioprinting provides controlled deposition of hydrogels, biological matters or biomaterials to fabricate complex cell-laden structures in a layer-by-layer manner for various tissue engineering applications. Natural or synthetic biocompatible and biodegradable cell-laden hydrogels are commonly used to construct 3D environment with the ability to turn into gel at physiological conditions without impairing cell integrity and cell-to-cell interaction. Extrusion based bioprinting is one of the most common method to deposit cell-laden hydrogels in desired geometry with precise control in micrometer scale. The process requires gelation of liquid hydrogel either by physical, thermal or chemical crosslinking before, during, or after bioprinting. However, physical phase transition of hydrogels during extrusion might clog the nozzle and could disrupt the viability of the encapsulated cells (Guillotin et al. 2010; Ozbolat and Hospodiuk 2016). In addition, due to low mechanical strength, the printed hydrogels may not be strong enough to hold overhanging structures. Integration of the subsequent layers is another challenge which needs proper adjustment of hydrogel gelation time with the printing process (H. W. Kang et al. 2016; Jin et al. 2017). The level of humidity strongly affects cellular viability, which is not often preserved during in-air hydrogel extrusion bioprinting (Matsuzaki et al. 2019; McCormack et al. 2020). These limitations can arise due to both hydrogel properties such as viscosity and gelation time, and the printing parameters such as fabrication time, extrusion pressure and nozzle size. Among them, viscosity of the hydrogel has a pivotal role. Viscosity can be fine-tuned with increasing the concentration, which increases the hydrogel stiffness and subsequently might have an adverse effect on cell migration and functioning. A sacrificial secondary hydrogel with different gelation property, or a viscosity modifying biomaterial is generally introduced within the primary hydrogel to obtain a qualified structure during the extrusion based bioprinting process (Datta, Ayan, and Ozbolat 2017; C. J. Wu et al. 2011; Topuz et al. 2018; Peak et al. 2018).

Direct free form writing of hydrogels in a fugitive and sacrificial support-bath has addressed aforementioned limitations. A support-bath with the Bingham plastic flow behavior can provide a rigid supporting matrix and at the same time, instantaneous yielding and rapid recovery during and after passage of the extruding nozzle, respectively (Mezger 2006; Jeon et al. 2019; Howard A. Barnes 2000; Ding and Chang 2018;

McCormack et al. 2020). In addition to the adequate flow behavior, the support-bath should quickly provide the necessary gelation to control the spreading of the extruded viscous bioink and let the printed layers to be integrated, and concurrently avoiding nozzle clogging. This approach has been demonstrated by depositing liquid hydrogel precursors within self-healing support materials such as Carbopol, Laponite, gelatin, gellan, fumed silica particles, Pluronic and alginate (Bhattacharjee et al. 2015; Hinton et al. 2015; Duarte Campos et al. 2013; Jin et al. 2016; Jin, Chai, and Huang 2017; Hinton et al. 2016; Grosskopf et al. 2018; Compaan, Song, and Huang 2019). However, the functionality of the support-bath materials is influenced by several parameters. In addition, the compatibility of the support-bath with the printed hydrogel has also a crucial role for a successful bioprinting (Highley, Rodell, and Burdick 2015; Jin et al. 2016; Hinton et al. 2015; Duarte Campos et al. 2013). For example, hydrophobic perfluorotributylamine fluid was employed for the bioprinting of agarose hydrogel due to its high buoyant density (Duarte Campos et al. 2013). Since the approach of supporting is based on buoyancy, viscosity of the printed hydrogel might affect the structural resolution which limits the applicability of this support material in different types of hydrogels. In another study, two different types of hyaluronic acid which were modified with adamantane or β -cyclodextrin, respectively, were utilized as self-healing support material, by using their reverse assembly capability as host-guest interactions (Highley, Rodell, and Burdick 2015). Although methacrylated gels were successfully printed, the possible reaction of adamantane or β -cyclodextrin ends would limit the utilization of this technique to be used with different materials. Due to their stress-yielding properties, Carbopol microgels and gelatin microparticles have also been studied (Bhattacharjee et al. 2015; Hinton et al. 2015). However, ionic sensitivity of the Carbopol and, thermal instability and microparticle size-dependency of the gelatin slurry limit their use. Therefore, to address limitations and general requirements for bioprinting of hydrogels with various properties, new formulations of support-bath systems are needed.

Poly(ethylene oxide)-poly(propylene oxide)-poly(ethylene oxide) (Pluronic F127; PF) is one of the support-bath material candidates possessing concentration dependent-thermoreversible gelation property. It is in gel form at around body temperature (concentrations >18%) and turns into liquid below 10 °C (Jiang et al. 2008). Hence, it was implemented as support-bath or sacrificial fugitive ink at room temperature within the range of 25-40% concentrations (Kolesky et al. 2014; Rocca et al. 2018). However,

viscoelastic modulus of the material was not strong enough for micrometer scale resolution in a long time printing processes due to mechanical weakness and tendency of quick dissolving in physiological conditions (Rocca et al. 2018) (Jiang et al. 2008). Sol-gel transition concentration of PF was modified by addition of Laponite (C. J. Wu and Schmidt 2009; C. J. Wu et al. 2011). Laponite is a layered synthetic nanoclay with chemical formula of $\text{Si}_8\text{Mg}_{5.45}\text{Li}_{0.4}\text{O}_{24}\text{Na}_{0.7}$ similar to hectorite. It exists as a 2D disc-like structure, 25 nm in diameter and 1 nm in thickness with negative charges distributed on the faces (OH^-) and positive charges on the edges (Na^+). Due to its biocompatibility, low cost, availability, thermal stability, processability, ionic insensitivity, and anisotropic behavior, Laponite can be considered as a promising rheology-modifier, or used as mechanical reinforcing component and crosslinker with several hydrogel systems (Haraguchi et al. 2003; Chang et al. 2010; Boucenna et al. 2010). It was utilized in different applications of tissue engineering from composite hydrogel printing to support-bath material (Tomás, Alves, and Rodrigues 2018; Nadernezhad et al. 2019; Gaharwar et al. 2019; Dávila and D'Ávila 2017; Ding and Chang 2018). The gel-forming ability of Laponite involves a multi-step mechanism. When particles react with hydroxide ions in the water, phosphate ions dissolve. After the ion dissolution, the nanoclay particles start to interact with each other while the sodium ions diffuse towards the surfaces within the galleries, resulting in expanded thixotropic gel structure (Au et al. 2015; Jatav and Joshi 2014; Castelletto, Ansari, and Hamley 2003). Laponite RDS, a category of Laponite family, possesses an extra peptizing agent of sodium pyrophosphate ($\text{Na}_4\text{P}_2\text{O}_7$) at the edges which ionically stabilizes the structures and prevent the face-edge bond formation between particles (Pek-Ing and Yee-Kwong 2015). The pyrophosphates give a thixotropic behavior to the structure (Pek-Ing and Yee-Kwong 2015). These properties of Laponite would make it a suitable support-bath material, but the printed hydrogels have high viscosity with stiff network which is a disadvantage for cellular activities like cell adhesion, migration and proliferation (Ehrbar et al. 2011; Krishnamoorthy, Noorani, and Xu 2019; Ahearne 2014). In addition, the removal procedure of the supporting gel is complicated, often resulting in damage to the printed structure due to being strongly adherent nanoclay particles (Compaan, Song, and Huang 2019).

A composite support-bath based on the mixture of PF and Laponite (PF-RDS) in the presence of calcium ions was developed, to be used in freeform bioprinting of complex

cell-laden hydrogel structures (Afghah et al. 2020) and utilized throughout the thesis work. Although both materials show unique properties and have been individually employed as sacrificial support gels, they showed limited capacities in bioprinting of low viscosity inks at low concentrations and also the ease and efficiency of removal procedure (Ding and Chang 2018; Jin et al. 2017). By combining two components as a composite support-bath, it would be possible to employ the distinct characteristics of each, namely the thermoresponsive gelation of PF and the thixotropic behavior of Laponite. Different formulations with varying concentrations of PF-RDS and calcium chloride (CaCl_2) were also analyzed to achieve optimum rheological properties. Sodium alginate was utilized as a precursor solution to evaluate printability of complex and hollow structures by *in situ* crosslinking within the support-bath. Finally, cell-laden hydrogel structures were bioprinted in the support-bath and the cytocompatibility of the bioprinting process was analyzed by monitoring the viability after printing process.

1.2. Anatomy of Vascular Tissue

The functionality of body tissues and organs depends on the fulfillment of their needs. Circulatory system of the body is the responsible from this and synchronously functions to supply the demands. Blood vessels have a crucial role in the system by controlling the delivery of oxygen and nutrients to the tissues and organs throughout the body and removal of their waste metabolites. Blood vessels are categorized into three types including arteries, veins and capillaries. Arteries (~25 mm in diameter) transport the oxygen and nutrient-rich blood from the heart to the tissues and organs throughout the body by passing through the smaller artery branches (10-0.1 mm in diameter) and, the capillaries (5-10 μm diameter). In the capillaries, nutrients and oxygen are exchanged with metabolic wastes, which return back to the heart by passing through venules (smaller vein branches) and vein. Arteries and veins are comprised of three distinct layers: tunica intima, tunica media and tunica externa, whereas capillaries only have tunica intima layer. The relatively different compositions of the layers attain different functionalities to the arteries and veins. Arteries are round shaped tubular structures. They have relatively thick elastic walls with smaller lumen, which allow withstanding the high blood pressure pumped from the heart. On the other hand, veins have irregular-shaped thin walls. Veins

are subjected to the relatively low blood pressure and contain valves working against gravity to provide one-way flow towards to heart.

Tunica intima is the innermost layer of artery or vein, which directly interact with the blood flow and pressure. Basically, endothelial cells align in a single-layer on the basement membrane composed of laminin, collagen IV and proteoglycans (Pugsley and Tabrizchi 2000). The tunica intima layer shows some differences in the arteries and veins. A wavy-like appearance in the tunica intima layer of arteries is seen due to the constriction of smooth muscles. In addition, an internal elastic membrane between tunica intima and tunica media is found only in larger size arteries, which permits stretching of the vessel. Tunica media is the middle layer characterized by a thicker structure compared to other layers, and much thicker in arteries compared to veins (Halper 2018). Vascular smooth muscle cells (SMCs) are arranged in circular sheets in the connective tissue matrix formed mostly by elastin fibers in this layer. The SMCs are seen in longitudinal morphology towards the tunica externa. Circular SMCs are responsible for the contraction (vasoconstriction) and relaxation (vasodilation) behavior, which determine blood pressure and flow by causing decrease or increase in the diameter of the vessel lumen. The outermost layer of the vessels is called tunica externa composed of fibroblast and myofibroblast cells in a collagenous-fiber rich connective matrix (Coen et al. 2011). This layer stabilizes and keeps the vessel in relative position. A bunch of smooth muscle fibers in the tunica externa distinguishes veins from arteries. In addition, this layer in veins is thicker than arteries. There are also other critical components like small blood vessels (vasa vasorum), unmyelinated nerve fibers and lymphatic vessels at tunica externa of larger vessels to provide demands of the cells and regulate vasoconstriction and vasodilation (Halper 2018). The capillaries consist of a line of endothelial cells surrounded by basement membrane. Arteries and veins are connected by the capillaries that help the exchange of oxygen, nutrient and waste materials between blood and tissues.

The impairment in the structure of the blood vessels like hardening, enlarging, and narrowing trigger severe health problems such as atherosclerosis, coronary artery heart disease, cardiovascular disease, peripheral artery disease. Unless the development of effective treatment approaches, cardiovascular disease related annual mortalities will dramatically increase in worldwide (Jeong et al. 2020; Carrabba and Madeddu 2018; Nemen-Guanzon et al. 2012). The insertion of stents, surgical bypass grafting, and

angioplasty are currently used clinical strategies to repair vascularization. There are commercialized grafts, such as polytetrafluoroethylene (PTFE), gore-tex, and dacron, which were found as clinically effective when replacing large-diameter vessels (≥ 6 mm). However, it can cause thrombosis with the closing of the lumen and the lack of long-term patency as well as intimal hyperplasia when employed for smaller-diameter (≤ 6 mm) vessels. Other vascular graft candidates with biological origin have been successfully prepared using various tissue engineering approaches (Syedain et al. 2011; Schutte et al. 2010; L'heureux et al. 1998; V. A. Kumar et al. 2013; Othman et al. 2015; Ghanizadeh Tabriz et al. 2017; Wilkens et al. 2016; Seifarth et al. 2017; Saeidi, Sander, and Ruberti 2009), yet lack of anatomical complexity with heterogeneous organization limits their functionality (Holland et al. 2018). The integration of 3D printing technology to tissue engineering approaches has shown promising results with the fabrication of natural like tissue engineered vascular grafts (TEVG). In particular, clinical applications of the TEVG have addressed limitations and overcome the essential problems such as anti-thrombosis and long-term patency. Several interesting studies have been reported to date to generate tubular structures with capability of physiological remodeling (Jeong et al. 2020).

Generation of vascular networks embedded structures also has vital role in the generation of sophisticated and functional artificial tissue and organ structures and their clinical transition. Requirement of vascularized tissue and organs at clinically-relevant sizes has been investigated to be addressed by variety of tissue engineering approaches but still resides as a grand challenge.

In the following section, different multimaterial bioprinting approaches are introduced thoroughly together with their superior and inferior aspects to demonstrate their implementations in the biofabrication of vascular and vascularized tissues.

1.3. Multimaterial Bioprinting

Human tissues are inherently complex structures composed of multiple types of cells hierarchically arranged within an extra-cellular environment. 3D printing technology has enabled the biofabrication of complex-shaped tissue structures through spatial patterning

of biological materials in a controlled manner yet, there are still many challenges that needs to be addressed to reach the bio-mimicry of the sophisticated nature of the living tissues and organs.

Multimaterial bioprinting approaches have achieved several milestones within this scope thanks to its capability to recapitulate multiscale microarchitecture of living tissues and organs including multiple cell types and ECM components. It has become possible through the simultaneous or sequentially deposition of several categories of biomaterials including cell-laden or pure ECM components, sacrificial materials and scaffolding polymers. While patterning of multiple hydrogel compositions loaded with different cell types has provided the biomanufacturing of tissue mass in a compositionally controlled manner, extrusion of sacrificial materials has enabled the formation of open lumens inside the tissue model. Printing of scaffolding polymers together with other biomaterials such as hydrogels have been utilized for contributing mechanical stability.

Conventional bioprinters allow deposition of multicomponent bioinks from a single nozzle. In this regard, different combinations of multicellular and multimaterial bioinks have been developed for different purposes. While many types of cells have been mixed in the same bioink and simultaneously co-extruded together, various biomaterials have also been blended and co-extruded for several reasons including viscosity modification, mechanical reinforcement and drug release. Even though patterning of multicellular and multicomponent single bioinks fulfill the biological complexity by enabling the interaction between different cell types and extracellular cues, it does not provide control over spatial heterogeneity like in living tissues. Replication of heterocellular and hierarchical composition of living tissues and organs requires more advanced multimaterial bioprinting tools and techniques.

In multimaterial bioprinting, different materials delivered from separate reservoirs or cartridges are simultaneously or alternatively deposited. Depending on their printhead system and working mechanism, multimaterial bioprinting approaches would be classified into four divisions: Multi-head multimaterial bioprinting, coaxial multimaterial bioprinting, microfluidic multimaterial bioprinting and laser-based multimaterial bioprinting. Each multimaterial bioprinting technique exhibits unique principles of material patterning for the bioengineering of physiologically relevant tissues.

1.3.1. Multi-Head Multimaterial Bioprinting

The principle of multi-head multimaterial bioprinting approach relies on the swapping of bioink dispensing systems in a controlled manner for the biomanufacturing of heterogeneous constructs with numerous bioinks. Separated and distinct multiple printheads sequentially deposit individual materials to recapitulate multimaterial architecture of native tissues.

Merceron et al. provided comprehensive demonstration of this multimaterial bioprinting technology through developing integrated tissue-organ printing (ITOP) system for biofabrication of heterogeneous tissue interface (Figure 1.2(a)) (Merceron et al. 2015; H.-W. Kang et al. 2016). Their bioprinting platform included four separate extrusion-based printheads, which were loaded with two different synthetic thermoplastic polymers and two different cell-encapsulated hydrogels to obtain biomechanically strong and biologically functional integrated structure composed of two distinct muscle-tendon unit. The system was automated to print different categories of polymers with different rheological properties sequentially. The scaffold designed for muscle unit was composed of C2C12 cell-laden bioink reinforced with polyurethane (PU) while tendon unit was comprised of NIH/3T3 cell-laden bioink reinforced with polycaprolactone (PCL). Beside representing tensile features of skeletal muscle and tendon tissues in a single scaffold, the construct exhibited upregulated expression of genes associated with muscle-tendon junction. Absence of these zone-specific markers in solely muscle bioprinted constructs indicates that this multimaterial bioprinting approach possesses the potential of biofabrication of anatomically and functionally correct tissues. The same multimaterial bioprinting platform, ITOP system, was also employed for the development of contractile cardiac tissues with multifaceted functionalities, ranging from molecular level to system level (Z. Wang et al. 2018). For the bioengineering of heart tissue, Das et al. also utilized co-printing of designed bioink with a thermoplastic polymer, poly (ethylene/vinyl acetate) (PEVA), to provide supportive framework and anchoring regions (Das et al. 2019). However, dispensing biocompatible thermoplastic polymers from an extrusion-based printhead and dispensing cell-laden bioinks from another extrusion-based printhead have especially gained considerable attention for the biofabrication of tissues exposed to

high mechanical loads (Khani et al. 2017; Ruiz-Cantu et al. 2020; Yun et al. 2019; Antich et al. 2020; Y. Sun et al. 2019; J. L. Song et al. 2020).

In addition to advantages of multimaterial bioprinting approaches for bioengineering of tissues and organs, they have also been utilized to understand the effects of drugs and progress of diseases through developing miniaturized tissues and organ-on-a-chip platforms (Levato et al. 2020; Dreher and Starly 2015). Heinrich et al. biofabricated a miniaturized brain model to understand cellular interaction of glioblastoma-associated macrophages (GAMs) with glioblastoma cells and to assess emerging therapeutics which target to inhibit this cellular interaction (Heinrich et al. 2019). First of all, brain model with an empty cavity was bioprinted with macrophage-laden bioink, and then empty cavity was filled by bioprinting with glioblastoma-laden bioink extruded from second nozzle. Lee et al. introduced one-step production of an organ-on-a-chip by multimaterial bioprinting of various cell types and ECM components (H. Lee and Cho 2016). In their study, a housing with an empty cavity was printed with PCL and cell-laden gelatin-based and/or collagen-based bioinks were bioprinted into the empty cavity for biofabrication of different organ-on-a-chip platforms. Besides providing spatially heterogeneity, the developed organ-on-a-chip fabrication approach showed its potential to overcome the issues of current organ-on-a-chip fabrication methods such as protein absorption. Further, Skardal et al. employed multimaterial bioprinting technology in the development of three-tissue organ-on-a-chip platform for investigating intertissue interactions (Skardal et al. 2017).

Multimaterial bioprinting strategies usually employ EBB modality. But it is noteworthy to mention that DBB modality also enables multimaterial bioprinting through the deposition of different materials from multiple nozzles. Early attempts of this technique include the ejection of cell-laden precursor solution from one nozzle and subsequent ejection of crosslinker from another nozzle for rapid gelation (Faulkner-Jones et al. 2015; C. Li et al. 2015). Through the improvements in this technique, different types of hydrogels with or without cells have been inkjet bioprinted from separate nozzles (Zimmermann et al. 2019; Negro, Cherbuin, and Lutolf 2018; Sakai et al. 2018).

Each of the bioprinting modalities have demonstrated their potential for the manufacturing of tissues in a spatially and compositionally controlled manner. However,

biofabrication of biologically and physiologically-complex fully functional tissues and organs might require co-working of different bioprinting modalities within the same process. In this context, multiple printheads working through different bioprinting modalities have been combined in various studies, such as using extrusion-based and droplet-based printheads for biofabrication of articular cartilage substitutes (Campos et al. 2019) or using digital light processing (DLP) and extrusion-based system for bioengineering of corneal substitutes (B. Zhang et al. 2019). Kim et al. provided extensive representation of this multimaterial bioprinting technology through manufacturing of human skin model *in vitro* via developed hybrid printing platform which accommodates extrusion-based and inkjet-based dispensers (B. S. Kim et al. 2017, 2018).

Recently, multi-head multimaterial bioprinting approach was combined with embedded bioprinting technique. Lee et al. recruited extrusion from multiple printheads for replication of human left ventricle model through extrusion of collagen ink and cell-laden bioink inside thermoreversible support bath made up of microgranular gelatin slurry (Figure 1.2(b)) (A. Lee et al. 2019). In this study, fabricated left ventricle model included two compartments: ellipsoidal core region including patterned human embryonic stem cell-derived cardiomyocytes and inner and outer walls created by extruding collagen ink for structural integrity and shape fidelity. Beside accurate replication of the desired model, printed ventricle demonstrated synchronized contraction with directional wave propagation and wall thickening functionalities.

Major limitation of multi-head multimaterial bioprinting is the feasibility of printing only one material at a time, which considerably slows down the fabrication process. Even though there is no limit for the number of printheads for dispensing many types of cells and biomaterials within one construct, printing process takes more time with increasing the number of printheads. Moreover, multiplication of printheads introduces alignment problem. Nozzles should be aligned and bioink flow should be started and stopped carefully in each swapping of dispensing systems to achieve a smooth interface between material changes. These challenges have been addressed in different multimaterial bioprinting techniques.

1.3.2. Coaxial Multimaterial Bioprinting

Coaxial bioprinting approach allows simultaneous extrusion of several concentric layers of materials by utilizing co-axially fashioned distinct nozzles. The approach is inherently a multimaterial bioprinting approach as the printhead system contains at least two compartments in its nature. This direct extrusion strategy is adapted to bioprinting from microfluidic-based wet spinning technique (B. R. Lee et al. 2011; Onoe et al. 2013; E. Kang et al. 2012), in which cell-laden or acellular microfibers are formed by flowing precursor hydrogel solution and crosslinker solution inside microfluidic device with core-sheath microchannels. In coaxial bioprinting, also called as core-shell bioprinting, solid or hollow filaments can be fabricated. When precursor solution is dispensed from inner channel and crosslinking agent is dispensed from outer channel, solid microfibres are manufactured. Reverse arrangement of precursor solution and crosslinker inside the channels enable the formation of microfibers with lumen inside. Following the flow of precursor solution and crosslinker from separate channels, precursor solution should be crosslinked rapidly when they contact with each other to sustain shape fidelity. Owing to its fast gelation mechanism, alginate-based systems were utilized and crosslinked with CaCl_2 broadly. However, it should be noticed that different coaxial bioprinting techniques were also developed such as incorporation of different crosslinking mechanism (Duchi et al. 2017) or delivery of crosslinker in a different way (Yeo et al. 2016). For example, Yeo et al. performed crosslinking of core/shell bioprinted cell-laden collagen/alginate construct by treating the extruded filament with aerosol CaCl_2 (Figure 1.2(c)) (Yeo et al. 2016).

Coaxial printing has been utilized for enhancing mechanical stability and robustness of soft hydrogels by surrounding low concentration ones with another supportive shell hydrogel (Akkineni et al. 2016). Liu et al. performed coaxial multimaterial bioprinting by delivering cell-laden gelatin methacrylate (GelMA) pre-hydrogel containing CaCl_2 from inner channel and delivering alginate from outer channel (W. Liu et al. 2018). In this study, core-shell bioprinting was utilized for the extrusion of very low viscosity cell-laden GelMA hydrogel without any structural deformation with the assistance of alginate template. Following the extrusion of inks from core-shell nozzle and patterning into pre-designed 3D shape, hydrogel structure was stabilized and formed through photo-crosslinking mechanism.

Coaxial bioprinting facilitates precise spatial distribution of multiple cell types in a controlled manner. Moreover, heterogeneity and complexity of the multicellular structures can be expanded by increasing the number of concentric nozzles to three or more (J. He et al. 2018; Dai et al. 2017). For this reason, this multimaterial bioprinting approach was employed in various tissue engineering applications by extruding multiple cell types encapsulated within different hydrogels from inner and outer channels. One example includes utilization of this bioprinting approach for pancreatic islet transplantation, a promising treatment strategy for Type I diabetes (X. Liu et al. 2019). In that work, cells were encapsulated within alginate-GelMA blend and while pancreatic islet cells were extruded from inner tube, islet-related cells were extruded from outer tube to improve revascularization and immunosuppression. Islet cells preserved its viability following the bioprinting process. Another example would be from application of coaxial bioprinting for *in vitro* tissue model fabrication to mimic tumor microenvironment. Wang et al. fabricated *in vitro* glioma model through co-axially extruding glioma cells from inner tube and glioma stem cells from outer tube (X. Wang et al. 2018).

Coaxial extrusion technique was also combined with other bioprinting strategies for hybrid biofabrication of complex constructs (Zhu et al. 2018; Ozbolat, Chen, and Yu 2014). Ozbolat et al. established a multi-arm bioprinter system, enabling simultaneous multimaterial patterning from different nozzles (Figure 1.2(d)) (Ozbolat, Chen, and Yu 2014). Unlike other multi-head multimaterial bioprinters, printheads are able to move at the same time with independent tool paths as they are actuated independently. In that study, coaxial printhead dispensed alginate and CaCl_2 from inner and outer tubes, respectively into 0-90° oriented filaments and another extrusion-based printhead deposited cell spheroids concurrently into gaps between the filaments. Duchi et al. developed a handheld printer for *in situ* biofabrication of cartilage tissue (O'Connell et al. 2016) and further improved the handheld device by incorporating coaxial multimaterial bioprinting technology (Figure 1.2(e)) (Duchi et al. 2017). Both of the inner and outer tubes included GelMA-Hyaluronic acid methacrylate (HAMA) blend hydrogel but adipose stem cells and photoinitiator material were additionally mixed with bioinks in the inner and outer tubes, respectively. Bioprinted structure exhibited high mechanical strength and cell viability.

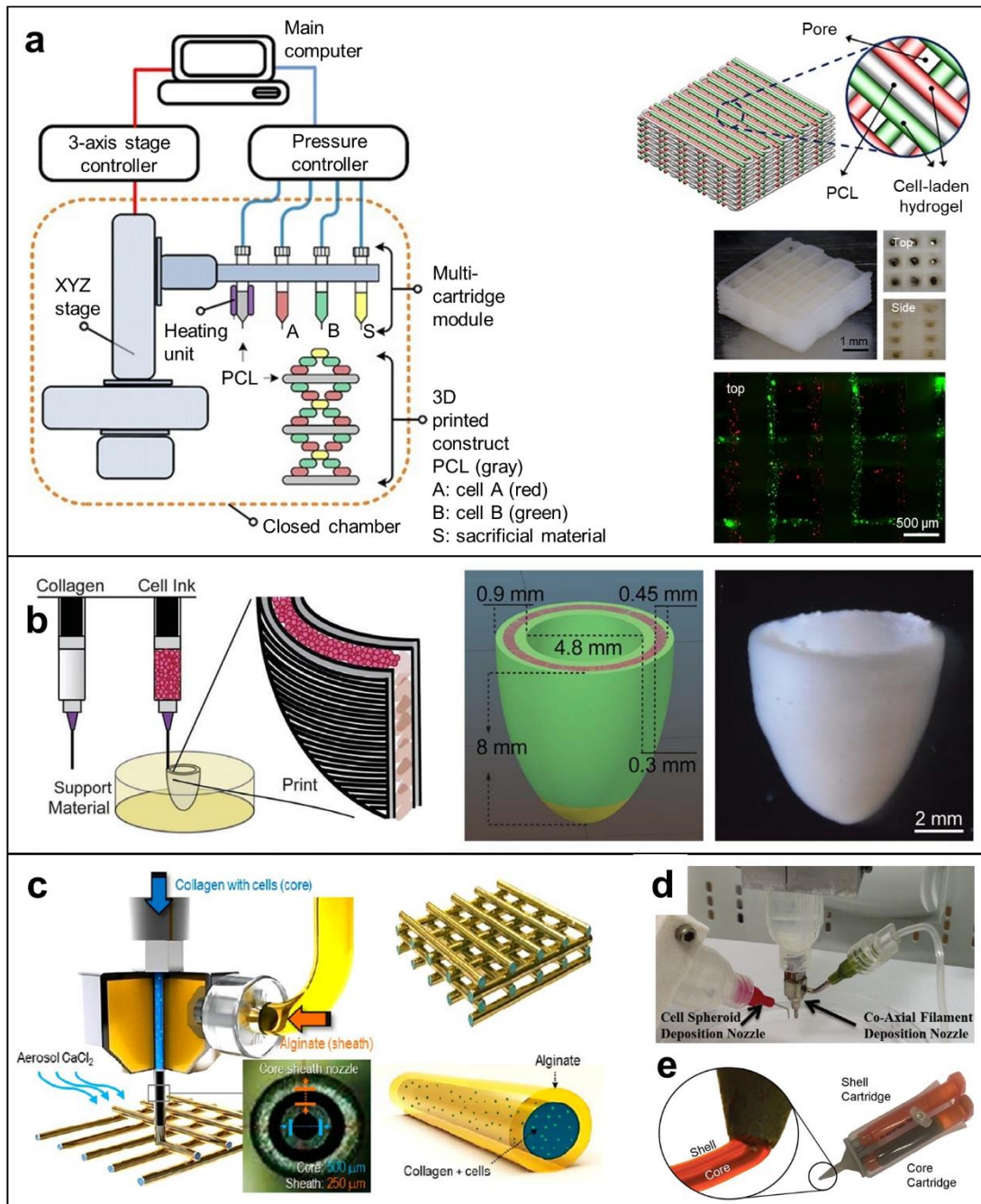


Figure 1.2 Different biofabrication platforms employing multi-head and coaxial multimaterial bioprinting approaches: **a**) ITOP system, which is a multi-head multimaterial bioprinting platform with the capability of dispensing multiple types of thermoplastic polymers and bioink formulations (left) and illustration, photograph and fluorescent image of a construct fabricated by ITOP system (right). Reproduced/adapted with permission from Ref. (H.-W. Kang et al. 2016). Copyright 2016, Nature America. **b**) Combination of multi-head multimaterial bioprinting approach with embedded bioprinting technique for the fabrication of cardiac ventricle model. Reproduced/adapted with permission from Ref. (A. Lee et al. 2019). Copyright 2019,

AAAS. **c)** Coaxial printheads enable the simultaneous extrusion of several concentric layers of materials and the developed printheads may be integrated with different crosslinking techniques such as aerosol delivery. Reproduced/adapted with permission from Ref. (Yeo et al. 2016). Copyright 2016, American Chemical Society. **d)** Multi-arm bioprinter system incorporating coaxial printhead and cell spheroid depositing secondary printhead for multimaterial patterning. Reproduced/adapted with permission from Ref. (Ozbolat, Chen, and Yu 2014). Copyright 2013, Elsevier. **e)** Handheld printer for *in situ* biofabrication of cartilage tissue by coaxial deposition of GelMA-HAMA hydrogels. Reproduced/adapted with permission from Ref. (Duchi et al. 2017). Copyright 2017, Springer Nature

1.3.3. Microfluidic Multimaterial Bioprinting

Microfluidics technology enables manipulation of various fluidic functions at micro-scale. Recently, this technology was transferred from microfluidic devices to additive manufacturing platforms as microfluidic techniques allow spatiotemporal coding of heterogeneous materials with high precision, which is an insertion of additional control and capabilities to printing systems. Hardin et al. performed multimaterial printing of viscoelastic polydimethylsiloxane (PDMS) inks by developing a microfluidic printhead with rapid switching capability and also analyzed the relationship between printing parameters, ink rheology and dispensed filament composition by mathematical models (Hardin et al. 2015). In another study, the same group assembled a rotating impeller into the microfluidic printhead to provide active mixing of viscoelastic inks at pre-determined ratios (Ober, Foresti, and Lewis 2015). Moreover, Serex et al. implemented various microfluidic functions performed in lab-on-a-chip devices into 3D printing system by integrating a microfluidic printhead (Serex, Bertsch, and Renaud 2018).

Microfluidics technology also demonstrated great advancements in the field of tissue engineering through the controlled manipulation of different types of cells, biomolecules, ECM components and other biological materials in precise configuration. By this means, several organ-on-a-chip platforms and tissue engineering techniques were developed for the generation of constructs mimicking biological functions of the native tissues in small scales (Zheng et al. 2016; Pi et al. 2018). Together with the integration of microfluidic

printheads with various 3D bioprinting platforms, another type of multimaterial bioprinting approach, microfluidic multimaterial bioprinting, has emerged for the biofabrication of anatomically-correct, multimaterial and heterocellular constructs mimicking the complex organization of native tissues and organs. This approach addressed scaling up issues observed in the microfluidic systems and also improved the printing resolution of the bioprinting platforms (J. Ma, Wang, and Liu 2018). In microfluidic multimaterial bioprinting, each of the bioinks coming from different reservoirs are connected to the inlets of the microfluidic printheads and bioinks flowing through the microchannels are simultaneously or alternatively dispensed from the single nozzle. Depending on the both arrangement of microchannels in the microfluidic system design and actuation adjustments of the pumps, distinct bioinks can be extruded separately or mixed together.

Beyer et al. developed a microfluidic chip printhead with coaxial flow focusing feature for 3D printing hydrogel constructs (S. T. Beyer et al. 2013). In the study, alginate stream was coaxially focused with CaCl_2 solution delivered from the two side flows and then deposited as a gelled microfiber with decreased diameter. Beyer et al. further improved the designed printhead for multimaterial printing of heterogenous hydrogel constructs by incorporating pneumatic valves that enable switching in between the different materials (Simon Travis Beyer, Mohamed, and Walus 2013). Recent studies also demonstrated the applicability of the microfluidic chip-based printheads with coaxial flow focusing and multimaterial switching capabilities for different bioprinting applications (Figure 1.3(a)) (Dickman et al. 2020; Sharma et al. 2020).

Combination of coaxial needles with microfluidic chips constitutes another microfluidic multimaterial bioprinting approach that enable switching between multiple bioinks or dispensing in combination. In this approach, alginate containing different bioink formulations are flown through the microchannels of the microfluidic chip with Y-junction (two inlets and one outlet) and then *in situ* crosslinked by calcium containing solution delivered from the coaxial nozzle at the tip of the microfluidic chip (Costantini et al. 2017; Colosi et al. 2016). Maiullari presents the flexibility of this multimaterial bioprinting approach on the biofabrication of multimaterial and heterocellular constructs with different geometries, where the bioinks with different cell types are deposited individually in each layer or dispensed together (Figure 1.3(b)) (Maiullari et al. 2018).

Idaszek et al. further improved the technique by incorporating passive mixing unit into the microfluidic chip design, which enabled the deposition of bioinks as continuous gradient (Idaszek et al. 2019). Moreover, Feng et al. increased the inlets of microfluidic chip to three and also added rotating motor to substrate for dispensing heterogenous filaments in different printing path directions (Feng et al. 2019).

Liu et al. developed capillary-based microfluidic printhead for the multimaterial bioprinting of tissue constructs, which holds major differences than microfluidic chip-based printheads (W. Liu et al. 2017). In this system, each of the bioink reservoirs are connected to the distinct capillaries bundled together and bioinks are individually or simultaneously ejected from different capillaries in a continuous manner (Figure 1.3(c)) (W. Liu et al. 2017; Zhou et al. 2018). There is no contact in between the bioinks till the end of single printhead with multiple capillaries which avoids intermixing of bioinks. Rocca et al. further optimized the developed capillary-based microfluidic printhead for embedded multimaterial bioprinting (Rocca et al. 2018).

1.3.4. Laser-Based Multimaterial Bioprinting

In conventional SLA-based bioprinting technique, UV light cures a photosensitive bioink in a layer-by-layer approach by tracing the two-dimensional (2D) cross-sections of the 3D construct in each layer. This was improved by pattern projection technique in which UV light was projected through masks enabling the polymerization of whole 2D cross-section in one exposure for each layer. Pattern projection was further advanced by employing digital micro-mirror device (DMD) chip made up of millions of mechanically adjustable micro-mirrors as a dynamic photo-mask (Y. Lu et al. 2006; Han et al. 2010; Soman et al. 2013). Digital light processing (DLP) technology employs DMD chips for bioprinting. Both SLA-based and DMD-based bioprinting techniques enable multimaterial and multicellular patterning of heterogenous constructs (Chan et al. 2010; Zhu et al. 2015; X. Ma et al. 2016). Multimaterial bioprinting is achieved by sequentially delivering input bioinks into the platform and photo-crosslinking layer-by-layer with the directed UV light. Ma et al. provided a comprehensive demonstration of this type of multimaterial bioprinting through employing DMD-based 3D bioprinting platform for the fabrication of *in vitro* triculture hepatic model (X. Ma et al. 2016). In their work,

hexagonal liver lobule architecture with multiple cell types was fabricated by sequential patterning of two bioink formulations encapsulated with human induced pluripotent stem cell (hiPSC)-derived hepatic cells and supporting endothelial and mesenchymal cells. Further, Miri et al. developed a stereolithographic multimaterial bioprinting platform by incorporating bioink switching capability to DMD-based bioprinters (Figure 1.3(d)) (Miri et al. 2018). In their bioprinting platform, bioinks with multiple cell types were flowed through a microfluidic chip with pneumatic valves for material switching and then patterned via layer-by-layer photo-crosslinking.

LIFT technology enables patterning of small volume of materials with high resolution and speed by focusing laser pulse to ribbon to eject material droplets onto receiving substrate (Antoshin et al. 2019). Barron et al. developed a LIFT-based bioprinting system for the deposition of biological materials and also proposed that multicellular patterning could be achieved in this technique by designing a donor slide with multiple-wells or with separated areas for different cell types (Barron et al. 2004). In their work, multiple cell types were deposited in the immediate vicinity to each other by employing a donor slide with multiple-wells. Initial attempts on LIFT-based bioprinting technique relied on the deposition of single type of cells in 3D (Barron et al. 2004; Othon et al. 2008) or patterning of multiple cell types in 2D (Guillotin et al. 2010; Koch et al. 2009), however multimaterial and multicellular 3D heterogeneous constructs have also been generated with further developments in the bioprinting technique (Figure 1.3(e)) (Gruene et al. 2011; Koch et al. 2012; Sorkio et al. 2018).

1.1.Multimaterial Bioprinting of Vascular Tissues

In this section of the thesis, the implementation of multimaterial bioprinting approaches explained above were elaborated on the fabrication of hollow vascular constructs. These multimaterial bioprinting applications overwhelm the inadequacies of current tissue engineering techniques from different perspectives by enabling construction of anatomically-correct, multi-layered and multicellular vascular tissues.

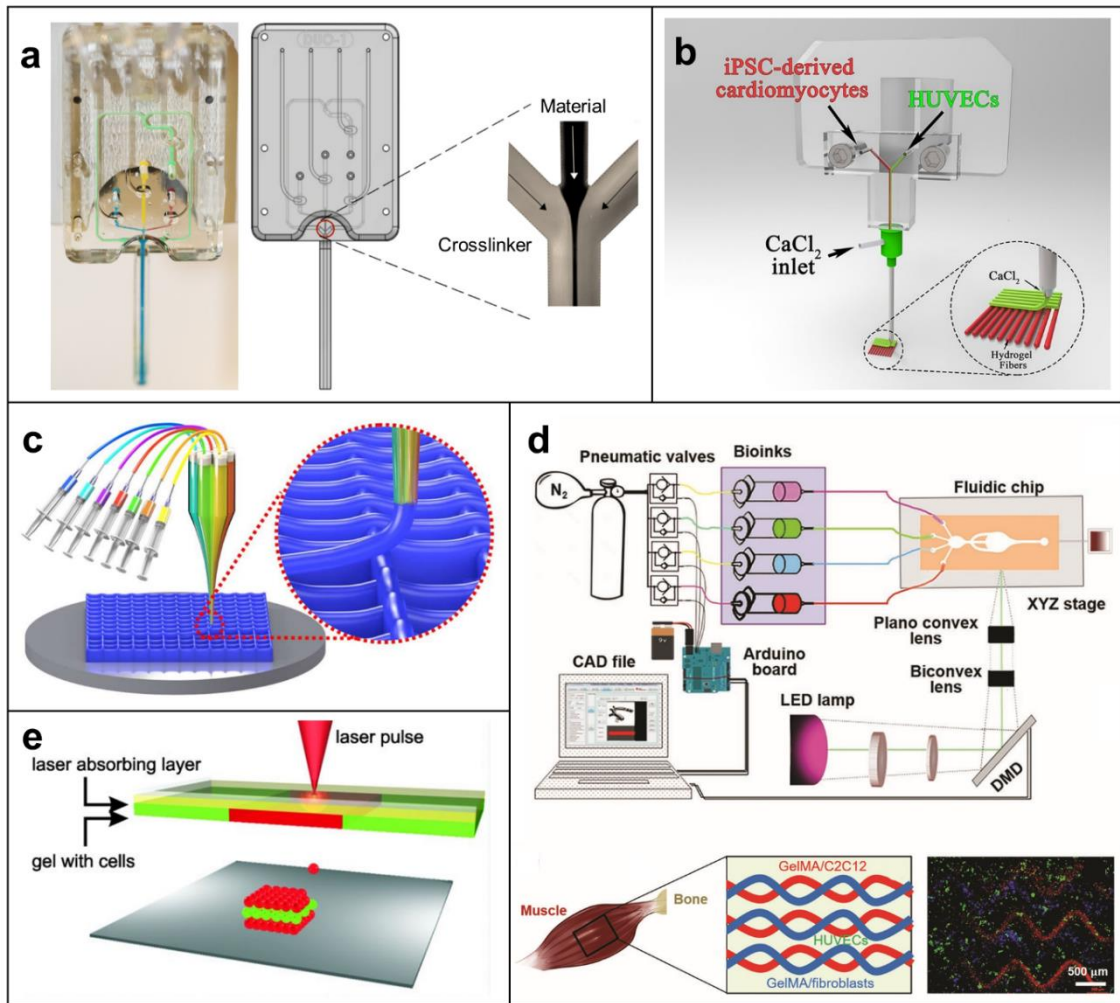


Figure 1.3 Different biofabrication platforms employing microfluidic and laser-based multimaterial bioprinting approaches: **a)** Microfluidic printhead with on-the-fly multimaterial switching capability. Reproduced/adapted with permission from Ref. (Dickman et al. 2020). Copyright 2019, FASEB. **b)** Combination of coaxial needles with microfluidic chips, where bioink solutions are delivered from the microfluidic printhead and then crosslinked by CaCl_2 supplied from the coaxial needle. Reproduced/adapted with permission from Ref. (Maiullari et al. 2018). Copyright 2018, Springer Nature. **c)** Capillary-based microfluidic printhead, in which bioinks are flowed through separate capillaries without any contact with each other till the end of the nozzle. Reproduced/adapted with permission from Ref. (Zhou et al. 2018). Copyright 2018, American Chemical Society. **d)** Setup of DMD-based, microfluidics-enabled multimaterial bioprinting platform (up) and a skeletal muscle model fabricated with this platform (bottom). Reproduced/adapted with permission from Ref. (Miri et al. 2018). Copyright 2018, WILEY-VCH Verlag GmbH & Co. KGaA, Weinheim. **e)** LIFT setups

also include multimaterial bioprinting capability. Reproduced/adapted with permission from Ref. (Koch et al. 2012). Copyright 2012, Wiley Periodicals

Multimaterial bioprinting oriented vascular tissue fabrication strategies are categorized into scaffold-based and scaffold-free multimaterial bioprinting approaches. The basis of scaffold-based multimaterial bioprinting depends on the use of supporting biodegradable polymers or hydrogels resembling the biological and mechanical characteristics of target tissue until cells get mature. Whereas in scaffold-free approaches, neo-tissues are formed from the cells and then bioprinted without any exogenous material (Bakirci et al. 2017).

1.1.1. Scaffold-Based Multimaterial Bioprinting Approaches

Various scaffold-based multimaterial bioprinting techniques have been administered for the recapitulation of zonally stratified, multicellular and concentric arrangement of natural blood vessels. Tan et al. achieved fabrication of concentric and self-supporting tubular structure via multi-head multimaterial bioprinting strategy based on EBB in both printheads (E. Y. S. Tan and Yeong 2015). In the study, first printhead was used to extrude alginate-xanthan gum hydrogel blend in circular pattern and secondary printhead was programmed to extrude crosslinker solution into inner-side of the printed circular pattern to provide mechanical stability and to optimize tube wall properties. Study of Campbell et al. further integrated a single printhead equipped with selector valve to switch between separate syringe pumps of multi-head multimaterial bioprinting platform (Campbell et al. 2015). By this modification, various hydrogels were extruded sequentially within a controlled manner, which could allow multilayered and heterocellular arrangement of multiple types of materials and cells in a vascular tube complexity. Viscous, pre-crosslinked alginate-collagen blends loaded with different cells were prepared as bioink and extruded from the printhead sequentially. A ring of endothelial cell laden bioink was deposited, which was further surrounded by a ring of smooth muscle cell laden bioink.

Coaxial multimaterial bioprinting techniques have been broadly utilized for the biofabrication of vascular constructs as the design of the bioprinting system perfectly complies with the concentric layer arrangement of blood vessels. Ozbolat and colleagues demonstrated the first application of coaxial bioprinting for the manufacture of vessel-

like tubular microchannels (Yu et al. 2013b) and further implemented the technique for the fabrication of vascular tissue (Y. Zhang et al. 2015). They followed a vascular design by co-axial extrusion where human umbilical vein smooth muscle cells (HUVSMCs) encapsulated alginate was flowed through outer channel of the coaxial nozzle, while crosslinker solution was dispensed from inner channel. Together with providing structural integrity, the engineered vascular conduit also enabled fluid transport through the lumen (Y. Zhang et al. 2015). In another study, Dolati et al. included carbon nanotubes into bioink dispensed from outer channel for the mechanical reinforcement of fabricated vascular conduit (Dolati et al. 2014). Further, in addition to the delivery of the crosslinker from inner channel, Jia et al. enrolled crosslinker spraying from outer side to enhance temporal stability of the construct during the manufacturing process (Jia et al. 2016). In their work, a blend bioink encapsulated with human umbilical vein endothelial cells (HUVECs) and human mesenchymal stem cells (MSCs) were ionically crosslinked from both inner and outer surfaces during bioprinting and photo-crosslinked after printing procedure.

Coaxial multimaterial bioprinting technique requires immediate gelation of the bioink after extrusion for the maintenance of shape fidelity, which makes alginate a typically employed hydrogel due to its quick ionic crosslinking. However, lack of binding sites in alginate for the attachment and migration of cells hinders the biofunctionality of engineered vascular tissues. In this regard, various biomaterials have been employed as a bioink or combined with alginate, including GelMA (Jia et al. 2016; Pi et al. 2018), tyramine-modified gelatin (Hong et al. 2019), collagen (J. He et al. 2018) and decellularized extracellular matrices (dECM) (G. Gao et al. 2017). Gao et al. combined vascular-tissue-derived dECM with alginate as a bioink and further loaded with endothelial progenitor cells (EPCs) and proangiogenic drug to engineer blood vessels that can treat the ischemic injuries (G. Gao et al. 2017). In the study, while an alginate-based hybrid bioink was flowed through outer tube, CaCl₂ containing Pluronic F127 (CPF127) was dispensed from inner tube for establishing the gelation via Ca²⁺ release of CaCl₂ and for supporting the lumen of tubular structure via Pluronic F127, which could be removed after providing enough mechanical strength. In a similar work, Gao et al. further utilized the designed dECM-based bioink for *in vitro* modeling of blood vessel (G. Gao et al. 2018). In their work, perfusable and biofunctional vascular model was generated by coaxial bioprinting of HUVEC-laden bioink and fugitive CPF127 onto a perfusion

platform, which was previously 3D printed by another printhead. In their following study, they mimicked multilayered and concentric arrangement of native vascular tissue by modifying a triple-coaxial bioprinting (Figure 1.4(a)) (G. Gao et al. 2019). The constructed vascular structure was functional enough that endothelial cells-laden layer of the engineered vascular graft inhibited thrombosis, smooth muscle cells-laden outer layer exhibited contraction for withstanding blood pressure.

Coaxial multimaterial bioprinting technique was further advanced by dispensing coaxially extruded bioinks onto a rotating rod. Quing Gao et al. provided comprehensive demonstration of this multimaterial bioprinting technique for biomanufacturing of vascular constructs with macro- and micro-channels (Q. Gao et al. 2017). In the study, smooth muscle cells and fibroblasts encapsulated within alginate were sequentially dispensed from outer channels of two separate coaxial printheads along the rotating rod (Figure 1.4(b)). Upon the fusion of nearby hollow filaments, a macrochannel formed in the middle after removing the rod and two microfilaments formed due to dispensing bioinks from coaxial printheads. After obtaining two-layered tubular structure, collagen was injected into the macrochannel for supporting the adhesion of endothelial cells, HUVECs were seeded onto collagen. Tubular structure printed with this technique exhibited more consistent geometry compared to the tubular structure fabricated through dispensing of hollow filaments in circular pattern along the vertical direction (Q. Gao et al. 2015). Biofabricated vessel-like structure also demonstrated sufficient mechanical strength and cellular viability. Jang et al. also performed similar studies in which bioinks were dispensed onto rotating rod either in cross-striped form or in helical form for biofabrication of artificial blood vessels (K. W. Lee et al. 2018; Jang et al. 2020). While biodegradable PCL was deposited into first and third layer, cell-laden alginate was dispensed as second layer from another nozzle. It should be noted that even though techniques employing rotating rod enable biofabrication of multi-layered and self-supporting tubular structures, geometry and arrangement of printed structure depend on the shape of rotating rod.

Microfluidic multimaterial bioprinting techniques have also been utilized for the biofabrication of vascular constructs (R Attalla, Ling, and Selvaganapathy 2016; Rana Attalla et al. 2018). Attalla et al. engineered tubular constructs with hierarchical architecture by depositing various viscous hydrogels from a microfluidic multi-axial

printhead (Rana Attalla et al. 2018). In the study, cell-laden bioinks and the crosslinker solution were flowed from the needles with different gauges inside the microfluidic chip and dispensed from the nozzle in a concentric arrangement. Further, Zhou et al. bioprinted a vessel-like tubular construct by employing capillary-based microfluidic printhead (Zhou et al. 2018). Cell-laden alginate was delivered from six outer channels of the multi-barrel capillary nozzle and CaCl_2 was delivered from the central channel to crosslink the bioink solution and to create a lumen. It is also noteworthy to mention the study of Feng et al. as the developed multicomponent bioprinting system holds great potential for the biofabrication of artificial vessels (Feng et al. 2019). In their work, two alginate-based bioinks encapsulated with HUVECs and embryonic rat cardiomyocytes were extruded from the coaxial microfluidic printhead onto rotating substrate which enabled the layer-by-layer fabrication of concentric ring structure.

Schöneberg et al. revealed the potential of DBB for the biofabrication of stratified, heterocellular and functional vascular channels (Figure 1.4(c)) (Schöneberg et al. 2018). In their approach, first of all, sacrificial rod made up of endothelial cell-laden gelatin was printed from the first printhead. Next, thrombin crosslinker solution from the second printhead and SMCs-laden fibrinogen from the third printhead were sequentially deposited onto the sacrificial rod until fully covering the rod surface. Further, fibroblast-laden collagen and fibrinogen blend was casted onto the printed structure. Following the dissolution of sacrificial rod, hollow vascular structure consisting of a single endothelial layer mimicking the tunica intima, SMCs deposited layer mimicking the tunica media and a fibroblast casted layer mimicking the tunica adventitia was fabricated. The engineered perfusable vascular model reproduced the physiological functions of the native tissue.

Even though laser-based platforms possess highest resolution and highest cell viability compared to other bioprinting modalities, current applications on vascular tissue fabrication are generally limited with the deposition of single type of hydrogel encapsulated with single type of cell, which is not adequate to recapitulate multilayered and multicellular structure of native vessels. A limited number of works has exploited printing capabilities of laser-based bioprinting modalities for multimaterial bioprinting of vascular constructs. Wu et al. designed a branched vascular architecture by depositing HUVECs from a laser-based bioprinter onto hydrogel surface (P. K. Wu and Ringeisen 2010). Deposited endothelial cells formed interconnections with each other, however

branched architecture exhibited poor stability. For this reason, HUVSMCs were deposited onto the HUVEC layer. Guillotin et al. also demonstrated the potential of laser-based platforms for the biofabrication of stratified and heterocellular constructs (Guillotin et al. 2010).

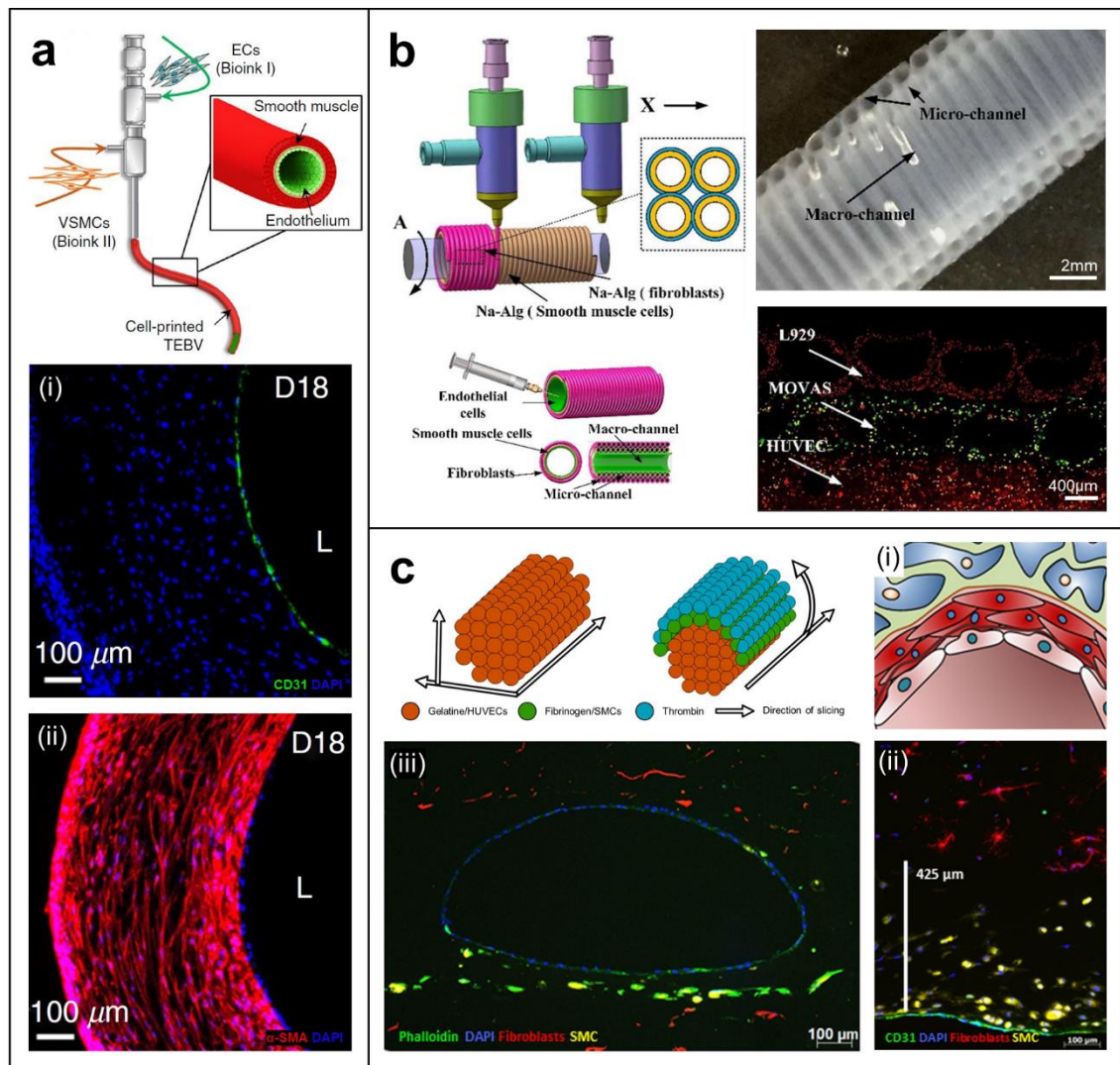


Figure 1.4 Scaffold-based multimaterial bioprinting approaches enable the fabrication of multilayered and concentric vascular tissue analogs with functionality by depositing cells within exogenous materials. **a)** Coaxial multimaterial bioprinting of vascular construct with endothelial and muscular layers by dispensing Pluronic F127 from inner channel (core), endothelial cell-laden bioink from middle channel and SMC-laden bioink from outer channel of triple coaxial nozzle. Following the *in vitro* remodeling process that include incubation, and static culture and pulsatile conditioning, fabricated vascular construct exhibited (i) intact monolayer formation in endothelial cell layer and (ii) circumferentially-oriented SMCs at muscular layer at day 18. Reproduced/adapted

with permission from Ref. (G. Gao et al. 2019). Copyright 2019, AIP Publishing. **b)** Biofabrication of vascular construct with micro- and macro-channels by co-axially extruding SMC-laden and fibroblast-laden bioinks onto a rotating rod, followed by the delivery of endothelial cells into the lumen. (i) Longitudinal section of the fabricated construct clearly demonstrates the presence of multi-level channels. (ii) Confocal imaging showed distribution of three different cell types and presence of apparent micro-channels within the vessel-like construct. Reproduced/adapted with permission from Ref. (Q. Gao et al. 2017). Copyright 2017, American Chemical Society. **c)** Multimaterial bioprinting of a multilayered vascular model by employing droplet-based printheads. Cell-laden gelatin was deposited to manufacture sacrificial rod, which was followed by deposition of SMC-laden fibrinogen and thrombin solutions from two droplet-based printheads onto the fabricated sacrificial rod. Further, a fibrinogen loaded bioink formulation was casted onto the printed structure. (i) Schematic cross section of the vascular model illustrating single layer of endothelial cells and a SMC layer. (ii) Fluorescence microscopy image after seven days dynamic cultivation, demonstrating the combination of endothelial layer and the muscular layer, where SMCs distributed close to the lumen. (iii) Cross-sectional fluorescence micrograph of multilayered vascular model after 4 days dynamic culture, exhibiting the localization of endothelial cells in the inner wall that was encircled by SMCs and fibroblasts. Reproduced/adapted with permission from Ref. (Schöneberg et al. 2018). Copyright 2018, Springer Nature

1.1.2. Scaffold-Free Multimaterial Bioprinting Approaches

Exogenous scaffolds have been broadly utilized in many tissue engineering strategies since the beginning of the tissue engineering field as they provide temporary support for the growth of the cells and even further deliver biological and mechanical cues for guiding the growth. However, scaffold-based tissue engineering approaches also face with challenges originating from the scaffolds such as undesirable host reactions, necrosis due to limited diffusion of oxygen and nutrients, mechanical mismatch between the biomaterial and the native tissue. For this reason, scaffold-free approaches have been implemented for the engineering of vascular constructs. Scaffold-free bioprinting applications have also been performed and further equipped with multimaterial bioprinting tools (Ozler et al. 2017).

Forgacs and colleagues provide a comprehensive demonstration of scaffold-free multimaterial bioprinting for the biofabrication of multilayered and multicellular vascular tubes (Figure 1.5(a)) (Norotte et al. 2009). In the study, both multicellular spheroids and multicellular cylinders were utilized as building blocks. For the bioprinting of vascular tubes, one of the printheads deposited agarose rods to be used as molding template and the other printhead extruded either multicellular spheroid or cylinder in a pre-programmed pattern. Deposition of molding template together with building blocks enabled the fabrication of vascular constructs with accurate dimension and geometries. Following the fusion of multicellular building blocks, supporting agarose rods were removed. Various vascular tubes were fabricated in linear and bifurcated geometries. Further, double-layered vascular tissue with inner layer (composed of HUVMSCs cylinders) and outer layer (composed of human dermal fibroblast (HDF) cylinders) was fabricated which replicates structural arrangement of tunica media and tunica adventitia of native blood vessels.

Tan et al. developed another scaffold-free biofabrication technology to promote fusion of tissue or cell spheroids by printing alginate mold (Y. Tan et al. 2014). In their work, alginate micro-droplets were deposited onto the calcium-containing gelatin substrate layer-by-layer to print alginate mold, which was followed by robotically dispensing tissue spheroids made up of smooth muscle cells and endothelial cells into the ring-shaped alginate mold. Together with showing the possibility of the developed technology, results also revealed the role of cell-secreted collagen type I on cell-to-cell adhesion and tissue maturation.

Kucukgul et al. proposed an algorithmic model for the generation of biomimetic and self-supporting macrovascular constructs (Figure 1.5(b)) (Kucukgul et al. 2015). In the study, scaffold-free bioprinting of aortic tissue constructs was conducted based on medical images of real human aorta and by the capillary-based extrusion of mouse embryonic fibroblast (MEF) aggregates and agarose support structures from two separate printheads according to the developed toolpath planning.

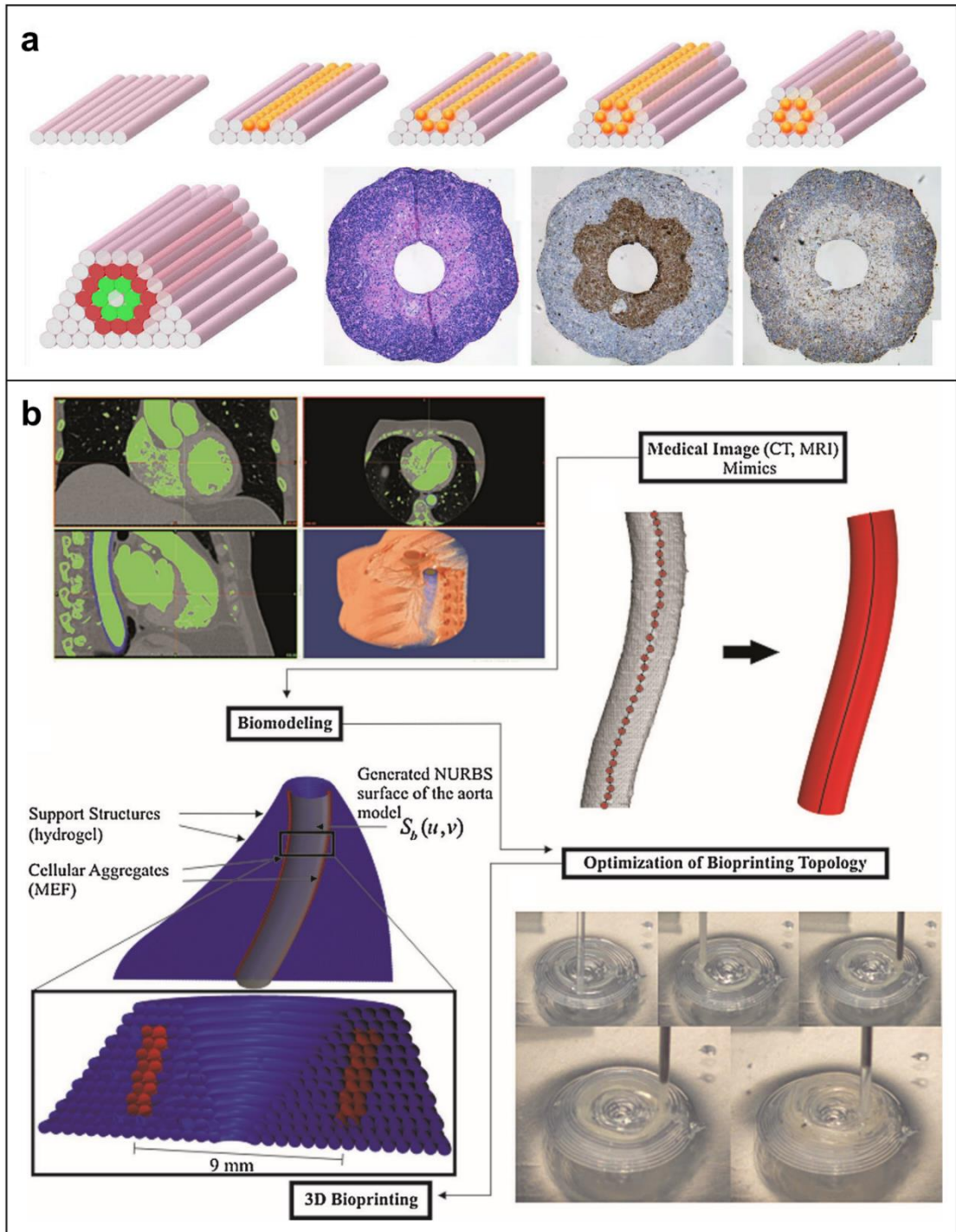


Figure 1.5 Scaffold-free multimaterial bioprinting approaches allow fabrication of vascular constructs by dispensing cells without encapsulating them within any exogenous material. **a)** Step-by-step illustration of scaffold-free multimaterial bioprinting, where agarose rods and multicellular aggregates extruded from different printheads are deposited layer-by-layer (up). Fabrication of multilayered vascular construct by assembling HUVMSC and HSF multicellular cylinders in pre-determined pattern. While HUVMSC cylinders form inner layer, HSF cylinders form outer layer of

vascular construct which may also be identified in histological examinations (bottom). Reproduced/adapted with permission from Ref. (Norotte et al. 2009). Copyright 2009, Elsevier. **b)** Roadmap for scaffold-free multimaterial bioprinting of biomimetic and self-supporting macrovascular constructs by employing algorithmic model developed by Kucukgul et al. Reproduced/adapted with permission from Ref. (Kucukgul et al. 2015). Copyright 2014, Wiley Periodicals

1.2. Multimaterial Bioprinting of Vascularized Tissues

3D printing technology allows the fabrication of architecturally and biologically relevant tissue structures, but the main concern arises afterwards to maintain survival, maturation and development of the fabricated structures over a prolonged time and to make them eligible for *in vivo* transplantation. Delivery of necessary nutrients especially oxygen has an essential role for the maintenance. However, the diffusion of nutrients and oxygen through the tissues is limited to approximately 200 μm distance, thus microchannels are introduced to the structures to be located in close proximity to the cells and biological factors to provide better diffusion of oxygen, nutrients and removal of wastes in conventional tissue engineering strategies. The fabrication of vascularized tissue structures resembling native tissues is now possible by employing multimaterial bioprinting technologies. Deposition of sacrificial materials is one of the commonly preferred strategies to obtain vascular channels. The sacrificial materials have reversible gelation property like alginate, gelatin and Pluronic F127, which can be removed for the formation of open lumens (V. K. Lee, Lanzi, et al. 2014; V. K. Lee, Kim, et al. 2014; S. Yang et al. 2020; N. K. Singh et al. 2020). The generated microchannels are decorated with the endothelium by perfusion of endothelial cells or by encapsulation of endothelial cells within the sacrificial bioink.

The attempts for the fabrication of vascularized heterogeneous structures have been demonstrated by using various multimaterial bioprinting approaches incorporate microfluidic and coaxial bioprinting, multi-head 3D bioprinting systems or dual printing platforms. Among them, coaxial multimaterial bioprinting is practical and commonly employed to manufacture the constructs containing stacked perfusable tubular networks.

The lumen is commonly supported with sacrificial fugitive bioink to provide physical support during bioprinting until sufficient crosslinking is provided to the inner wall of the vessel, then which is washed out (V. K. Lee, Lanzi, et al. 2014; V. K. Lee, Kim, et al. 2014; Cui et al. 2019; D. Kang et al. 2020; Qin et al. 2020). The sacrificial fugitive ink can be supplemented with the crosslinker to increase mechanical strength of the inner wall of vascular structure (D. Kang et al. 2020; Qin et al. 2020). In addition, endothelial cells can be encapsulated into these sacrificial materials to mature an endothelial layer at the inner wall (Cui et al. 2019). The development of all-in-one coaxial nozzle or microfluidic coupled systems have enabled fabrication of vascularized heterogeneous structures by using a single nozzle system (Colosi et al. 2016; Shao et al. 2020; N. K. Singh et al. 2020). For example, Shao et al. designed a two-in-one coaxial bioprinting system (Shao et al. 2020). Gelatin was utilized as the sacrificial material extruded from the inner channel of the coaxial nozzle while cell-laden GelMA was separately and simultaneously printed from the outer channel of the coaxial nozzle and irreversibly photocrosslinked. Afterwards gelatin was dissolved, and endothelial cells encapsulated within the gelatin were released and adhered to the inner wall of the vascular structure. A heterogeneous structure with two different components was successfully constructed by sequentially switching the different bioinks. Depending on the encapsulated cell-types in GelMA, this approach was suggested to be used for the construction of different vascularized tissue models larger than one cm scale.

A triple coaxial nozzle bioprinting system was used for the construction of perfusable renal tubular tissue in another study (N. K. Singh et al. 2020). Functional hybrid hydrogel composed of kidney dECM and alginate was used to encapsulate either renal proximal tubular epithelial cells or ECs and simultaneously extruded to the outer or inner layer of the tubular structure, respectively. Pluronic F127 containing CaCl_2 was used as fugitive sacrificial material extruded to support the lumen and to provide adequate crosslinking for alginate. The continuous hollow tubular structures were bioprinted in mono- or bi-layered-wall structures by using on/off tunable feature of the coaxial nozzle system (Figure 1.6) and then the Pluronic F127 was washed out from the lumen. Due to the capability of bioprinting monolayer and bilayer structures with desired intervals, a realistic renal proximal tube structure could be constructed which was revealed by the expression of functional marker proteins, and successful integration with the host tissues

in vivo. These results have demonstrated the capability of fabricated perfusable renal tubular tissue to be used in regenerative medicine.

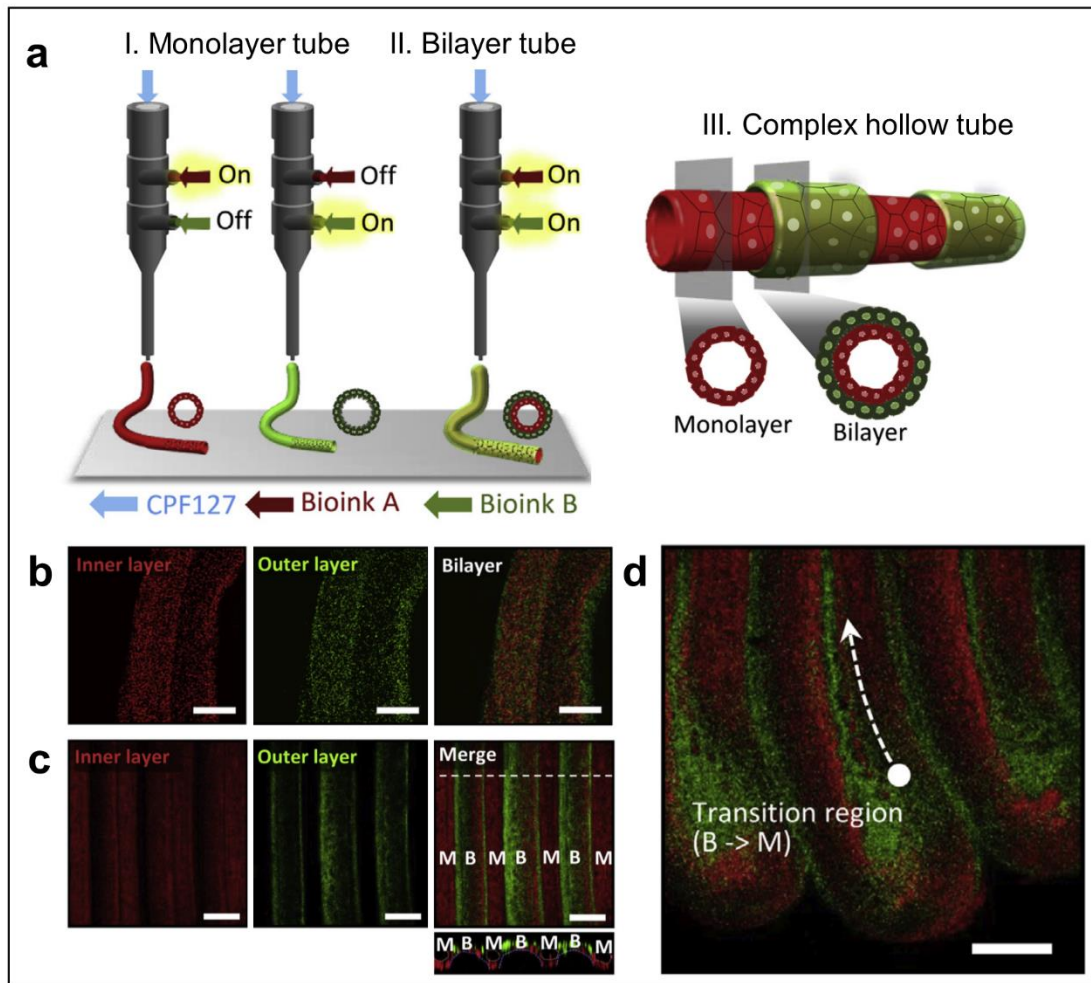


Figure 1.6 Vascularized tissue biofabrication through coaxial multimaterial bioprinting. **a)** Schematic diagram of microfluidic co-axial nozzle system for monolayer (M), bilayer (B) and complex hollow tube bioprinting and representative views. **b)** Confocal images of bilayered hollow tube, **c)** complex hollow tube with monolayer and bilayer structures and **d)** their transitional region. Inner and outer shells were demonstrated with red and green fluorescent beads embedded in the ink, respectively. Copyright 2019, with permission from Elsevier. Readapted from Ref. (N. K. Singh et al. 2020)

There are other biological designs for coaxial nozzle extrusion systems without utilizing a sacrificial material. A vascularized muscle construct was fabricated by simultaneously printing muscle cells encapsulated by skeletal muscle dECM from the inner core of the coaxial nozzle while endothelial cells-laden vascular dECM were extruded to the outer

shell (Y.-J. Choi et al. 2019). The design allowed the formation of pre-vascularized muscle structures, and showed functional recovery with integration within the host tissue and muscle regeneration. In another study, the complex anatomical structure of an intestinal villi model with blood capillaries was established by simultaneous extrusion of HUVEC cells from the core region of coaxial nozzle and Caco-2 human colon epithelial cells from the shell region in a collagen matrix (W. Kim and Kim 2018). To mimic biological and physical properties of the villus structure, the design of first two layers before coaxial bioprinting was as follows: HUVEC containing bioink was bioprinted in a flat mesh structure in the first layer and Caco-2 containing bioink was deposited to the second layer. In the complete bioprinted construct, Caco-2 cells were differentiated and enhanced the barrier function, which would be suggested as promising platform for the organ-on-a-chip systems or human intestine regeneration.

Multi-head multimaterial bioprinting platforms have also been systematically used to manufacture vascularized, perfusable and heterogeneous tissue constructs at clinically relevant volumes. First studies were based on rapid prototyping with double-nozzle assembling printing technique (S. Li et al. 2009). The control over printing parameters allowed fabrication of adipose-derived stromal cells (ADSC) laden gelatin/alginate/fibrinogen bioink in a vascular-like network which was surrounded by hepatocyte laden gelatin/alginate/chitosan bioink in a mesh-like structure. The process was followed by layer-by-layer deposition, where the nozzles were switched at each layer. The bioprinting parameters did not affect the cellular viability and functionality of hepatocytes, and ADSCs were successfully differentiated to endothelial-like structure. The development of liver like construct was achieved, which was suggested as a promising technology for drug screening systems.

ECs are commonly used for the endothelialization of larger perfusable channels or for the formation of capillaries in the bioprinted constructs, but it is difficult to maintain their viability in hypoxic conditions (V. K. Lee, Lanzi, et al. 2014; V. K. Lee, Kim, et al. 2014; W. Liu et al. 2017). Embedded microchannels are commonly built by the inclusion of sacrificial fibrous structures between the layers of bioprinted structure, which can be evacuated after the structure is strengthened enough while ECs can be introduced into the bioinks to form capillaries that would grow toward larger vessels. However, ECs cannot maintain their viability in larger structures and mostly undergo apoptotic or necrotic cell

death. It was reported that the presence of MSCs in close proximity supported and stabilized ECs for neovasculature (Gaebel, Furlani, et al. 2011). LIFT-based multimaterial bioprinting technique was utilized to deposit ECs and MSCs on a Polyester urethane urea (PEUU) cardiac patch to enhance angiogenesis and cardiac regeneration (Gaebel, Ma, et al. 2011). ECs were patterned in a mesh-like structure, subsequently where MSCs were printed with 150 μm gap-distance in a square shape within ECs mesh structure. The design and strategy for the biofabrication resulted in the formation of pre-vascularized patches, which showed enhanced angiogenesis and improvement at the infarcted hearts after in vivo transplantation.

Some approaches do not need a sacrificial material to build perfusable channels based on the computational design and the control over the printing technology. For example, DLP technology was employed to construct vascularized network in a shorter time (Zhu et al. 2017). As previously mentioned, this technology utilizes a micromirror array device to project the dictated the pattern on the digital mask to the fabrication state. A mixture of photopolymerizable glycidyl methacrylate-hyaluronic acid and GelMA encapsulating ECs and fibroblast cells solution was used to fabricate designed microchannels while GelMA was used to fabricate base layer. UV light was reflected with a pre-designed pattern while unpolymerized parts are washed away. This technology promises the fabrication of vascularized large tissue constructs in a high resolution with easy modification of bioink compositions with various multi-materials without influencing cell viability.

Lewis' group is the first that developed a custom-made 3D bioprinter with more than two independently controllable printheads to construct wholly functional, scalable and vascularized tissue structures (Kolesky et al. 2014). Since then, several multi-head multimaterial bioprinting systems have been implemented for the construction of various functional and vascularized tissue structures such as bone, cartilage, skeletal muscle and proximal tubule of kidney, within a particular architectural design (Kolesky et al. 2014; H.-W. Kang et al. 2016; Kolesky et al. 2016; Yi et al. 2019). These systems have enabled the extrusion of different types of inks such as hydrogels, fugitives and elastomers. For example, PDMS, Pluronic F127 and two different GelMA bioinks were separately loaded to the four separate printheads for the following purposes: PDMS was used to print the borders to surround the printed construct; Pluronic F127 was used as a fugitive sacrificial

material for the formation of embedded microchannels; GelMA was used to encapsulate the green or red fluorescence expressing fibroblast cells and to provide ECM like microenvironment. GelMA and Pluronic F127 were co-printed in multilayers at 20-22 °C while pure GelMA was used to encapsulate the bioprinted cell laden-GelMA and Pluronic F127. After photopolymerization of GelMA, the temperature was decreased to liquefy and evacuate the Pluronic F127 from the microchannels of the construct. Then, ECs were injected through the microchannels under mild shaking conditions for endothelization. The processes yielded in the fabrication of vascularized heterogeneous tissue constructs with high resolution and shape fidelity, and cell viability. In their other study, a vascularized bone structure was fabricated by using multiple bioinks composed of hMSC, HUVEC and human neonatal dermal fibroblasts (HNDF) encapsulated separately within gelatin–fibrinogen hydrogel and by using PDMS to construct a 3D perfusion chip (Kolesky et al. 2016). After fabrication of the perfusion chip, cell-laden bioinks and Pluronic F127 as sacrificial material were printed onto the chip and encapsulated with ECM via casting. The biofabrication workflow was as follows: The hMSCs were bioprinted in a special geometry intervening in- and out-of-plane of fugitive ink. HUVEC-laden bioink was bioprinted in a line for ultimate branched vascular network formation. The HNDF cells laden ECM bioink was casted in the interstitial space in order to support the hMSC and HUVEC. The bioink was crosslinked enzymatically with thrombin and transglutaminase (TG) and fugitive ink was evacuated with the same procedure indicated in their previous study. Perfusion of osteogenic differentiation factors through the vascular network induced osteogenic tissue formation (determined by alkaline phosphatase expression and mineral deposition) after 30 days. It was reported that fibroblasts were used as model cells that surrounded the heterogeneously patterned stem cells and vascular network which can be replaced with other cell types like support cells (e.g., immune cells or pericytes) or tissue-specific cells (e.g., hepatocytes, neurons, or islets) in future studies.

With the understanding of the multimaterial bioprinting principle, investigations proceed with the development of constructs in different areas. Li et al. developed a microfluidic-based chip for glioblastoma (GBM) cancer model using multi-head bioprinting system with a similar approach (Yi et al. 2019). Three individual printheads were loaded with silicone, brain-derived decellularized ECM (BdECM) bioinks separately laden with HUVECs and GBM cells. After printing of a silicone chamber, HUVEC-laden bioink was

printed in a ring shape followed by the deposition of GBM-laden bioink that filling inside the ring shape. The gelation of the bioink was provided by incubating in humidified cell culture incubator, and culture medium was perfused through the silicon chamber. It was found that GBM cancer model exhibited pathological features and showed high sensitivity against potential drugs when tested in the chips constructed with the dECM from different patients. The presented personalized GBM cancer model would help to identify patient specific drugs for the efficient treatment. In another study, a personalized thick, vascularized and perfusable cardiac patch was constructed by using multi-head extrusion based 3D bioprinting platform (Noor et al. 2019). By using the patient's own cells, it was aimed to develop a personalized treatment by eliminating the immunological response. The ECM-based bioink was prepared by decellularization of human omental tissues, which was used to encapsulate induced pluripotent stem cells (iPSCs)-derived cardiomyocytes (CMs) and ECs to demonstrate the ability to reprogram the patient's own cells. Like a sandwich model, a crisscross geometry was used to print two lower layers of patch using CMs laden bioink. After printing the third layer with omentum hydrogel, ECs were deposited within sacrificial gelatin bioink to provide a vascular network. The extrusion of CMs laden omentum bioink was followed with the continuous two layers in crisscross model. A support medium (gelatin slurry) was used to show the printability of the complex and volumetric anatomical structures (Figure 1.7). A small-scale human heart structure with major blood vessels was bioprinted using two distinct bioinks laden with Cy5-prestained CMs or RFP-expressing ECs. After removal of support medium, an integrated heart structure with robust and mechanically stable perfusable vessels was obtained.

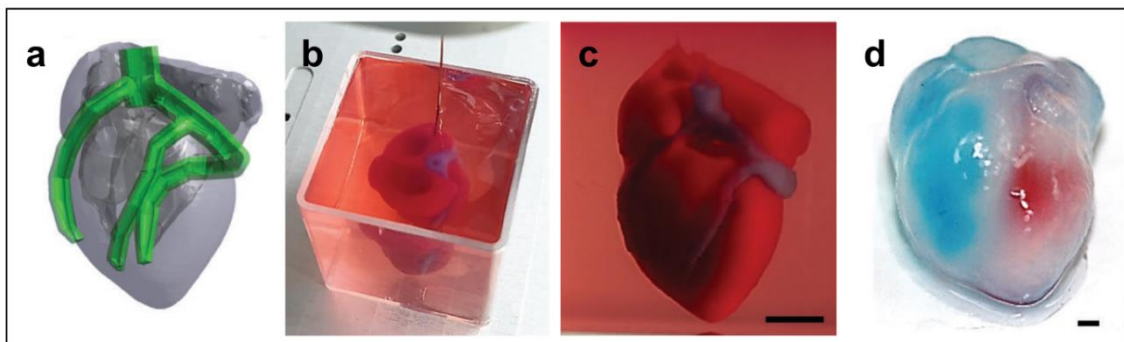


Figure 1.7 Printability of multiple materials in a support medium using multi-printheads. **a)** computer-aided design (CAD) model for human heart, **b)** printed heart within a support bath, **c)** after removal of support medium and **d)** after perfusion of red

and blue dyes. Copyright 2019, The Authors. Published by WILEY-VCH Verlag GmbH & Co. KGaA, Weinheim. Reused from Ref. (Noor et al. 2019)

Dual 3D printing systems incorporating multiple bioprinting strategies are also used to construct scalable vascularized structures (Cui et al. 2016; B. S. Kim et al. 2019; S. Yang et al. 2020; Cui et al. 2019). For example, Cui et al utilized a 3D dual-printing system involving extrusion-based and SLA-based platforms and applied an integrated bio-architectural design to construct vascularized bone construct by alternately patterning PLA fibers and cell-laden GelMA bioink (Cui et al. 2016). PLA fibers were printed in a honeycombed pore structure modified with bone morphological protein (BMP2) and then ECs and hMSCs loaded, VEGF modified GelMA was deposited to promote regional osteogenesis and angiogenesis. Spatial localization of the biofactors and physical porous structure in a controlled manner and the followed four weeks perfusion of the structure facilitated the formation of interconnected vascularized channels in bone construct. In a similar study, PCL and cell-laden PEGDA bioink was printed alternatively layer-by-layer to construct an integrated soft to hard multi-phasic hybrid construct with a vascular conduit using melt mediated extrusion (MME) and SLA techniques (Shanjani et al. 2015). The MME at high temperature did not affect the viability of cells encapsulated within PEGDA bioink and provided mechanical support to the construct. The conduit provided enough diffusion of media to the cells, which help to sustain their viability. In another study, a full-thickness vascularized skin tissue model was constructed layer-by-layer by employing multiple printing strategies including extrusion, and inkjet bioprinting (B. S. Kim et al. 2019). The biofabrication process is schematically illustrated in Figure 1.8. First, a PCL porous transwell system was fabricated using extrusion printing. The pores of the transwell were filled with sacrificial gelatin hydrogel to prevent their blockage with the diffusion of the subsequently printed bioink in the following layer. A PCL mesh structure with 100 μm pores was printed on top of the transwell, which was followed with the extrusion bioprinting of the bioink composed of fibrinogen and adipose-derived dECM that was encapsulated with human adipocytes and pre-adipocytes to mimic hypodermis layer. Since vascularization occurs between dermis and hypodermis layers of skin tissue, in the next layer, endothelial cells encapsulated within thrombin containing gelatin in a cylindrical shape. Thrombin was employed to irreversibly crosslink the fibrinogen while endothelialized vascular channels formation was targeted with thermal assisted evacuation of gelatin from the hypodermis layer. In the following layer, fibroblast

cells were extruded in skin-dECM and fibrinogen containing bioink. Meanwhile, thrombin solution was sprayed and temperature was increased to 30°C to provide enough crosslinking of fibrinogen and collagen, respectively, and to integrate hypodermis and dermis layers. The construct was matured for 7-day incubation facilitated with the incubation with multiple culture medium. After maturation, keratinocytes were placed to the last layer by the aid of inkjet bioprinter. The formation of vascularized channels between dermis and hypodermis layers helped to the maturation of epidermis layer with almost human skin-like structure.

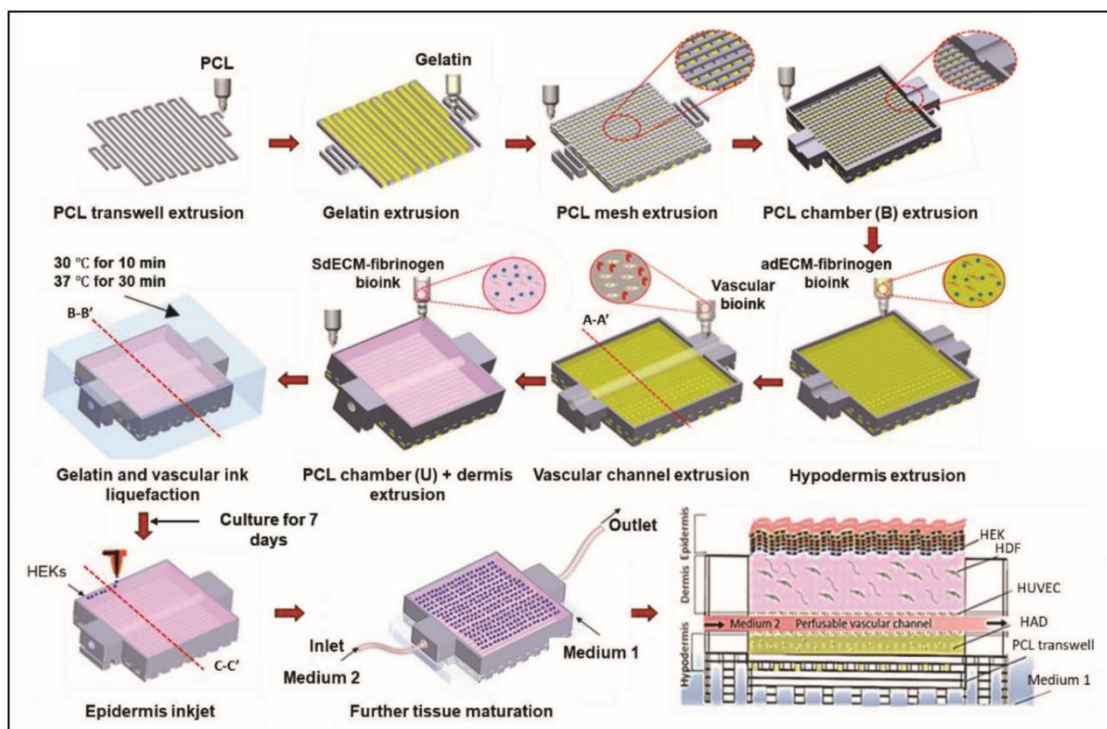


Figure 1.8 Dual bioprinting platform. Schematic diagram exhibiting step-by-step fabrication process using EBB and inkjet bioprinting technologies to generate full-thickness skin model. Copyright 2018, WILEY-VCH Verlag GmbH & Co. KGaA, Weinheim. Reused from Ref. (B. S. Kim et al. 2019)

A vasculature was sandwiched into a thick tissue by a dual bioprinting platform employing coaxial extrusion and stereolithography by Cui et al (Cui et al. 2019). First, a thick vascular construct was bioprinted by extrusion of human coronary artery smooth muscle cells-laden catechol modified GelMA (GelMA/C) bioink from the outer channel of coaxial nozzle while HUVECs laden Pluronic F127 sacrificial ink was simultaneously extruded from the inner channel in a grid pattern. Sodium periodate was also included in

the Pluronic F127 to crosslink the inner layer of GelMA/C. Pluronic F127 was removed by using their thermoreversible characteristic and released HUVEC adhered to the inner surface of the channels. SLA bioprinter was used to deposit MSC-laden GelMA for covering printed vasculature structure. The bioprinted vascular construct showed biomimetic properties with the biomechanics, perfusability and permeability to the surroundings.

As different than other approaches, Byambaa et al. utilized a capillary-based extrusion bioprinting approach to manufacture the vascularized bone structure by sequentially aspirating and depositing bioink with different multimaterial components (Byambaa et al. 2017). A gradient structure with perfusable microchannel was constructed within a hollow architectural design using distinct bioink compositions including GelMA and VEGF modified GelMA encapsulating HUVEC and MSCs (Figure 1.9(a)). In another study, a pre-set cartilage system was used to construct vascularized hepatic lobule (D. Kang et al. 2020). The cartridge was designed with three separate channels for extrusion of hepatocyte-laden bioink, EC laden bioink and sacrificial biomaterial such that the final structure resembled complex human hepatic lobule structure (D. Kang et al. 2018). A precursor cartridge was prepared as follows: Alginate was used as sacrificial material to build a microchannel at central vein of hepatic lobule while a high density of ECs laden bioink was positioned at the lumen or exterior surface with an interconnection to mimic the sinusoid network (Figure 1.9(b)). The gap between exterior surface and lumen was filled with the bioink including high density of hepatic cells for the formation of liver cords. The alginate was washed out, and the final structural outcome was preserved structural integrity with a lumen. The larger size vascularized hepatic lobe structures were generated by layer-by-layer deposition of the multiple precursor cartridges. The constructs showed hepatic cell functions by secretion of albumin and urea at higher levels.

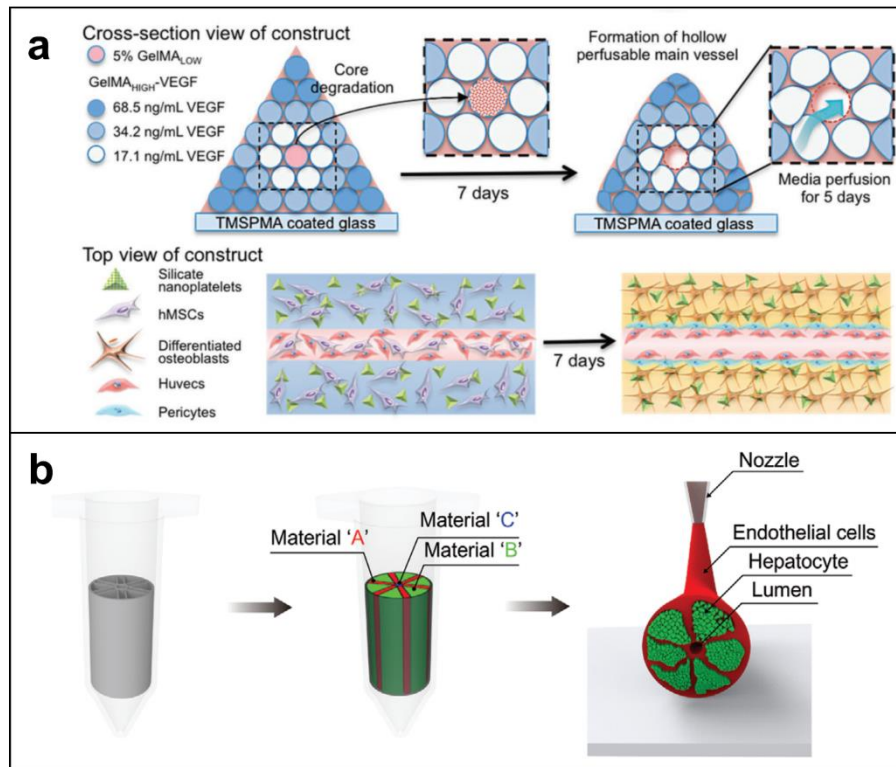


Figure 1.9 Capillary based and preset extrusion-based multimaterial bioprinting systems for vascularized tissue biofabrication. **a)** Capillary (Copyright 2017, WILEY-VCH Verlag GmbH & Co. KGaA, Weinheim. Reused from Ref. (Byambaa et al. 2017)) and **b)** preset extrusion (Copyright 2020, WILEY-VCH Verlag GmbH & Co. KGaA, Weinheim. Reused from Ref. (D. Kang et al. 2020)) based multimaterial bioprinting to generate vascularized tissues.

2. EXPERIMENTAL

2.1. Design and Development of Embedded Multimaterial Bioprinting Platform

2.1.1. A General Overview on the Embedded Multimaterial Bioprinting Platform

For the biofabrication of zonally stratified vascular constructs, microfluidic multimaterial bioprinting approach incorporating a multiple-channel microfluidic printhead was combined with the embedded bioprinting technique which includes deposition of bioinks into a support bath.

Within this framework, backbone of the multimaterial printhead was fabricated, which was further equipped with three hydrogels reservoirs, connection parts and pulled multi-barrel microcapillary nozzle. Each of the bioinks coming from different reservoirs are connected to the separate solenoid valves that enable flowing of the bioinks through the microcapillaries and simultaneously or alternatively deposition from the single nozzle. Depending on the both arrangement of microchannels in the microfluidic system design and actuation adjustments of the pumps, distinct bioinks can be extruded separately or mixed together. Motion of three axis and open/close commanding of solenoid valves were controlled through the G-code and M-code. Tool path generation was specifically conducted for the fabrication of vascular-like constructs incorporating multiple layers with varying compositions. Simultaneously or alternatively extruded bioinks were deposited into hydrogel-nanoclay based support bath which enabled the biomanufacturing of geometrically complex constructs that is not possible through in-air bioprinting of precursor solutions.

2.1.2. Development of Multiple-Channel Microfluidic Multimaterial Printhead

2.1.2.1. CAD modelling and fabrication of multimaterial printhead backbone

Recapitulation of multilayered and multicellular organization of native tissues requires the biofabrication of tissue substitutes with different layers exhibiting distinct characteristics. Starting from this point of view, a multimaterial printhead harboring three hydrogel reservoirs was designed. Figure 2.1 illustrates both CAD modelling of the backbone of the multimaterial printhead and fabricated end product. Multimaterial printhead backbone was made up of three parts: main part which enables mounting of the multimaterial printhead onto the gantry system, support part which was included for increasing the stability of the main part and sliding part which allows positioning and immobilization of the connection in between flexible needle and microcapillary nozzle.

Backbone of the multimaterial printhead was designed and realized in a way that three hydrogels reservoirs will be located onto the backbone. While upper and lower parts of the multimaterial printhead backbone immobilizes the hydrogel reservoirs, screws positioned to the sides of each of the hydrogel reservoirs further fastened the reservoirs from slippage. Connection in between each of the hydrogel reservoirs and microchannels of the pulled multi-barrel capillaries was provided by flexible needles. While one side of the flexible needle assembles to the hydrogel reservoir through Luer lock system, other side of the flexible needle was fixed with the puller capillary by the designed slider part. Slider part was designed with the aim of holding connection section of the flexible needles to the pulled microcapillaries tight and also for the positioning of this connection section at the desired position. Slider part was mounted to the main part of the backbone through two screws.

CAD model of the multimaterial printhead backbone was developed in Rhinoceros 6 (Robert McNeel & Associates, USA) and then converted into stereolithography file. The exported file was sectioned and transformed into G-code in Ultimaker Cura (Ultimaker, Cambridge, MA, US). The designed and sliced multimaterial printhead backbone model was manufactured from Ultimaker-2 (Ultimaker, Cambridge, MA, US) 3D printer.

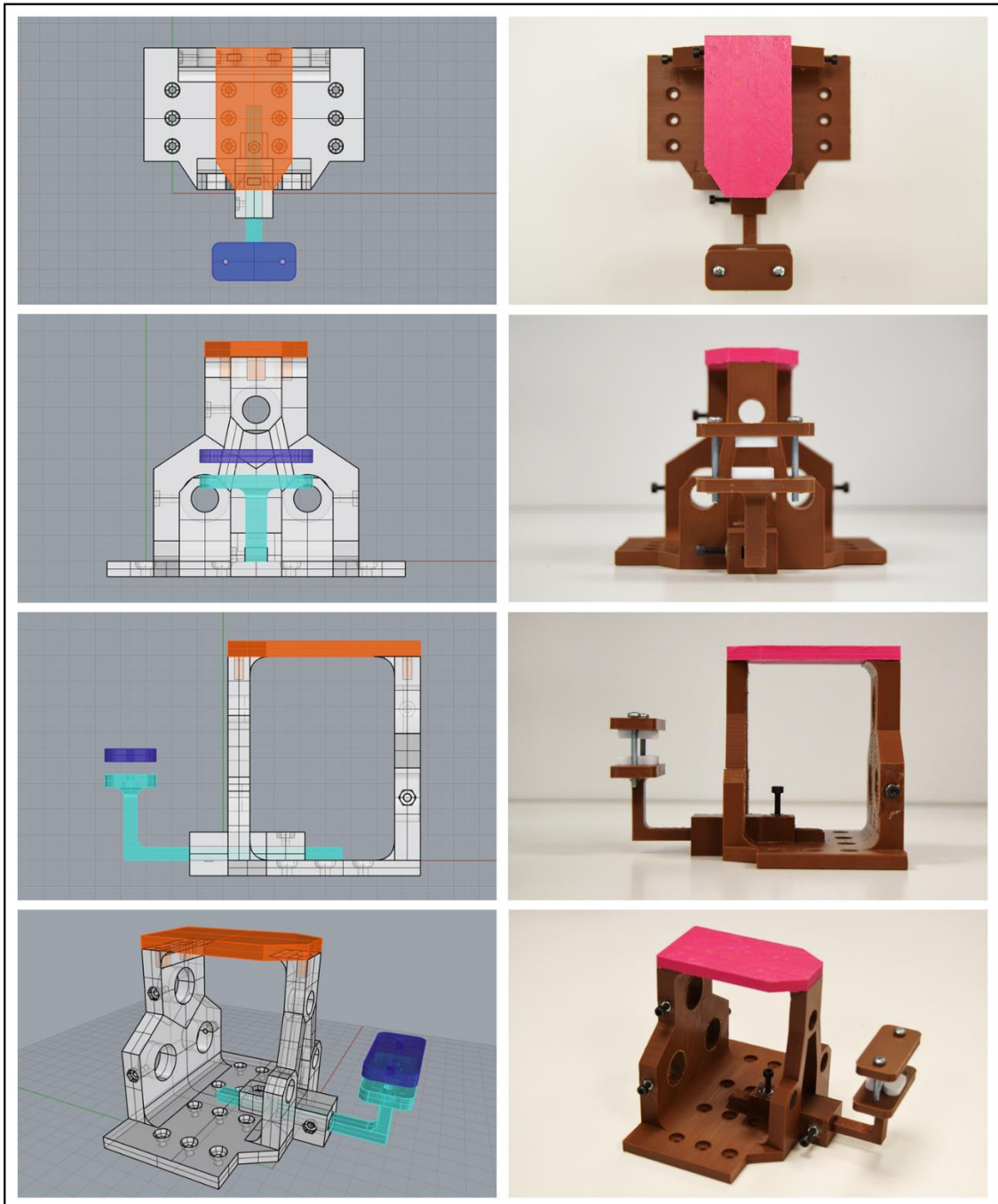


Figure 2.1 Top, front, right and perspective views of the modelled (left) and fabricated (right) multimaterial printhead backbone from top to bottom, respectively. Main part, supporting part and sliding part of the multimaterial printhead backbone were respectively illustrated in light gray, orange and blue colors in the designed CAD model.

2.1.2.2. Multi-barrel microcapillary pulling

To enable the extrusion of three different bioinks simultaneously or alternatively for the fabrication of zonally stratified vascular-like constructs, a multiple channel multimaterial nozzle was designed and fabricated by employing multi-barrel microcapillaries. The nozzle was fabricated by pulling three-barrel microcapillaries in Sutter P-97 Pipette Puller and then scoring the pulled microcapillaries from the desired point. Figure 2.2 illustrates the pulling procedure of a multi-barrel microcapillary within pipette puller and the inverted microscope image of the pulled microcapillary. Pulled three-barrel microcapillaries were scored in a way that inner diameters of each of the three channels are in compliance with the layer thickness of the targeted vascular construct. For instance, for the biofabrication of vascular construct that has layer thicknesses which are the multiples of $200\mu\text{m}$, then multi-barrel capillary was scored such that inner diameter of each capillary will have $200\mu\text{m}$. Each three channels of the pulled and scored microcapillary were fitted with three different flexible needles which provide connection in between the hydrogel reservoirs and the microcapillary nozzle.

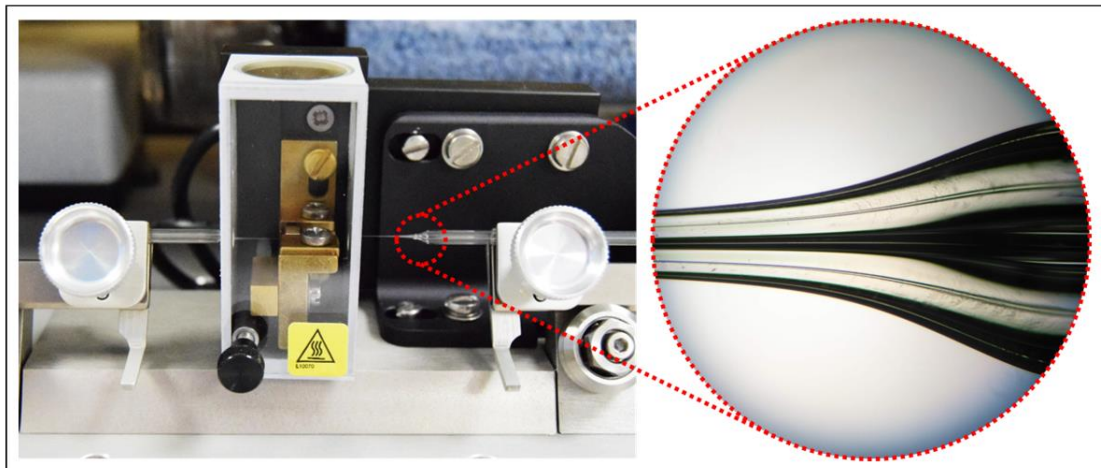


Figure 2.2 Multi-barrel microcapillary pulling for the fabrication of multiple channel microfluidic nozzle. Microcapillary pulling device (left) and 4X magnified inverted microscope image of the pulled multi-barrel microcapillary (right)

2.1.2.3. Construction of Multiple-Channel Microfluidic Multimaterial Printhead And Assembly of Multimaterial Bioprinting Platform Components

A custom-design three axes 3D bioprinter controlled by a motion controller software was modified for multimaterial bioprinting purposes. Solenoid valve control units were included into motion controller panel and multimaterial printhead setup was mounted onto the z-axes of the custom-design gantry system.

Three different bioink solutions were loaded into separate 10 mL material reservoirs which were positioned within the previously described multimaterial printhead backbone. These three separate hydrogel reservoirs were equipped with the three-channeled microcapillary nozzle by having connection through distinct flexible needles (Silkann filling cannula, 22G 70mm).

Material extrusion from the multiple-channel microfluidic multimaterial printhead (Figure 2.3) was provided through three pneumatic dispensing units (Nordson EFD Performus V). Three separate solenoid valves were assembled in between the material reservoirs and the pneumatic dispensing units for controlling open/close states of the pneumatic driving forces. Addition of solenoid valves into the multimaterial bioprinting platform and control of them through the developed M-codes have enabled the simultaneous or alternatively delivery of the different bioink formulations. By this means, multimaterial bioprinting of any multimaterial and multicellular structures having complex geometries might be conducted.

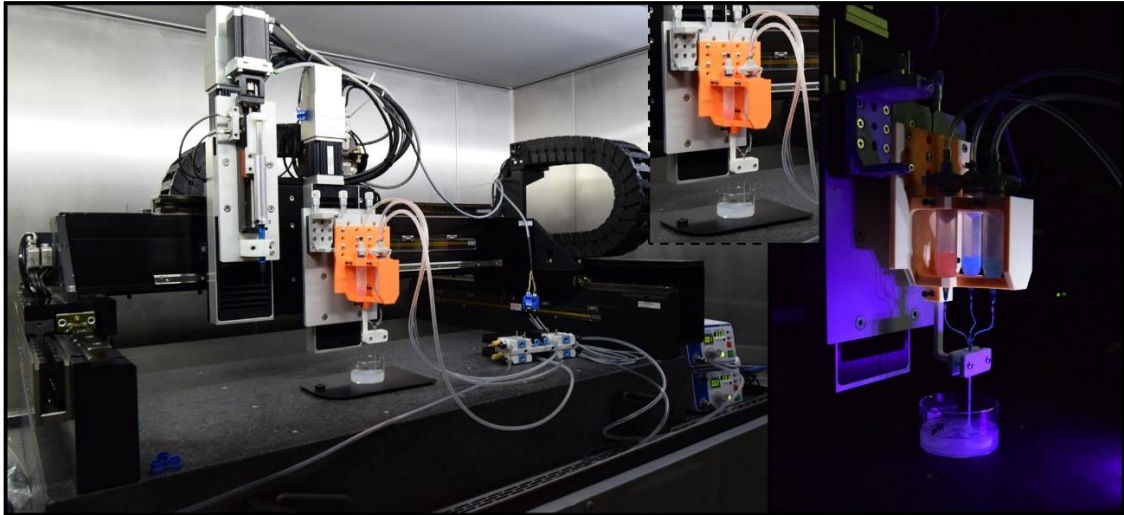


Figure 2.3 Embedded multimaterial bioprinting platform (left) and microfluidic multiple-channel multimaterial printhead (middle and right).

2.2. Preparation and Characterization of Nanoclay-Hydrogel Composite Support-Bath

2.2.1. Preparation of PF-RDS Support-Bath and Characterization

PF-RDS support-bath was prepared by slowly adding equal volume of PF-CaCl₂ (Sigma Aldrich) solution into Laponite RDS (BYK Additives & Instruments) suspension. Briefly, PF solutions with 15%, 20% and 25% concentrations were prepared by dissolving in 0.5, 1 or 2% (w/v) CaCl₂ solution at cold room (4°C) under continuous stirring. A 6% Laponite-RDS solution was prepared by suspending appropriate amount of dry Laponite-RDS powder in deionized (DI) water and vigorously stirring for minimum one hour at room temperature to allow fully exfoliation and dispersion of nanoclay particles with a transparent appearance (Jin et al. 2017; Nelson and Cosgrove 2004). Then, PF solution was added slowly into Laponite-RDS solution under continuous stirring at 4 °C to obtain final concentrations of 7.5, 10 and 12.5% for PF and 0.25, 0.5 and 1% of CaCl₂ with constant Laponite concentration of 3%. The mixture was further stirred for minimum one hour at 4 °C. The composite material was centrifuged at 4000 rpm for 3 min prior to incubation at 37 °C to remove the bubbles. It is worth to mention that final 2% of Laponite was also prepared and examined but the electrical repulsive forces were not enough to

make an ordered array of particles. Hence, the matrix storage and recovery was not appropriate for printing (Sakairi, Kobayashi, and Adachi 2005; Gaharwar et al. 2019; Sheikhi et al. 2018) and it was omitted from further experiments (data not shown). The composite material was stable and could be stored at 4 °C for a long time with no changes in its properties (K. Sun and Raghavan 2010). Based on rheological data, 3 % of Laponite-RDS, 10 % of PF, and 0.5% of CaCl₂ concentrations were selected for the support bath formulation.

2.2.2. Rheological Measurements

All rheological characterizations were performed on a MCR302 (Anton Paar, Austria) equipped with a Peltier plate for temperature control. A stainless steel parallel plate of 25 mm diameter with a gap distance of 0.5 mm was utilized for all the experiments. A low viscosity silicon oil was used as the solvent trap during the measurements. Rotational and oscillatory measurements were performed to investigate the flow and viscoelastic behavior of the support-baths. Gel yield stresses and linear viscoelastic (LVE) regions were measured by strain sweep from 0.01-100% at a constant angular frequency of 10 rad/s. Oscillatory angular frequency sweeps were carried out within the LVE range (0.6% strain and angular frequency of 0.1-100 rad/s) to monitor the dynamic rheological behavior. Temperature sweep experiments were conducted from 4-37 °C with 5 °C/min ramp to observe gelation temperature and evolution of the structure's moduli. To investigate the recovery behavior of the support-bath during hydrogel extrusion, cyclic strain test at low and high oscillatory strains of 0.6 and 50% at constant angular frequency of 10 rad/s and 10 s duration per cycle was performed. Shear rate sweeps were conducted to monitor the shear thinning behavior and viscosity changes of the formulations between 0.01-100 1/s.

Samples were incubated at 37 °C for 2 h with a pre-shear rate of 1/s prior to each run. Three measurements were taken for each sample and mean values were reported. The effect of different compositions of PF and CaCl₂ on flow behavior of the support material was investigated. Control groups were selected as CaCl₂-PF named as Control 1 and CaCl₂-Laponite RDS named as Control 2 with different concentrations of CaCl₂. Control 1 contained 10 and 1% for PF and CaCl₂, respectively to observe the effect of Laponite

on rheological properties. Control 2 were included constant Laponite-RDS of 3% and 0.125, 0.25, 0.5, and 1% of CaCl₂.

2.2.3. CAD Design of Complex Structures and 3D Printing Inside Support-Bath

A customized three axes 3D bioprinter controlled by MACH3 software (Newfangled Solutions) was used to print different structures. Hydrogel solution was loaded into a 10 mL material reservoir equipped with a double thread screwed plastic nozzle (Musashi Engineering, Japan) and material extrusion from the printing head was provided through a pneumatic dispensing unit (Nordson EFD Performus V). CAD models of the constructs were developed in Rhinoceros 6 (Robert McNeel & Associates, USA) and tool paths were generated and transformed into G-codes.

Star shape, grid pattern and branched vascular-like, and a nose shape structure in different scales were printed using 3% (w/v) sodium alginate (Sigma Aldrich) solution prepared in DI water. Star and grid-pattern structures were printed with a 25 Gauge nozzle and vascular-like and nose shape were fabricated via a 23 Gauge nozzle. For star shape printing, 15 layers of hydrogels were deposited by setting parameters as 140 mm/min print speed and 0.7 bar feeding pressure. The structure was formed by depositing two concentric contours without any gap in between them. The grid shape of 0-90° zig-zag 10 × 10 mm² deposition pattern including 9 stripes with 750 μm gap in between was extruded in each layer with 140 mm/min print speed and 0.7 bar feeding pressure. Branched vascular-like construct was printed at 150 mm/min print speed and 0.6 bar feeding pressure. Nose shape structure was printed with 2.7 cm length and 1.7 cm width using a 25 Gauge nozzle at 130 mm/min print speed and 0.5 bar feeding pressure by three offsetted counters.

Prior to support-bath removal, the structures were post-crosslinked in a 2% CaCl₂ solution for 10 min. Then, residual support-bath materials were removed from the beakers by pipetting 1% cold NaCl solution. To show the presence of lumen inside the structure and impermeability and its interconnectivity, diffusion test was performed by delivering blue food dye solution from one end of the branched vascular structure.

2.2.4. Bioprinting of Cell-Laden Alginate in PF-RDS Support-Bath

All components of support-bath and alginate were sterilized by autoclaving. Dry powder of PF was sterilized at 105 °C for 30 min as suggested in the previous study to prevent rheological property changes (Burak et al. 2018). CaCl₂ and Laponite-RDS were also autoclaved in their powder forms. Then, the support-bath was prepared as explained above. Alginate solution was prepared in 3% (w/v) concentration in 1×PBS and autoclaved at 121°C for 15 min before encapsulating the cells.

NIH-3T3 cells (ATCC) were grown in Dulbecco's Modified Eagle Medium (DMEM, Sigma) supplemented with 10% fetal bovine serum (FBS, Sigma) and 1% penicillin-streptomycin (Gibco) at humidified atmosphere containing 5% CO₂ at 37 °C. The cells with a 1×10⁶ cells/mL density were prepared by suspension in 3% alginate solution at room temperature. A 0.5 bar pressure was applied to extrude cell-laden hydrogel from a 30 Gauge nozzle with 150 mm/min print speed. After printing, the alginate structures were washed with 1% ice-cold NaCl solution and DMEM. They were placed into 12 well-plate with fresh DMEM and incubated at the incubator.

2.2.5. Evaluation of In-Gel Bioprinting Biocompatibility

The viability of 3T3 cells-encapsulated in the alginate was evaluated on Day 1, Day 3, and Day 7 after bioprinting. At the end of incubation points, the samples were transferred into glass bottom Petri dishes and washed with 1×PBS. Calcein AM/PI staining was used to evaluate live/dead cells. Briefly, cells were first stained with 1 μM Calcein-AM (Invitrogen, green fluorescence) for 30 min and then, with 0.75 μM propidium iodide (Invitrogen, red fluorescence) for 5 min in 1×PBS at 37 °C, followed by washing in 1×PBS for three times. The viable cells were monitored with maximum excitation/emission wavelengths of 488/515 nm, respectively while the dead cells were monitored at maximum excitation/emission wavelengths of 561/625 nm, respectively, using inverted confocal microscope (Carl Zeiss LSM 710). 3D images were obtained

using tiled z stacks with 5.00 μm intervals and 2.77 μm pixel size. The live/dead cells were analyzed quantitatively by using ImageJ 1.48v software.

2.2.6. Statistical Analysis

All values for cell viability and rheological assessments are presented as the mean \pm SD (n=3). P Students *t*-test was used to analyze the significant difference. P values <0.05 and <0.01 are considered statistically significant.

2.3. Preparation and Characterization of Alginate-GelMA Blend Bioink

Alginate has been frequently employed as a bioink solution in variety of bioprinting applications due to its biocompatibility, fast ionic crosslinking kinetics and affordability. However, lack of binding sites in alginate for the attachment and migration of cells hinders the biofunctionality of engineered vascular tissues. In this regard, various biomaterials have been employed as a bioink or combined with alginate, including GelMA (Jia et al. 2016; Pi et al. 2018), tyramine-modified gelatin (Hong et al. 2019), collagen (J. He et al. 2018) and decellularized extracellular matrices (dECM) (G. Gao et al. 2017).

Among different hydrogels, GelMA has distinctive properties. Biological motifs, especially arginine-glycine-aspartic acid (RGD) peptide sequence, present within the GelMA hydrogel promote attachment and proliferation of almost all types of cells. RGD peptide sequence allows the attachment of cells to the GelMA network and further maintenance of the biological processes. Hydrogels that will be utilized as bioink solution should also bear biodegradability for promoting healing process of the body. Matrix metalloproteinase (MMP) regions within the GelMA are recognized by the cells as enzymatic degradation sites. Following the encapsulation of cells within the native cells inside GelMA hydrogels, cells start synthesizing their own ECM and degrade GelMA network. Another characteristic that highlights GelMA among other hydrogel candidates

is the adjustability of viscosity and mechanical properties of the bioink solution by changing the degree of functionalization (DoF).

Together with functioning as a thermoreversible polymer, GelMA also behaves as a thermoset polymer following the covalent crosslinking. Another property of GelMA comes from the heterogeneity of the gelatin in molecular level. Due to its heterogeneity in molecular level, seeding different types of cells within GelMA turns this hydrogel into a single structure harboring various cellular micro-environments. By this way, GelMA becomes an ideal material that has different strength and ductility degrees which can mimic *in vivo* conditions in a better way compared to other hydrogels. Another reason which makes GelMA as a typically utilized bioink material is the ability to fabricate constructs with complex shapes. Integration of GelMA hydrogel into additive manufacturing has enabled the biomanufacturing of intricate 3D structures which can also promote development of cells inside.

2.3.1. Methacrylated Gelatin Synthesis

GelMA is a semi-synthetic polymer which is obtained by modifying natural polymer gelatin with methacrylate groups. GelMA is synthesized through the reaction of amine groups of lysine amino acids within the gelatin with the methacrylic anhydride inside phosphate buffered saline (PBS) at 50°C (Van Den Bulcke et al. 2000). Figure 2.4 demonstrates the schematic illustration of GelMA synthesis.

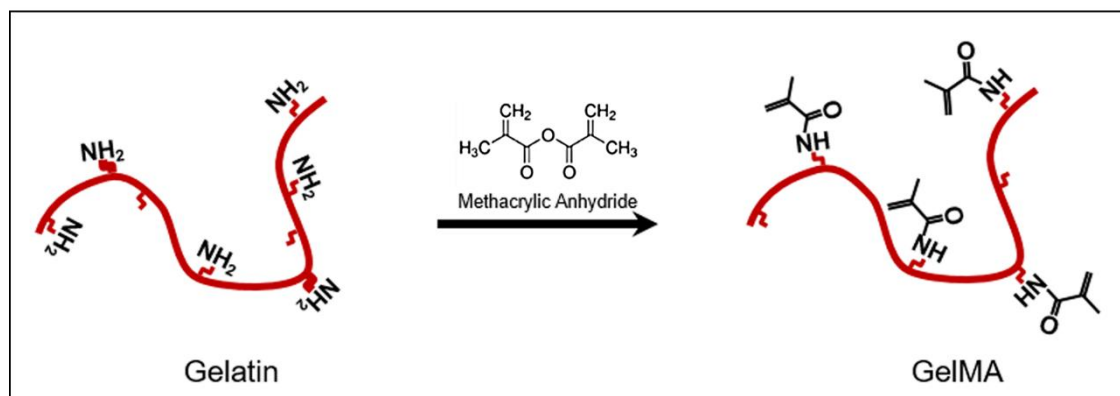


Figure 2.4 Synthesis of GelMA by the addition of methacrylate groups to the gelatin. Reproduced under the terms of the Creative Commons CC-BY 4.0 License

(<https://creativecommons.org/licenses/by/4.0/>) from Ref. (Yoon et al. 2016). Copyright 2016, Yoon et al.

Synthesis of methacrylated gelatin was performed according to the protocol previously explained in elsewhere (Loessner et al. 2016). Briefly, 10% (w/v) gelatin solution was prepared by dissolving gelatin type A (Sigma Aldrich) within PBS at 60°C and stirring until the solution becomes completely transparent. Following the preparation of gelatin-PBS solution, methacrylic anhydrite (MA, Sigma Aldrich) was added into solution drop by drop under hood. To be able to obtain high methacrylation degree, 0.6g of MA was added per 1g of gelatin. Without having a contact with air, the prepared solution was stirred for three hours to continue the modification reaction. After three hours of stirring, the solution homogeneously turned into opaque. As an alternative to mass ratio between gelatin and MA, stirring time can also be increased to increase the methacrylation degree of the modification reaction. Following the stirring of the solution, centrifugation at 3500 rpm was performed for 3 minutes to remove MA that did not react with the gelatin. To terminate the modification reaction, supernatant solution was diluted by adding PBS twice volume of supernatant solution at 40°C. Following the termination of the modification reaction, the solution was transferred into 12-14 kDa dialysis membranes (Sigma Aldrich) and dialyzed within distilled water for one week. GelMA solution's pH value was set to 7.4 by adding 1M sodium bicarbonate (Sigma Aldrich) for the elimination of materials that may cause impurity. As a last step of synthesis, GelMA solution was lyophilized. In this regard, GelMA solution was transferred into 50mL falcon tubes and stored at -80°C for one day. Following the storage of GelMA solutions at refrigerator, lyophilization was performed for three days at freeze-dryer. Dried GelMA samples were stored at -20°C until use (Loessner et al. 2016).

2.3.2. Characterization of Synthesized Methacrylated Gelatin and Determination of Degree of Functionalization

Modification of GelMA and its degree of functionalization was investigated by proton nuclear magnetic resonance (¹H NMR) spectroscopy. Before measurement, gelatin and lyophilized GelMA was dissolved inside deuterium oxide, D₂O (30 mg / ml) at 40°C. ¹H NMR measurements were performed at 40 °C by using 500 MHz Varian Inova (Varian

Inc., Palo Alto, CA, USA) spectrometer. Degree of methacrylation of GelMA was determined by utilizing MestreNova NMR analysis software (version 6.0.2, Mestrelabs Research).

2.3.3. Preparation of Alginate-GelMA Blend Bioink

As previously mentioned, alginate has been utilized as a commonly used bioink due to several reasons and was also selected as the precursor solution for the experiments performed for investigating the printability of complex constructs inside the developed support bath. To reinforce biological functionality of bioink solution that was employed for the vascular tissue bioprinting studies, synthesized GelMA was included into the bioink formulation.

While hydrogel formation of alginate involves physical crosslinking through ionic interaction in between sodium alginate and calcium ions, formation of hydrophilic and water-insoluble networks from GelMA incorporates chemical crosslinking through free-radical photopolymerization. Alginate, a seaweed derived natural polysaccharide, is made up of α -D-mannuronic acid and β -D-guluronic acid and polymer chains are formed through ionic crosslinking of the carboxylate groups of the guluronate groups in the presence of divalent cations such as Ca^{+2} and Mg^{+2} (Burdick and Stevens 2005). As illustrated in Figure 2.5, GelMA hydrogel was yielded by chemical crosslinking through exposure to 365nm UV light in the presence of photoinitiator. In all of the experiments incorporating GelMA, 2-hydroxy-1-[4 (hydroxyethoxy)phenyl]-2-methyl-1-propanone photoinitiator solution (Irgacure 2959, Sigma Aldrich) was employed as a photoinitiator. Absorption of incident UV light photons by the Irgacure 2959 causes the cleavage of the photoinitiator which results in the formation of free radicals. Through the propagation of these reactive species along the vinyl groups of the methacrylated pre-polymer backbone, chemical crosslinks are created between polymer chains and further free radicals are generated (Pereira and Bártolo 2015; J. R. Choi et al. 2019). As procedure advances, number of covalent crosslinks rises and strongly crosslinked polymer networks form via chain-growth mechanism.

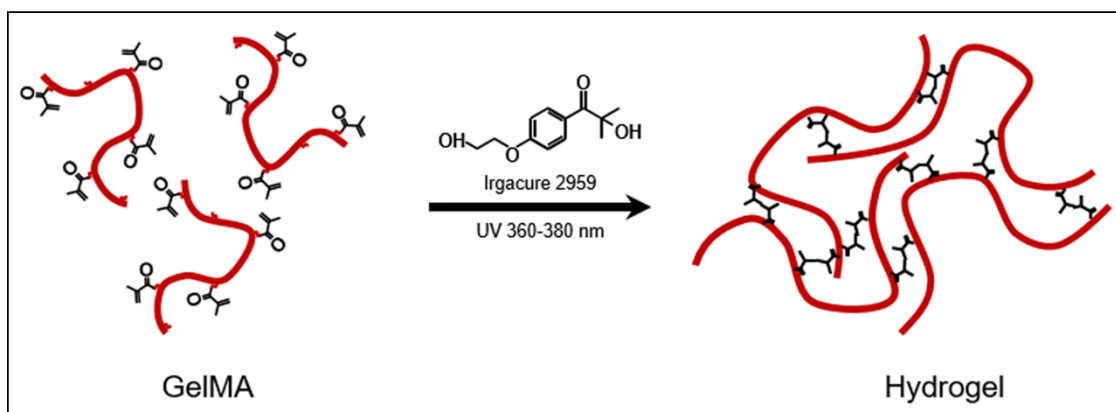


Figure 2.5 Crosslinking of synthesized GelMA into hydrogel through exposure to UV light in the presence of Irgacure 2959. Reproduced under the terms of the Creative Commons CC-BY 4.0 License (<https://creativecommons.org/licenses/by/4.0/>) from Ref. (Yoon et al. 2016). Copyright 2016, Yoon et al.

The designed bioink solution was made up of 3% sodium alginate, 4% GelMA and 0.5% Irgacure2959. For the synthesis of designed bioink, lyophilized GelMA was dissolved within distilled water at 40°C and stirred until it gets completely transparent. Then, sodium alginate was included into the solution. Finally, Irgacure2959 was added into the suspension as it is required for the crosslinking of GelMA. While alginate was physically crosslinked inside the support bath following the deposition from the printhead, GelMA was covalently crosslinked through exposing the printed complex structure into UV light. For increasing the visualization of the printed structures, fluorescent dyes with three different colors were included to the prepared hydrogel precursor solution.

2.4. CAD Modelling and Tool Path Planning for the Generation of Multilayered Vascular-Like Constructs

CAD models of the complex-shaped structures and vascular constructs were developed in Rhinoceros 6 (Robert McNeel & Associates, USA) and tool paths were generated and transformed into G-codes by using the same software's Rhinoscript extension. Biomimetic biomodelling of aortic constructs were initiated in Mimics software for segmentation of the patient-specific data and then converted to Rhinoceros 6 software.

2.4.1. Biomodelling of Vascular Constructs

Aorta was chosen as the native vascular tissue and its spatial heterogeneity, multicellular and multimaterial composition and hierarchical microarchitecture were aimed to be recapitulated. For the biofabrication of vascular constructs with anatomically-correct geometry, geometrical data of the aorta was obtained from the medical image and then converted into CAD model rather than modelling in CAD software directly which lacks significant anatomical considerations.

Geometry of the targeted tissue was obtained through imaging and segmentation of the patient-specific computed tomography data in Mimics (Medical Image Segmentation for Engineering on Anatomy) software (Figure 2.6). In the software, Thresholding was applied to the medical image with a minimum limit of 280 Hounsfield Unit (HU) and a maximum of 3071. Thresholding reduces the interaction of the targeted section of the overall scan with the surrounding tissues. Software's "edit masks" tool was utilized for masking vascular part of the image from the other parts of the scan. Lastly, segmented human abdominal aorta was captured by employing "region growing" tool of the software. Segmented abdominal aorta was exported in the Stereolithography (STL) format.

However, STL files tessellate the surface of the model with triangles, which causes the generation of 3D models not having smooth surfaces. For tool path planning of vascular tissue biofabrication, Mimics software output (mesh model made up of triangular facets) were converted into smooth parametric surfaces in Rhinoceros 6 software. Conversion of mesh model into non-uniform rational basis spline (NURBS) was obtained through "MeshtoNURB" command. To obtain abdominal aorta model with smooth surface, parametric polysurface was sectioned through the intersection of many planes with abdominal aorta model. These intersection curves were transitioned into smooth abdominal aorta model surface by "Loft" command.

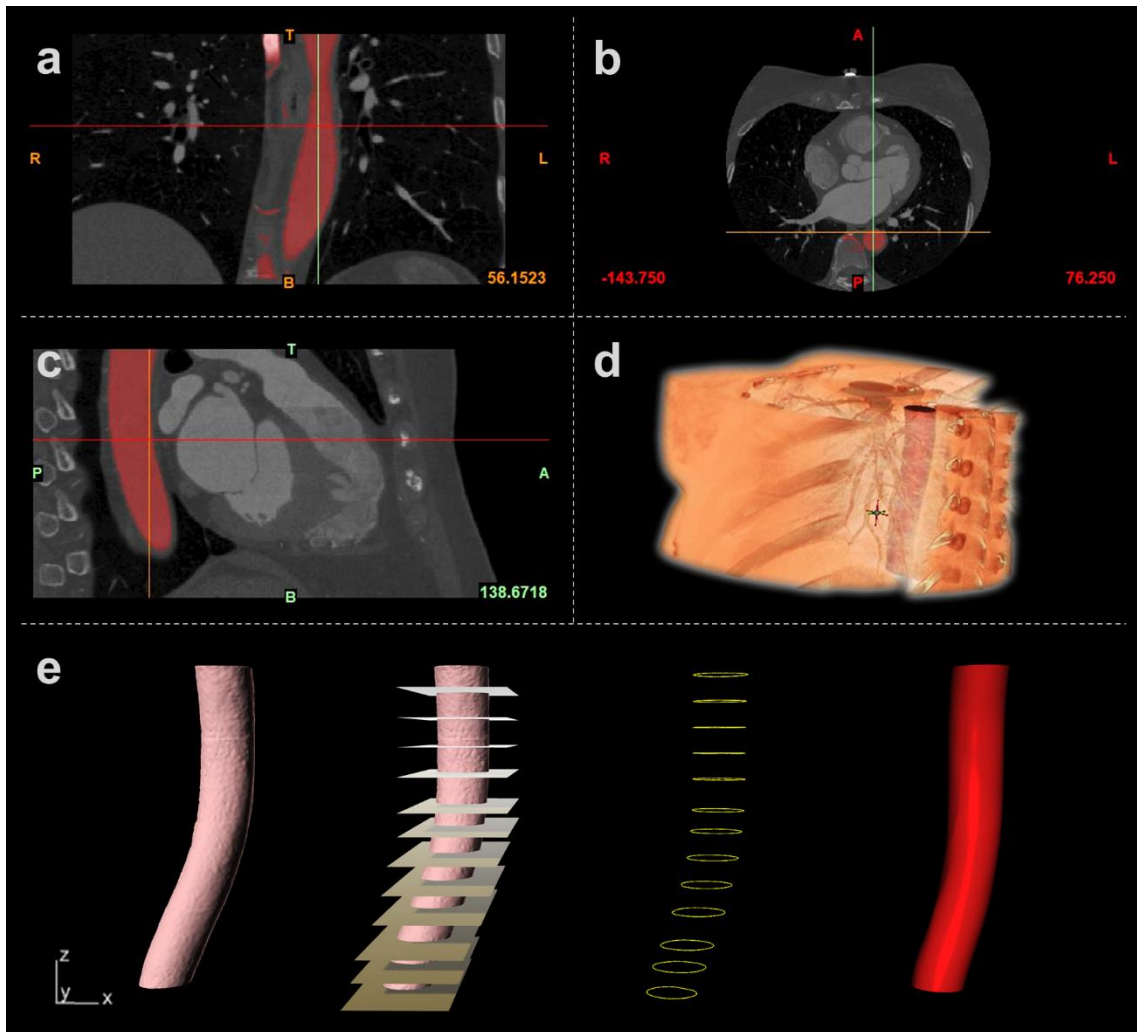


Figure 2.6 Biomodelling of an aortic construct from a medical image. (a) Coronal, (b) axial, (c) sagittal and (d) 3D rendered views of the aorta segmentations. (e) Surface improvement on the segmented model.

Holzapfel et al. have comprehensively demonstrated the thicknesses of different layers of the abdominal aorta and their findings were employed as thickness parameters on the CAD modelling of the aorta. According to their findings, thickness ratios of adventitia: media: intima were determined 33:48:19 in axial direction (Holzapfel et al. 2007). In their previous studies performed on iliac arteries, average ratio of intima: media: adventitia was documented as 13: 56: 31, which shows similarity (Schulze-Bauer, Mörth, and Holzapfel 2003). Total thickness of the abdominal aorta was reported as 1.64 ± 0.44 mm right after the preparation of the axial strip and as 1.60 ± 0.46 after 16 hours. Following the six hours of equilibrium, thicknesses of adventitia, media and intima layers were recorded as 0.40 ± 0.08 , 0.57 ± 0.16 and 0.23 ± 0.06 , respectively (Holzapfel et al. 2007). Measurements on the circumferential directions have also demonstrated similar results.

In the light of these findings, macro-vascular tissue model with three layers having the thicknesses of 400, 600 μm and 200 μm was modelled, where three layers represent adventitia, media and intima layers of the native vascular tissues, respectively.

2.4.2. Tool Path Planning for Multimaterial Bioprinting

In this thesis, a microfluidic and multimaterial printhead was developed with the main concentration on the biofabrication of vascular tissue analogs. Both the development of multimaterial bioprinting platform and recapitulation of hierarchically organized microarchitecture of native vascular tissues necessitate the development of a novel tool path algorithm (**Algorithm 1**). Moreover, continuous layer-by-layer deposition of bioinks with no or minimum hopping is crucial for bioprinting process and movement disruption might affect the printed construct quality. With this regard, a continuous tool path generation was performed (Figure 2.7).

Tool path algorithm was initiated through providing parameters of vascular construct CAD model, layer thickness, number of layers, offset number, gap thickness, resolution and feed rate into the script as an input, which were represented as C_{vascular} , t_{layer} , n_{layer} , n_{offset} , t_{gap} , R and F in the Algorithm 1, respectively. Vascular construct model was sliced based on the layer thickness and then cross-sectional contours (C_{intersec}^i) were obtained through intersecting vascular construct model with plane (p) generated by the bounding box parameters of the vascular construct in each layer. Layer-by-layer movement of multimaterial printhead was developed in a way that, while the printhead moves towards the center of the cross-sectional contour in one layer, printhead moves from center to the border of the contour in the consecutive upper layer. Movement direction of the printhead in each layer was determined by assigning if conditional that changes in each two layers depending on the value of even/odd variable (s) in particular layer. Then, in each layer, cross-sectional contour was offsetted several times depending on the n_{offset} input of the user. By this way, biofabrication complex-shaped constructs having varying features in different layers was made possible as the number of curves that will be generated in each layer may be specified through few modifications in the algorithm. In the algorithm, each of the curves obtained through offsetting the cross-sectional contour in each layer were divided into equal distances depending on the resolution of the 3D bioprinter and dividing


```

15.          TGcode(c) = PCGcode ; c = c + 1
16.                                          }      /*End of 3rd For-loop*/
17.      Else
18.          }      /*End of 2nd If statement*/
19.      Pcentroid = AreaCentroid (cinterseci)
20.      doffset = tgap * x
21.      Coffset = OffsetCurve (cinterseci, Pcentroid, doffset)
22.      Pintersec = DivideCurve (Coffset, R)
23.      For (m = 0 to UBound(Pintersec)-2 step 1) {
24.          n = m + 1
25.          PGcode = Pintersec(n)
26.          PCGcode = PointCoordinate (PGcode)
27.          TGcode(c) = PCGcode ; c = c + 1
28.          }      /*End of 4th For-loop*/
29.      }      /*End of 2nd For-loop*/
30.  Else
31.      For (x = 1 to noffset step 1) {
32.          Pcentroid = AreaCentroid (cinterseci)
33.          If (x = noffset) Then {
34.              nrevoffset = 0.01
35.          Else
36.              nrevoffset = noffset - x
37.          }      /*End of 3rd If statement*/
38.          doffset = tgap * nrevoffset
39.          Coffset = OffsetCurve (cinterseci, Pcentroid, doffset)
40.          Pintersec = DivideCurve (Coffset, R)
41.          For (m = 0 to UBound(Pintersec)-2 step 1) {
42.              n = m + 1
43.              PGcode = Pintersec(n)
44.              PCGcode = PointCoordinate (PGcode)
45.              TGcode(c) = PCGcode ; c = c + 1
46.          }      /*End of 6th For-loop*/
47.      }      /*End of 5th For-loop*/
48.  }      /*End of 1st If statement*/
49.  s = s + 1
50.  }      /*End of 1st For-loop*/
END

```

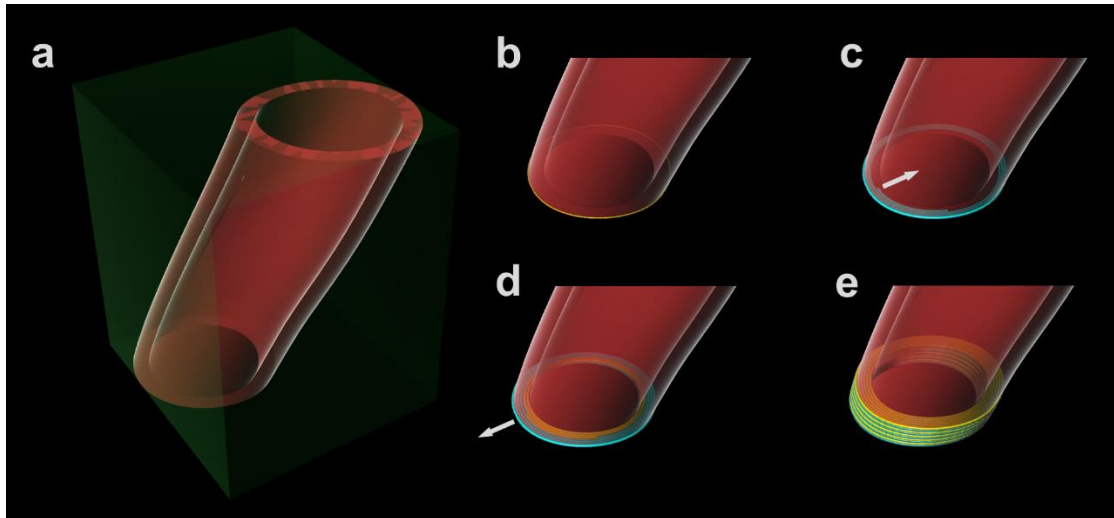


Figure 2.7 Main steps of tool path planning for the generation of multilayered and concentric vascular-like constructs: (a) generation of BoundingBox, (b) intersection of plane with aorta model, (c) generation of first layer by offsetting through the center, (d) generation of second layer by offsetting through the wall, (e) repeating offsetting through inside and outside for the generation of a structure with a specified layer number. White arrows represent offsetting direction in the specified layer.

2.5. Embedded Multimaterial Printing of Complex-Shaped Structures

Multimaterial printing of complex structures were performed by employing the developed embedded multimaterial bioprinting platform incorporating multiple-channel microfluidic printhead, which was demonstrated previously in Section 2.1. Single or multiple hydrogel precursor solutions were loaded into 10 ml hydrogel reservoirs that are connected to the multi-barrel glass capillary needle through tubing junctions. Hydrogels used for embedded multimaterial printing studies were colored by mixing precursor solutions with fluorescent dyes in 1:30 ratio. Before mixing with precursor solutions, blue, green and red fluorescent dyes were diluted in the distilled water with 1:10 ratio which were further sonicated two hours and then filtered from filter paper after dilution. Hydrogels were extruded from the microfluidic multimaterial printhead through three separate pneumatic dispensing units. On-off switching of these pneumatic dispensing units were enabled by solenoid valves that are controlled through M-codes written in the developed tool path algorithm. Extruded hydrogels were patterned inside support bath

according to the desired models that transformed into G-codes via generated tool path algorithm.

For the optimization of printing parameters, nine stripes with different feeding pressure and printing speed combinations were deposited into support bath. Hydrogels extruded through 0.1, 0.2 and 0.3 bar feeding pressures were patterned inside support bath with 1, 2 and 3 mm/sec printing speeds.

Printability of structures having multiple concentric contours in each layer was demonstrated through printing four layered cylinder with 2 cm diameter. The structure was formed by depositing six concentric contours with 200 μm gap in between them for increasing the visibility of each six contours. For the demonstration of smooth interchangeability in between valves which enables the sequential extrusion of different hydrogel solutions, single layer star shape with 60 mm diameter was patterned with 5 concentric contours having 2.5 mm gap thickness in between them. Hydrogels were either sequentially or simultaneously deposited from the microfluidic multimaterial printhead through switching the states of solenoid valves at the beginning of each concentric contours. Moreover, six stripes with 40 mm length were deposited inside the support bath for investigating transition from one hydrogel channel to another hydrogel channel. While one of the solenoid valves was closed at the middle of the stripe, another solenoid valve was opened. To demonstrate fabrication of complex-shaped structures including at least two different material compositions, initial letters of Sabanci University and a cylinder with 6 concentric contours were printed. Initial letters with 2.2 cm length were printed as a four layered construct having four concentric contours in each layer. While red fluorescent included hydrogel solution was deposited in outer two contours of Letter S and blue fluorescent included hydrogel solution was deposited in inner two contours of the same letter, deposition order was reversed for Letter U. By this means, continuous deposition of complex structures with two material compositions was confirmed. Before performing multimaterial bioprinting of aortic construct having six concentric contours patterned with one of the three bioink formulations, multimaterial printing of the same structure was conducted through three fluorescent dyed hydrogels. While two outermost contours of the structure were patterned with blue hydrogel solution, three middle contours were patterned with red hydrogel solution and single innermost contour was deposited with green fluorescent hydrogel solution.

Following the completion of multimaterial printing process, complex-shaped structures were recovered from the support bath by treating them with ice-cold CaCl₂ and NaCl solutions. After transferring the samples into glass bottom petri dish and exposing to UV light from 10 cm distance for 60 sec, 3D images were obtained using tiled z-stacks with 10.00 μm intervals.

2.6. Embedded Multimaterial Bioprinting of Vascular Constructs

2.6.1. Cell culture

For embedded multimaterial bioprinting of vascular constructs with three distinct concentric layers, three different cell types, which are human primary umbilical vein endothelial cells (HUVEC, ATCC), human aortic smooth muscle cells (HASMC, ATCC) and human dermal fibroblast (HDF, ATCC) were cultured. Vascular cell basal medium (ATCC) supplemented with endothelial cell growth kit (ATCC), vascular cell basal medium supplemented with vascular smooth muscle cell growth kit (ATCC) and Eagle's minimum essential medium (EMEM, ATCC) supplemented with 10% fetal bovine serum (FBS, Sigma) and 1% penicillin-streptomycin (Gibco) were employed as growth media for the culture of HUVECs, HASMCs and HDFs, respectively.

Cells received from liquid nitrogen tank were thawed at 37°C inside water bath. 1mL cryovial content was transferred into 15 mL falcon tube and 5 mL growth media was added drop-by-drop. Following the centrifugation of falcon tube at 1100 for 5 minutes, supernatant containing dimethyl sulfoxide (DMSO) was removed. Cell pellet remaining at the bottom of the falcon tube was resuspended in 3 mL of growth media and transferred into T75 flask which was previously filled with 7 mL growth media. Cells were maintained in humidified atmosphere containing 5% CO₂ at 37 °C and subcultured when they reach ~80% confluency. For subculturing of the confluent cells, consumed growth media was discarded, and cell surface was washed with 5 mL Dulbecco's phosphate-buffered saline (DPBS), which was followed by covering surface of cell monolayer with 1.5-2 mL 0.25% trypsin-EDTA solution. Cells incubated at 37 °C for 4 minutes were

observed under microscope for checking detachment of the cells from the surface of the flask. Fresh growth media with double volume of trypsin-EDTA was added into the flask for neutralizing proteolytic activity of trypsin and then all of the suspension was transferred into 15 mL falcon tube which was centrifugated at 1100 rpm for 5 minutes. Following this step, cell pellet obtained after the removal of the supernatant was either transferred into another flask for subculturing purposes or used for bioink preparation.

2.6.2. Preparation of Bioinks Encapsulated with Different Cells

Three bioink solutions including different type of cells were prepared for the biofabrication of vascular constructs with three distinct layers. 6% alginate dissolved within 1X DPBS was autoclaved. On the other hand, 8% GelMA and 1% Irgacure 2959 were dispersed within the three different growth medias belonging to each three cell types and then filtered. Trypsinized and growth media added cell suspension was counted in hemocytometer and then centrifuged. The cells with a 2×10^6 cells/mL density were prepared by resuspending cell pellet within GelMA and Irgacure 2959 containing solution at room temperature. Then, equal volume of 6% alginate and cell-loaded 8% GelMA and 1% Irgacure 2959 solutions were mixed. At final volume, three different bioinks including 3% alginate, 4% GelMA and 0.5% Irgacure 2959 encapsulated with cells having 1×10^6 cells/mL density were obtained.

2.6.3. Multimaterial Bioprinting Inside Support Bath

Support bath ingredients were autoclaved in their powder forms and then support bath was prepared as previously mentioned in Section 2.2. However, all of the preparation steps were held in biosafety cabinet except stirring the materials at 4°C. Three bioink solutions including either HUVECs, HAMSCs or HDFs were loaded into hydrogel reservoirs and then positioned within multimaterial printhead. Respectively, two outer, three middle and one inner concentric contours resembling adventitial, medial and intimal layers of the native vascular tissue were patterned inside support bath by extruding corresponding bioink solutions at 0.1 bar and with 3 mm/sec feed rate. Three-layered

aortic constructs having six concentric contours were biofabricated and prior to removal from support-bath, they were post-crosslinked in a 2% CaCl₂ solution for 10 min. Then, residual support-bath materials were removed from the beakers by pipetting 1% ice-cold NaCl solution. Bioprinted aortic constructs were transferred into 6-well plates containing growth media blend and incubated at 37°C. Growth media blend was prepared mixing equal volumes of growth medias of each three cell types. Before addition of growth media into the six well plates, bioprinted constructs were exposed to low intensity UV light (3 W/cm²) from 10 cm distance for 60 sec which enabled secondary crosslinking of the bioinks.

2.7. Investigation of Bioprinted Vascular Constructs

2.7.1. Live / Dead Assay

The viability of three different cell types encapsulated within alginate-GelMA blend bioink was investigated through live-dead fluorescence assay on Day 1, Day 4 and Day 7 following the multimaterial bioprinting process. Calcein was employed for the indication of living cells within the bioprinted constructs and was prepared through dilution of 1 mg/ml stock solution in 1x PBS with calcium and magnesium in 1:500 ratio. In the same way, 1 mg/ml propidium iodide stock solution was diluted in 1x PBS with calcium and magnesium in 1:1500 ratio for the indication of dead cells.

Following the termination of each incubation points, the bioprinted aortic constructs were transferred into glass bottom petri dishes. After washing each sample with 1x PBS, 5 mL calcein staining solution (0.8 µl calcein /1 ml 1x PBS) was transferred into each well and incubated for 30 min. Then, calcein staining solution was aspirated and 5 ml propidium iodide staining solution (0.5 µl propidium iodide /1 ml 1x PBS) was transferred into wells and incubated for 5 min. At the end of incubation period, bioprinted aortic constructs were washed with 1x PBS three times.

The viable cells were monitored with maximum excitation/emission wavelengths of 488/515 nm, respectively while dead cells were monitored at maximum

excitation/emission wavelengths of 561/625 nm, respectively, using inverted confocal microscope (Carl Zeiss LSM 710). 3D images were obtained using tiled z stacks with 5.00 μm intervals in 2.77 μm pixel size. Live/dead cells were analyzed quantitatively by using ImageJ 1.48 v software.

2.7.2. Cellular Labelling

Zonally stratified arrangement of the bioprinted vascular constructs was evaluated through staining the cells present in distinct vascular layers with two different dyes: SP-DilC18 (Molecular Probes) emitting red fluorescence and SP-DiOC18 (Molecular Probes) emitting green fluorescence. While HUVECs and HSFs were stained with green membrane-intercalating fluorescent stain, HASMCs were stained with red membrane-intercalating fluorescent stain. These carbocyanine-based dyes were dissolved within 1x DPBS with 1.5 $\mu\text{g}/\text{ml}$ concentration. Growth media was discarded, and prepared dye solutions were transferred into cell culture flasks. Following the 30 minutes incubation period, cells were trypsinized and then prepared for the bioprinting in a similar order as explained above. Biofabricated vascular constructs were observed under the inverted confocal microscope after 1 day incubation period.

3. RESULTS AND DISCUSSIONS

3.1. Preparation and Characterization of Nanoclay-Hydrogel Composite Support-Bath

3.1.1. Rheological Characterization of the Support Bath

The weak interactions of the support-bath components play a critical role in the formation of network and its stability and hence the preservation of the printed hydrogel structures in over-hanged and complex geometries (Mezger 2006; Jeon et al. 2019; Howard A. Barnes 2000). In this work, thermoresponsive behavior of PF was combined with the thixotropic behavior of the Laponite to obtain yielding and easily removable support-bath structure. Laponite RDS is selected due to formation of a stable polymer-nanoclay complex with the presence of Ca^{2+} and possession of a neutral isoelectric point providing a biocompatible environment (Castelletto, Ansari, and Hamley 2003; Pek-Ing and Yee-Kwong 2015).

Thermoresponsive gelation behavior of the PF-RDS support-bath with different formulations was characterized through a typical temperature sweep test from 4 to 37 °C with a final dwelling time of 2 h by the evolution of storage (G') and loss (G'') moduli (Figure 3.1). By increasing temperature, G' and G'' moduli raised as a result of both liquid crystalline phase transition of PF in ionic media and the presence of Laponite particles (Castelletto, Ansari, and Hamley 2003; C. J. Wu and Schmidt 2009; Topuz et al. 2018). Then, G' and G'' reached a steady state by further incubation at 37 °C.

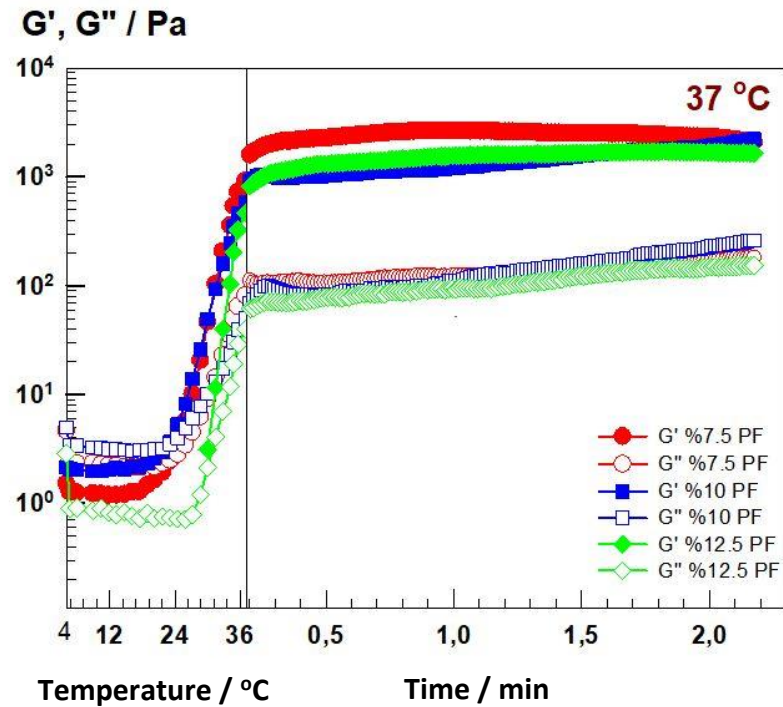


Figure 3.1 Time sweep measurement of the support-bath showing storage and loss moduli over time for different concentrations of PF. Laponite and CaCl_2 concentrations were set to 3% and 1%, respectively. Storage (G') modulus (filled symbols) and loss (G'') modulus (open symbols).

Effect of PF concentration. Figure 3.2 represents rheological characterization of different concentrations of PF in the presence of Laponite-RDS and CaCl_2 at constant concentration. Dynamic moduli of composites containing 7.5, 10, and 12.5% of PF, and 3% Laponite RDS, and 1% CaCl_2 are plotted during the strain amplitude (Figure 3.2(a)) and angular frequency sweeps (Figure 3.2(b)). Strain amplitude graphs demonstrate the flow point of the materials at which a transition between elastic gel state ($G' > G''$) to viscous liquid-like state ($G'' > G'$) is observed (K. Yang et al. 2018; Dávila and D'Ávila 2017). At very low strain amplitudes, G' and G'' values show the linear viscoelastic behavior (Q. He et al. 2012). Increasing the concentration of PF from 7.5% to 10% in the composite resulted in an apparent increase in both moduli during constant strain amplitude loading, however further increase to 12.5% induced a significant decrease (Figure 3.2(a)). The value of storage moduli of 7.5 and 12.5% PF containing composites were observed to be almost the same while the corresponding value for 10% PF one was 1.5-fold higher. The interactions of PF and RDS are considered to be very complex and have not been completely known, however it is assumed that electrostatic interactions as

well as hydrogen bonding are the dominant players in the final structural configuration (Gaharwar et al. 2011, 2019).

The observed developments in both G' and G'' by increasing the PF concentration can be attributed to the bridging effect of PF micelles and chains with their vicinal nanoclay particles which results in stabilization of the composite (K. Sun and Raghavan 2010; Gaharwar et al. 2019). In this way, it is speculated that there would be a threshold for such interactions, which could be translated to the surface capacity of the Laponite-RDS in such a system. A viscoelastic gel structure could be formed by increasing the PF concentration up to a certain value above which, the faces of the Laponite-RDS nanoclays would be already saturated by the adsorbed polymer. Further increase in the polymer concentration will not necessarily contribute in establishment of long-range elastic interactions between the two components of the system (Nelson and Cosgrove 2005; C. J. Wu and Schmidt 2009). The mixtures of PF and CaCl_2 (Control 1) and Laponite-RDS and CaCl_2 (Control 2) were selected as control groups to identify the contribution of each individual component of the composite in development of the viscoelastic properties. It should be noted that the exclusion of CaCl_2 from the mixture of PF-Laponite RDS resulted in formation liquid-like composite, failing to form a viscoelastic gel network (Castelletto, Ansari, and Hamley 2003; Pek-Ing and Yee-Kwong 2015). Hence, this composition was not included in the set of experiments. Control 1 failed to show a detectable linear viscoelastic limit within the range of strain values 10^{-3} to 10^3 (%). This can be explained by formation of clusters consisting of polymer chains at low concentration of PF as reported elsewhere (P. J. Lu et al. 2006). Control 2 showed a linear viscoelastic range during strain amplitude sweeps, however the storage modulus values were much lower than the corresponding region in PF-RDS composites containing PF at the same CaCl_2 concentration (Sheikhi et al. 2018). Both control groups showed less elastic moduli, since Laponite-RDS acts as a physical cross-linker to PF polymer chains in the presence of CaCl_2 which is in agreement with previous study of Wu *et. al* (C. J. Wu et al. 2011).

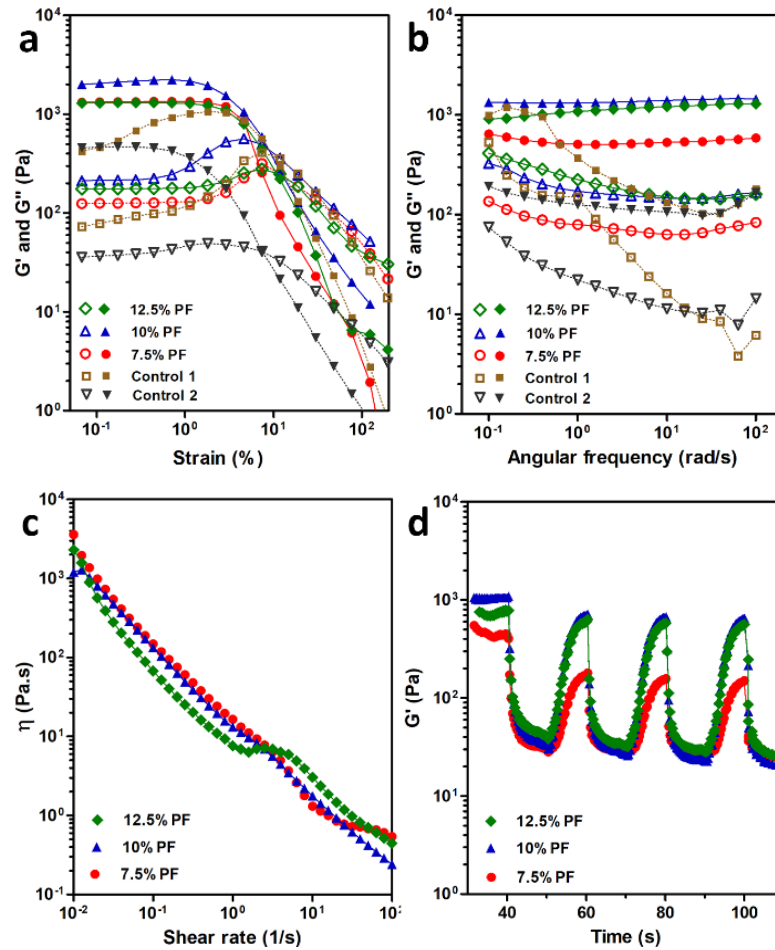


Figure 3.2 Dynamic rheological characterization of the support-bath representing the effect of PF concentration on flow behavior and recoverability of the structure at 37 °C (Laponite-RDS and CaCl_2 concentrations were constant at 3 and 1%, respectively except for control samples). Control 1 and control 2 included 10% PF, and 3% RDS, respectively at constant 1% CaCl_2 (a) Strain amplitude sweep profiles of supporting media, (b) frequency sweep profiles within the linear viscoelastic range, (c) viscosity vs. shear rate plots revealing the shear thinning behavior of the support material, (d) cyclic strain measurements at high (50%) and low (0.6%) strains showing storage (G') moduli of the samples in 4 cycles. Storage (G') modulus (filled symbols) and loss (G'') modulus (open symbols).

The dynamic viscoelastic properties of the formed networks of PF in the presence of Laponite-RDS and CaCl_2 were also probed by frequency sweep analysis (Figure 3.2(b)). The elastic features of the matrix were dominant throughout the whole measured frequencies, characterized by G' values higher than G'' values (K. Yang et al. 2018). The elastic modulus value at 7.5% PF was considerably lower than the other two

concentrations. By increasing the PF concentration to 10%, the interactions between PF and Laponite-RDS evolves from a viscoelastic-dominant gel state to a glassy state colloidal network, in which the elastic modulus is almost independent from the frequency of deformation. Further increase in PF concentration to 12.5% resulted in weakening of the elastic response of the system at low frequencies, an indication of the increased contribution of excess PF chains which are speculated to have no direct interactions with Laponite nanoparticles. The results demonstrate that concentration dependent interactions between polymer and clay nanoparticles allow the formation of suitable and stable network for support-bath (Jin et al. 2018; K. Sun and Raghavan 2010; Sheikhi et al. 2018). Control 1 showed a strong dependency of both elastic and loss moduli to frequency values. It could be due to testing parameters which was not in a viscoelastic region. Control 2 showed glassy gel-like behavior with almost constant elastic modulus values at all frequencies, revealing the effect of calcium ions in the formation of House of Cards-like structure which was utilized as support-bath material in previous studies (Ding and Chang 2018). However, the value of storage modulus was much lower compared to the composite with PF which needs more viscous bioink to be able to provide enough mechanical strength to hold the structure during bioprinting process.

Shear thinning behavior and yield stress values of the composite support-bath materials were investigated by a shear rate sweep test (Figure 3.2(c)). As the graph implies, all the tested concentrations showed the same trend of viscosity drop but the sample with 7.5% PF had the highest decrease in its viscosity while the sample with 10% of PF had the lowest change.

Figure 3.2(d) shows recoverability of the composite throughout cyclic deformation. Due to the thixotropic characteristics, the disturbed matrix result in rebuilding of the interactions by forming the matrix network over time (Dávila and D'Ávila 2017; Jin et al. 2017). The so-called self-recovery property represents an essential feature of the composite matrix to be utilized as a support-bath material. Dynamic strain tests were performed at high (50%) and low (0.6%) strains. The strain cycles were repeated in 10 seconds intervals to monitor how fast the composite material could recover itself. Thixotropic behavior was monitored within 16 cycles (data was clipped to 4 cycles to enhance the legibility) and the recovery time and the extent of drop in storage moduli after 3rd cycle of deformation were almost constant. As shown in the graph, even in a

short time of 10 seconds the structures with 10 and 12.5% of PF could almost reach to their initial storage moduli. The composite with 7.5% of PF showed lower recovery in storage modulus compared with the starting point. This could be due to lower amount of polymer-chains which could not enhance the composite matrix stiffness (K. Sun and Raghavan 2010) as the amount of PF was not enough to resist the high shear strain values to rapidly recover the physically crosslinked polymer chains attaching on the Laponite nanodiscs charged surfaces (K. Yang et al. 2018; Laxton and Berg 2006).

Effect of CaCl₂ concentration. The contribution of ionic content in the formulation to viscoelastic properties of the composite was systematically assessed by varying the CaCl₂ concentration with constant PF and Laponite-RDS which were set to 10 and 3%, respectively. We evaluated three different concentrations of 1, 0.5, and 0.25% for CaCl₂ in the formulation to provide a moderate crosslinking for dispensed liquid form of alginate and to obtain an integrated structure without diffusion into the support-bath (S. J. Song et al. 2011; Au et al. 2015; Sheikhi et al. 2018). It should be mentioned that the lowest concentration of Ca²⁺ were above the threshold of “gel” formation below which a “glass-colloid” would be formed as explained in the previous study (Nelson and Cosgrove 2004).

It is noteworthy to mention that low concentrations of CaCl₂ showed promising behavior to be used as an electrolyte together with Laponite nanoclay. In this study, we selected 0.5% CaCl₂ since it was not only a structural modifier for Laponite, but also a cross-linker for alginate. Our aim was to utilize a low concentration cell-laden hydrogel (3% alginate) to provide a cell-friendly bioprinting process with the utilization of a relatively low pressure for extrusion of bioink in a moderate CaCl₂ concentration to obtain sufficient cross-linking density for structural integrity among the subsequently printed layers.

3.1.2. Printability of Overhanging and Complex Structures in PF-RDS Support-Bath

The challenges of overhanging and tubular complex structure printing have been addressed with different approaches in the literature (Luo, Lode, and Gelinsky 2013; Yu et al. 2013a; Distler et al. 2019; Ruther et al. 2019; Dubbin, Tabet, and Heilshorn 2017; G. Gao et al. 2019). The principle of the printing mechanism of those tubular structures

are based on one-step extrusion of hydrogel in air, which is cross-linked by the inclusion of cross-linker through a coaxial nozzle system. These techniques are capable of printing hollow vascular-like structures in small dimensions by employing different formulations of bioinks, whereas construction of complex shapes in a layer-by-layer manner may not be applicable for integration of the extruded subsequent layers.

Printing in support-bath has been an emerging approach utilized by extrusion of hydrogels in a liquid form to have an appropriate shape fidelity, as well as to provide a more cell-friendly process compared to in-air extrusion bioprinting (Dubbin, Tabet, and Heilshorn 2017). Laponite support-bath was demonstrated as support bath for fabrication of overhanging and complex branched tubular structures for various hydrogel types with different crosslinking mechanism (Jin, Chai, and Huang 2018; Ding and Chang 2018). Although Laponite support bath was investigated individually with many aspects for printing, the extruded hydrogel concentration was very high which could affect living cell functionality (Ding and Chang 2018). The use of high concentration of hydrogel is expected due to the slow crosslinking kinetics of alginate in the presence of low concentration of CaCl_2 , which has a strong negative effect on viscoelastic properties of Laponite as it is demonstrated above.

Rheological characterization suggested that all the tested PF-RDS composites could be used as a support-bath for hydrogel printing. Three percent of alginate was used for printing inside the support-bath that has lower concentration compared to previous studies (Y. Wang et al. 2019; Ding and Chang 2018; Jin et al. 2017). Among PF concentrations, 10% showed better viscoelastic behavior in terms of storage modulus and self-recovery. Printability of alginate into the support-bath containing various CaCl_2 concentrations were investigated. In the previous report, concentration of CaCl_2 for the Laponite support-bath was 0.125% (Jin et al. 2017). However, our initial experiments showed that even the CaCl_2 concentration of 0.25% was not enough to efficiently cross-link 3% of alginate hydrogel during printing. This concentration was much lower than the hydrogel that was used in the mentioned study (8% alginate). On the other hand, increasing the concentration of CaCl_2 to 1% resulted in fabrication of structures with non-integrated fibers and occurrence of staircase effect (Ding and Chang 2018). Hence, the support-bath with composition of 10% PF and 0.5% CaCl_2 was used. Moreover, Ding *et al.* increased CaCl_2 concentration to 0.5% in a 4% Laponite support bath, while they used a

concentrated and more viscous hydrogel blend as the extruded bioink (3% alginate+10% gelatin) (Ding and Chang 2018). This could be correlated to the decreased self-recovery properties of Laponite support-bath in the presence of high CaCl_2 concentrations. It is worth mentioning that increasing the concentration of CaCl_2 above 0.125% causes the deterioration of the House of Cards-like structure and shear-thinning property of only Laponite support-bath. Formulation of the Laponite support bath with PF resulted in increased tolerance over the CaCl_2 content and allowed to dispense less viscous hydrogel with higher shape fidelity at low extrusion pressure, which would be a more cell friendly process.

A detailed overview of 3D printed overhanging hollow structures with different angular configurations before and after recovery from PF-RDS support-bath are demonstrated in Figure 3.3. Support-bathes were incubated at 37 °C in a humidified environment for two hours prior printing based on the rheological data explained above. Integrated and bended tubular structures perpendicular to the surface (90°) and with 60° and 45° angles and a conical structure with 60° angle were printed in 20 layers. The front views of the tubular structures in support-bath are presented in Figure 3.3(a, b, c, d). It is clearly seen that the angles of printed structures were the same as designed models. The front and top views of the printed structures after harvesting from support-bath demonstrated that structures were well-crosslinked with integrated layers and preserved angular configurations due to optimized concentration of CaCl_2 in the PF-RDS bath. The heights of the printed structures were measured as 7.58 mm \pm 0.9, 4.54 mm \pm 0.08, and 3.88 mm \pm 0.25 for tubular structures of 90°, 60°, and 45° angles, respectively. Based on computer-aided design (CAD) models, all the printed structures should have the same height. During printing of the tubular structure with 90° angle, the nozzle moved through the same x-y coordinates for 20 times. In contrast, the movement patterns of the nozzle for the other angled structures were not as repetitive in the same coordinates. As a result, diffusion of the hydrogel ink during printing of the structure with 90° angle was more and the final structure had higher height. Angles of the bended structures after removing from support-bath were measured as follows: 85.9° \pm 1.40, 59.4° \pm 2.33, and 47.8° \pm 5.34, which indicates a high printing resolution for the overhanging CAD models in the PF-RDS bath. The printed structures of alginate with 3% concentration demonstrated that the support-bath had proper viscoelastic characteristics which allowed printing of liquid-like

hydrogels with relative low viscosity in a defined geometry and *in situ* cross-linking while the shape fidelity of overhanging hollow structures was preserved.

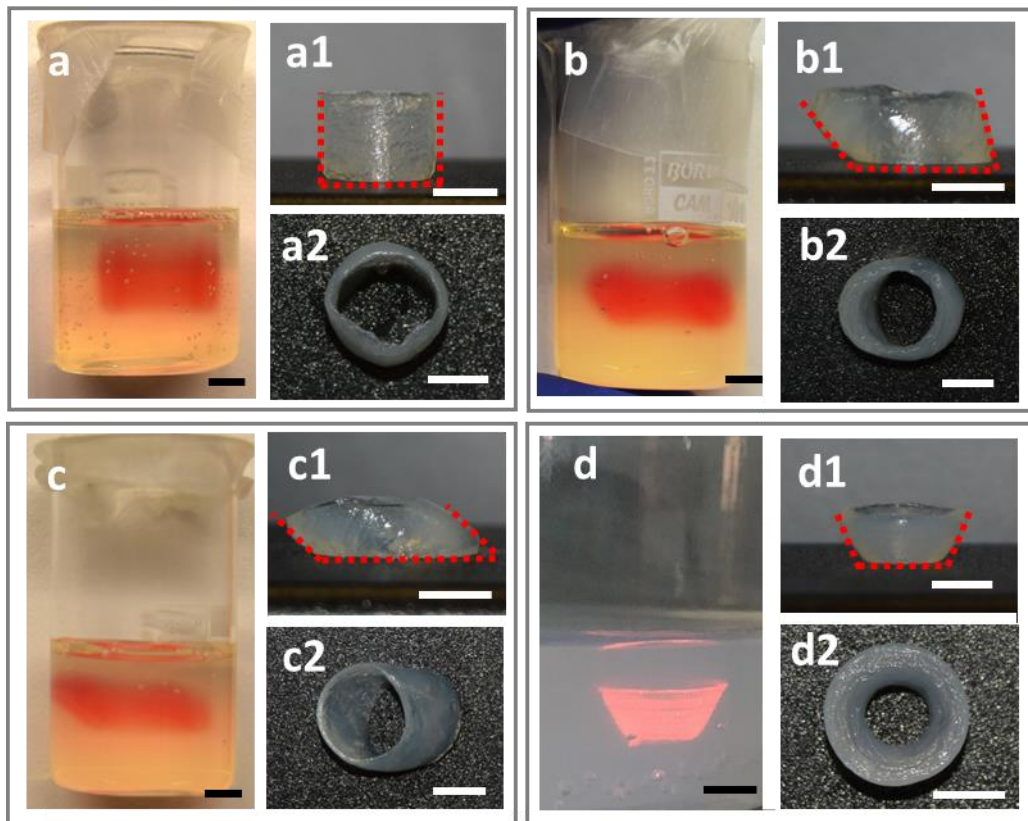


Figure 3.3 Characterization of PF-RDS support-bath for printability of tubular structures in various angular configurations. Digital images of the printed tubular alginate structures using 25 gauge nozzle in the support-bath angled at (a) 90°, (b) 60° and (c) 45°, and (d) a conical structure with 60° angle with respect to the surface. Digital images of front and top views of (a1, a2) 90°, (b1, b2) 60° and (c1, c2) 45° bended tubular structures and (d1, d2) conical structure after removal from support-bath. Scale bars indicate 5 mm.

Three different complex structures including star shape, grid and branched vascular structure were used to demonstrate printing capability of complex geometries with different scales inside the PF-RDS support-bath. Figure 3.4 shows the CAD models, top views of the printed structures before and after removal of the support-bath. Compared to reported Laponite support bath at which the sample was incubated for 6 h to obtain proper gelation (Jin et al. 2017), we could easily remove the printed constructs from the PF-RDS support bath just after printing. Increased concentration of CaCl_2 in support bath provided

enough crosslinking density and ice-cold NaCl solution facilitated the removal of PF coated RDS. A star shape with an outer diameter of 2 cm was selected to demonstrate the precise deposition of extruded filaments with sharp corners (Fig. 3.4(a1)). Shape fidelity and its high resolution after the support-bath removal are demonstrated in Figure 3.4(a2). A small square grid structure with one cm length was chosen to explore the recoverability of the support medium in a repetitive pattern. CAD model of grid structure is depicted in Figure 3.4(b). Despite the structural integrity and shape fidelity concerns for grid structure printing, the support-bath presented here allowed its fabrication (Figure 3.4(b1)). The structure was harvested without disturbing shape fidelity during removal from the PF-RDS as shown in Figure 3.4(b2).

A vascular structure plays an important role for living tissues in oxygen and nutrients transportation, and metabolic removal. Fabrication of the vascular network is essential for the functional structures. A CAD model for a branched vascular structure with an overall length of ~ 3 cm and a width of ~ 2 cm was designed (Figure 3.4(c)). The vascular structure with a wall thickness of ~ 0.95 mm and 6 mm height was printed by three offsetted contours in each layer. Figure 3.4(c1) shows the printed branched structure inside the support-bath that was printed in 50 min. After gently removal of the support material from the lumen, interconnectivity of the hollow vascular structure was monitored by passing a food dye through it. The diffusion test demonstrated no leakage from the walls.

To demonstrate the capability of our support-bath for printing of anatomically relevant and 3D complex structures, a nose shape with an overall 2.7 cm length and 1.7 cm width was printed using 25 Gauge nozzle (Figure 3.4(d)). It is to be noted that the printing path strongly affects the final structure as it was demonstrated before (Z. Zhang et al. 2018). When printing path started from the tip of nose inside the support-bath, we could obtain a smooth surface on the nose with apparent nostrils as represented in Figure 3.4(d3). This result also verifies the applicability of our support-bath for bioprinting of liquid hydrogels in various complex and large-scale structures.

The printed constructs demonstrated the feasibility of the support-bath for continuous and repeated retracing of the print-head. As stress-yielding phenomena happened around the local area where nozzle moves, overall rheological characteristics of the support bath did

not change and did not cause any disruption of the complex shapes, highlighting the stability of the support-bath for long-lasting printing procedures. Although printing speed is considered as a key parameter affecting the yielding properties of the support bath (Grosskopf et al. 2018; Ding and Chang 2018), the support-bath revealed a consistent recovery in different print speeds. In addition, shape fidelity preservation after structure removal from the support-bath has demonstrated the sufficient integration between the consecutive layers.

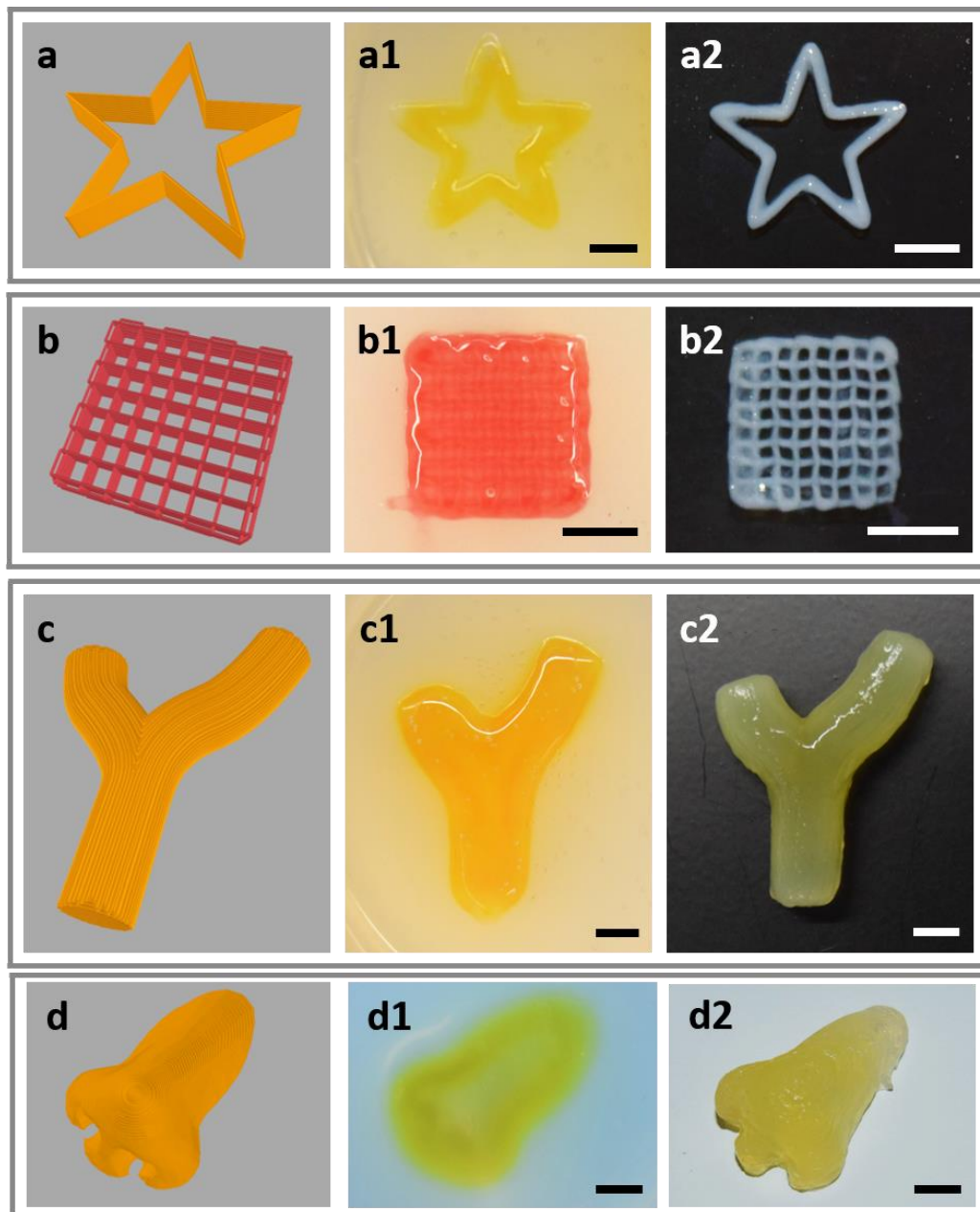


Figure 3.4 Fabrication of 3D complex constructs. CAD models of (a) star shape, (b) 0-90° grid pattern, (c) branched vascular structure, and (d) nose shape. Digital images of

the fabricated structures (a1, b1, c1, d1) before and (a2, b2, c2, d2) after recovery from PF-RDS support-bath. Scale bars indicate 5 mm.

3.1.3. Bioprinting of Cell-Laden Alginate Hydrogel in Support-Bath

Cell-laden hydrogels dispensed from a nozzle are being exposed to a shear stress, and followed by an invasive effect of cross-linking mechanism (Suzanne and Steller 2013; Dubbin, Tabet, and Heilshorn 2017). Therefore, fabrication process of cell-laden hydrogels inside the support-bath might affect the cellular integrity. Since the nozzle size and feeding pressure for the extrusion of cell-laden hydrogel have an inverse relation, the use of small needle size might have more negatively effect on cell viability. We selected a small nozzle (30-Gauge) to investigate the effect of bioprinting process in support-bath in intense conditions. Compatibility of the bioprinting process was evaluated by monitoring cell viability after bioprinting. Alginate used to encapsulate the cells in this study is commonly employed in 3D bioprinting applications due to the biocompatibility and fast crosslinking in the presence of Ca^{2+} ions despite its bio-inert nature and limited biodegradability. It is also used as a thickening hydrogel to enhance the bioprintability of the other, more bioactive hydrogels (Jin et al. 2017; Ding and Chang 2018). NIH-3T3 mouse fibroblast cells in a density of 1×10^6 cells/mL were encapsulated in 3% of alginate and bioprinted by feeding pressure of 0.5 bar and print speed of 150 mm/min. Well defined 3D hollow structure with a 5 mm diameter and average height of 0.6 mm was obtained by the integration of deposited four concentric fibers of cell-laden alginate. Figure 3.5 shows (a) bright field image of harvested bioprinted structure from the support-bath and (b) Calcein AM (green) and PI (red) stained, live and dead cells, respectively, in a complete bioprinted structure. The results demonstrated the structural integrity of the proposed structure for bioprinting and their efficient recovery from support-bath with high percentage of viable cells (Jin et al. 2017; Compaan, Song, and Huang 2019; Ding and Chang 2018). Live and dead cell numbers showed that $82.7 \pm 6.5\%$ cells in alginate hydrogel were viable after one day (Day 1) of incubation (Figure 3.5(c)). The percentage of viable cells did not change on Day 3 while the cell viability increased to $94.3 \pm 4.6\%$ at Day 7. The results indicated that extrusion pressure did not affect the cell viability significantly and the cells almost recovered at Day 7.

These results demonstrate that the bioprinting process in PF-RDS support-bath does not cause significant damage to the cells encapsulated within the hydrogel. Further long-term cell viability evaluations are necessary for bioactivity investigation of different hydrogels (Suzanne and Steller 2013; Dubbin, Tabet, and Heilshorn 2017).

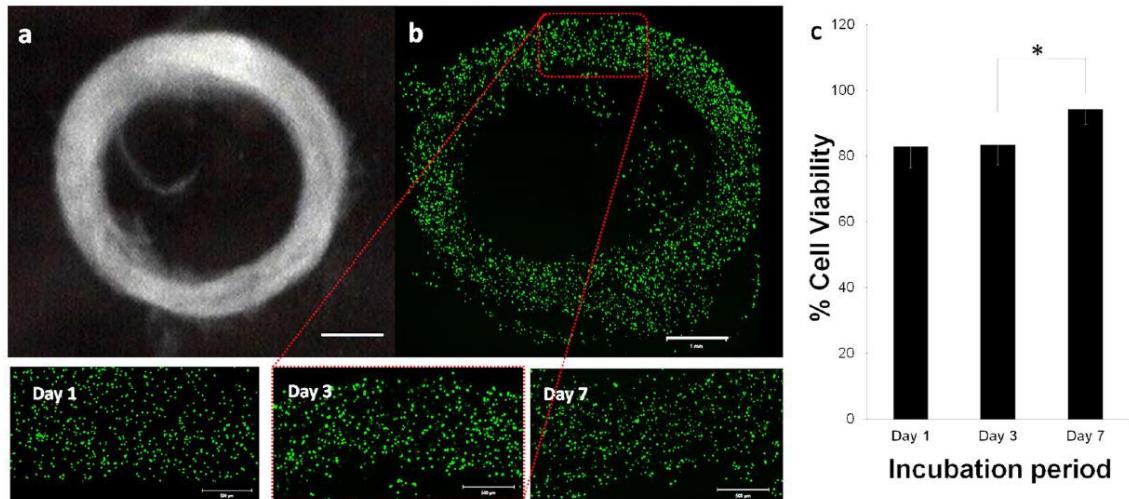


Figure 3.5 Fabrication of cell-laden alginate constructs using PF-RDS support-bath. (a) Image of harvested bioprinted tubular structure from support bath. (b) Confocal microscopy image of live/dead cells encapsulated in the alginate hydrogel in a complete 3D bioprinted hollow structure at Day 3 and the zoomed images of cells obtained on Day 1, Day 3 and Day 7. (c) Quantitative viability analysis of cells for Day 1, 3 and 7 after bioprinting. Two tail Students *t*-test was used to analyze the significant change in the cell-viability after bioprinting process. P-values $* < 0.05$ were considered as significant. Scale bars indicate 1 mm for (a) and (b) and 0.5 mm for the zoomed images.

3.2. Characterization of Synthesized GelMA for the Preparation of Alginate-GelMA Blend Bioink

Figure 3.6 shows the NMR spectrums of gelatin and GelMA. Following the modification of gelatin, peaks that are present in the NMR spectrum at the 5.5-6 ppm range and at the 3.2 ppm are the indicators of methacrylate groups and amine groups, respectively. Together with these two peaks, phenylalanine peak appearing at 7.5 ppm in both of the gelatin and GelMA NMR spectrums was used as reference peak for the normalization of

the graphs. In the other words, for the comparison of peaks belonging to methacrylate groups and amine groups, phenylalanine peaks of the two graphs were equalized.

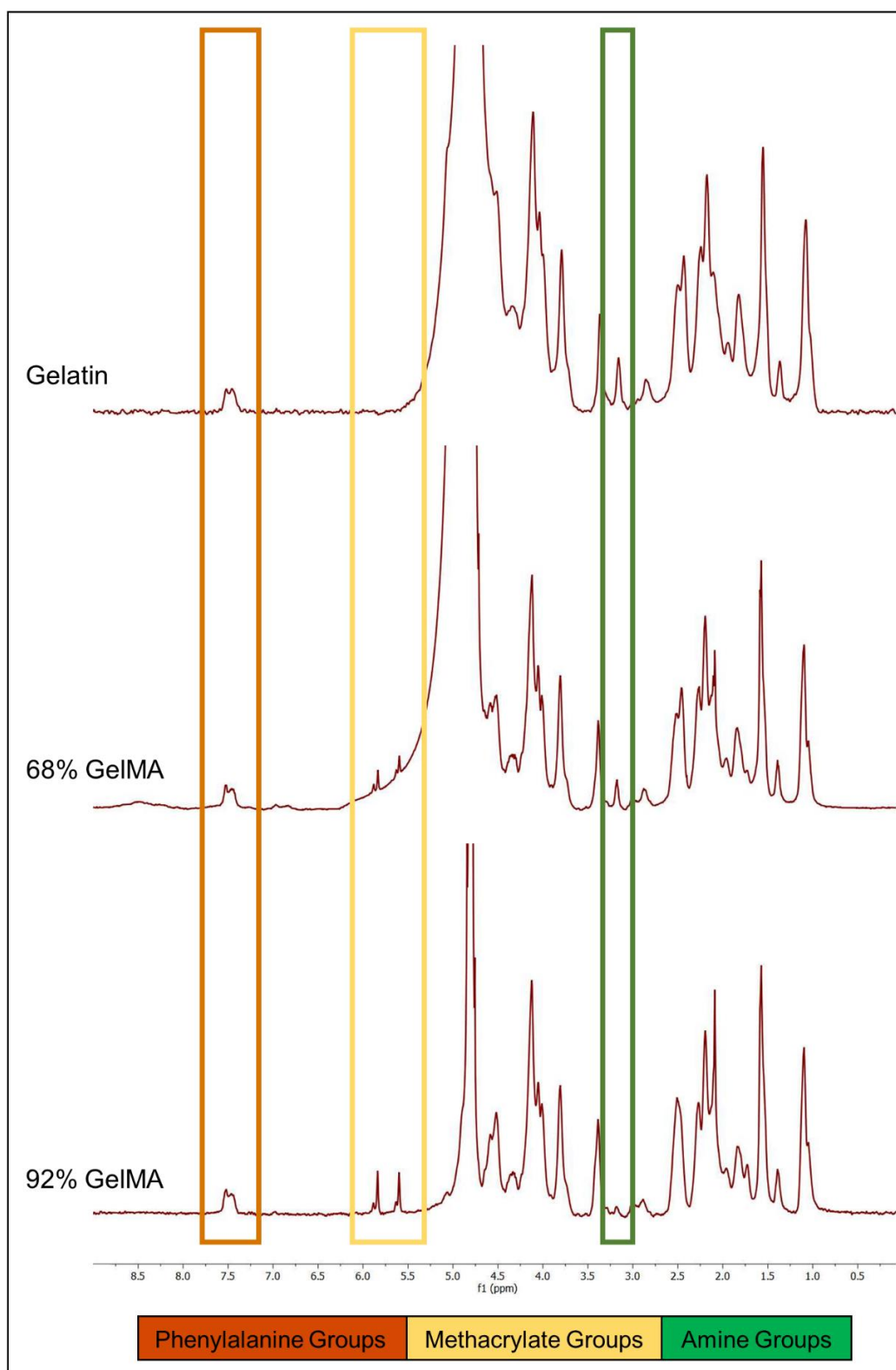


Figure 3.6 NMR spectrums of gelatin and synthesized GelMA with different DoF percentages

Degree of functionalization (DoF) is defined as the ratio of the number of methacrylate groups present in the structure of synthesized GelMA to the number of un-reacted amine groups (lysine, hydroxylysine) present in the structure of gelatin (Hoch et al. 2012). For the calculation of DoF, first of all, NMR spectrums were normalized according to the phenylalanine signals (6.9-7.5 ppm) as they do not participate to the modification reaction. Then, integral areas of the methyl lysine signals (2.8-2.95 ppm) for gelatin and GelMA spectrums were determined. Degree of methacrylation was calculated according to the Equation 1.

$$\% \text{ DoF} = \left[1 - \frac{\text{Area of lysine peak (GelMa)}}{\text{Area of lysine peak (Gelatin)}} \right] \times 100 \quad \text{Equation (1)}$$

Attenuation of lysine signal (including amine groups) intensities and formation of methacrylate peaks following the methacrylate modification process prove successful GelMA synthesis. Throughout the experiments, GelMA with 92% degree of methacrylation was employed. DoF difference shown in Figure 3.6 was obtained through altering the stirring time of the modification reaction.

3.3. Embedded Multimaterial Printing of Complex-Shaped Structures

3.3.1. Printing of Single-Material Multilayered Structures Inside Support Bath

Before proceeding to the multimaterial extrusion processes for multimaterial printing of complex-shaped structures and for multimaterial bioprinting of aortic constructs, the initial experiments were performed for the optimization of the printing parameters and then deposition of single type of hydrogel precursor solution from one channel of the microfluidic multimaterial printhead.

Feeding pressure which provides extrusion of the hydrogels from the printhead and printing speed defining how fast the printhead will move from one position to another position were optimized by patterning an array of nine stripes where feeding pressure and

printing speed vary in each stripe. While 0.1, 0.2 and 0.3 bar were investigated for the identification of optimal feeding pressure, 1, 2 and 3 mm/sec were employed as printing speed parameters. Diameter of the printed stripe increased as pressure applied to extrude hydrogel increases. For this reason, smallest available feeding pressure, which is 0.1 bar was selected for the rest of the experiments. On the other hand, leakage of the hydrogel inside the support bath was observed during patterning in low printing speeds. Even though higher printing speeds would lower the manufacturing process and enable generation of stripes with lower diameters, self-recovery of the support bath would be drastically affected. Printing speed that was utilized for the rest experiments was selected as 3 mm/sec, which is the parameter that structures were printable without damaging self-recovery of the support bath.

Subsequently, a four layered cylindrical model having six concentric contours in each layer was printed by extruding single-material from one of the channels of the multimaterial printhead (Figure 3.7). By this means, optimized parameters were investigated on the printing of structures with increasing geometrical complexity. Printed structures were visualized and photographed by exposing to UV light as fluorescent dye was included to the alginate-GelMA blend hydrogel solution. Addition of fluorescent dye rather than food dye significantly prevented the diffusion of the dye from hydrogel solution to the support bath. Following the extrusion of the fluorescent dyed precursor solution into support bath, the structure was removed from the support bath and patterned stripes were observed under confocal microscope. During the tool path planning of the targeted model, gap thickness in between in each concentric contours was defined as 300 μm for increasing the visibility of each contours. Confocal microscope image of the multilayered cylindrical construct clearly demonstrated the patterning of stripes with 200 μm diameter having 300 μm gap thickness in between them (Figure 3.7(d)).

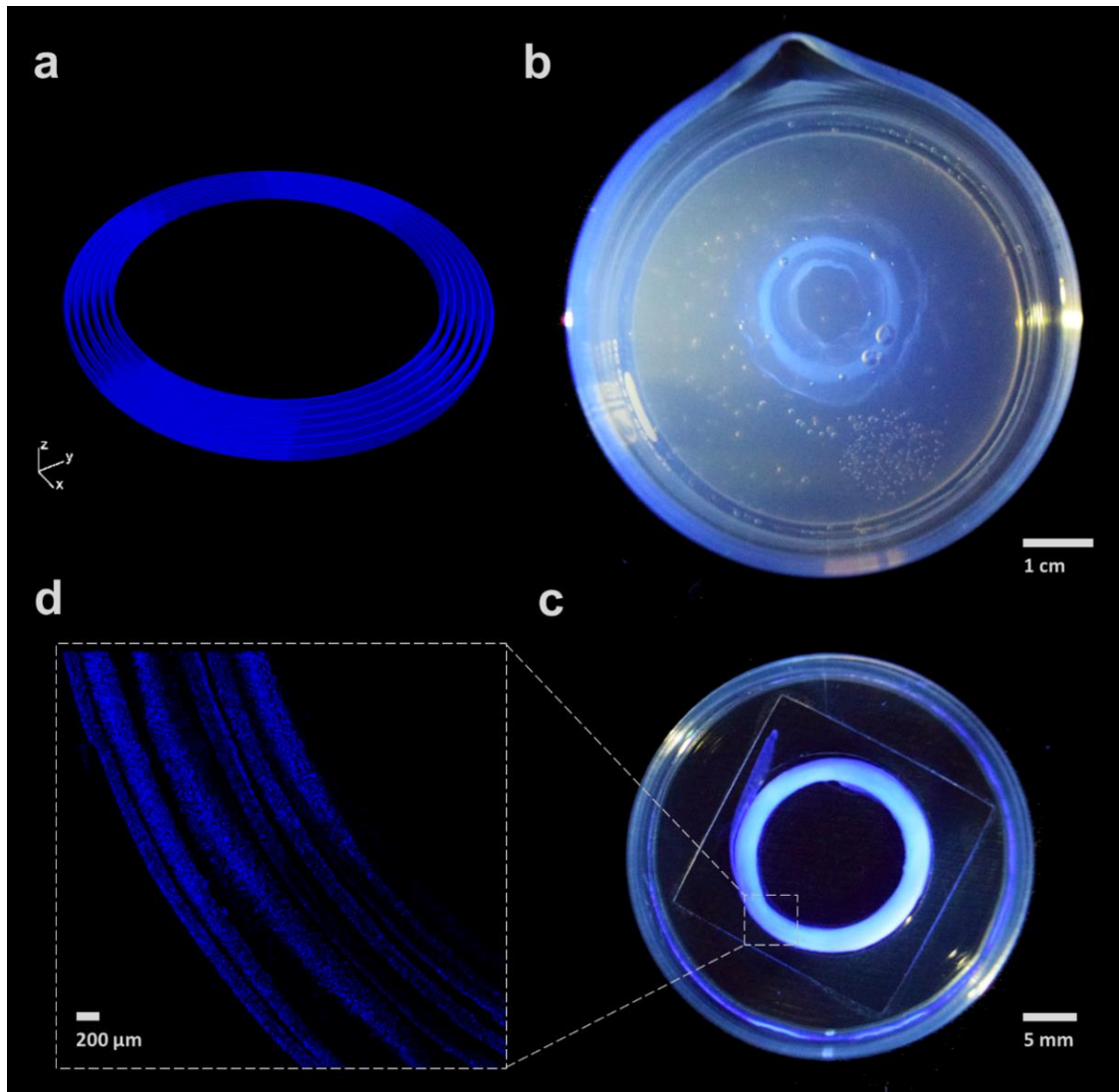


Figure 3.7 Embedded printing of a multilayered structure by microcapillary-based printhead. (a) CAD modelling of the multilayered structure with six concentric contours in each layer. Photographs of the four-layered structure (b) inside support bath and (c) after removal from the support bath. (d) Confocal image of one part of the structure.

3.3.2. Investigation of Valve Interchangeability for Multimaterial Extrusion

After optimizing printing parameters through single-material printing of cylindrical structure with geometrical complexity, transitions in between the pressure-driven valves were also investigated before passing to multimaterial extrusion studies. For this purpose, first of all, transitions in between the pressure-driven valves during simultaneous or sequential patterning of hydrogel solutions were investigated (Figure 3.8). Alginate-

GelMA blend hydrogel solutions were separately mixed with blue, red or green fluorescent dyes and then transferred to hydrogel reservoirs which are connected to distinct channels of the microcapillary tip. Fluorescent dyes in three colors were employed to distinguish hydrogels extruded from different channels in each transition.

A one-layered star shape with 60 mm outer diameter was patterned within the support bath with 0.1 bar feeding pressure and 3 mm/sec printing speed. On-off switching was performed at the beginning of each contour. Following the deposition of blue dyed hydrogel at the first contour (first valve is on), blue dyed hydrogel was simultaneously extruded with the red dyed hydrogel at the second contour by opening the second valve. Then, first valve was turned off and red dyed hydrogel was extruded individually at third contour. At the fourth contour, third valve was opened while first valve was off, and second valve was still on. At the innermost contour, all of the pressure-driven valves were opened, and three hydrogels were synchronously extruded from the distinct channels. Photographs taken has proven the successful on-off switching of the valves without encountering any delay or disruption (Figure 3.8(c)).

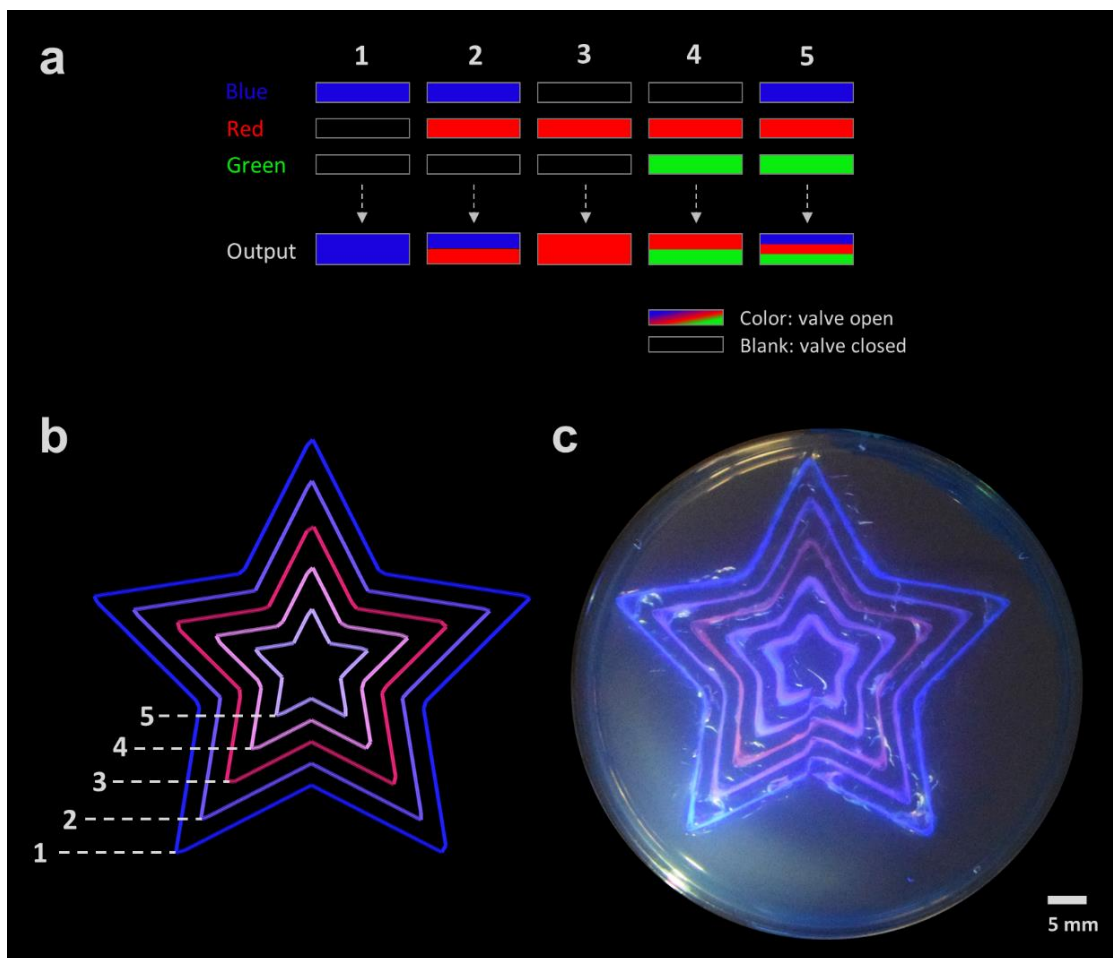


Figure 3.8 Investigation of valve interchangeability between different valves. (a) Schematic of a code including transitions in between pressure-driven valves for simultaneous and sequential extrusion. (b) Tool path planning of the single layered construct where valve transition occurs in between each contour. (c) Photograph of a multimaterial structure with valve transitions inside support bath.

Upon the investigation of valve transition in each contours for sequential or simultaneous extrusion of hydrogels from different separate channels, the study was elaborated on the investigation of transition regions. An array of six stripes with 40 mm length was patterned, where on-off switching takes place at the middle of each stripe (Figure 3.9). Following the multimaterial extrusion process, the stripes were harvested from the support bath and observed under confocal microscope. It was observed that a continuous switching in between the different hydrogels would be achieved within a few hundred micrometers. The length of transition region would be further lowered through decreasing the feeding pressure or increasing the printing speed. It is noteworthy to mention that the bioink formulation was kept constant for all the hydrogels that were delivered from

different channels to isolate issues that may arise during optimization process. However, the spatial resolution would change in case of the extrusion of materials with different compositions.

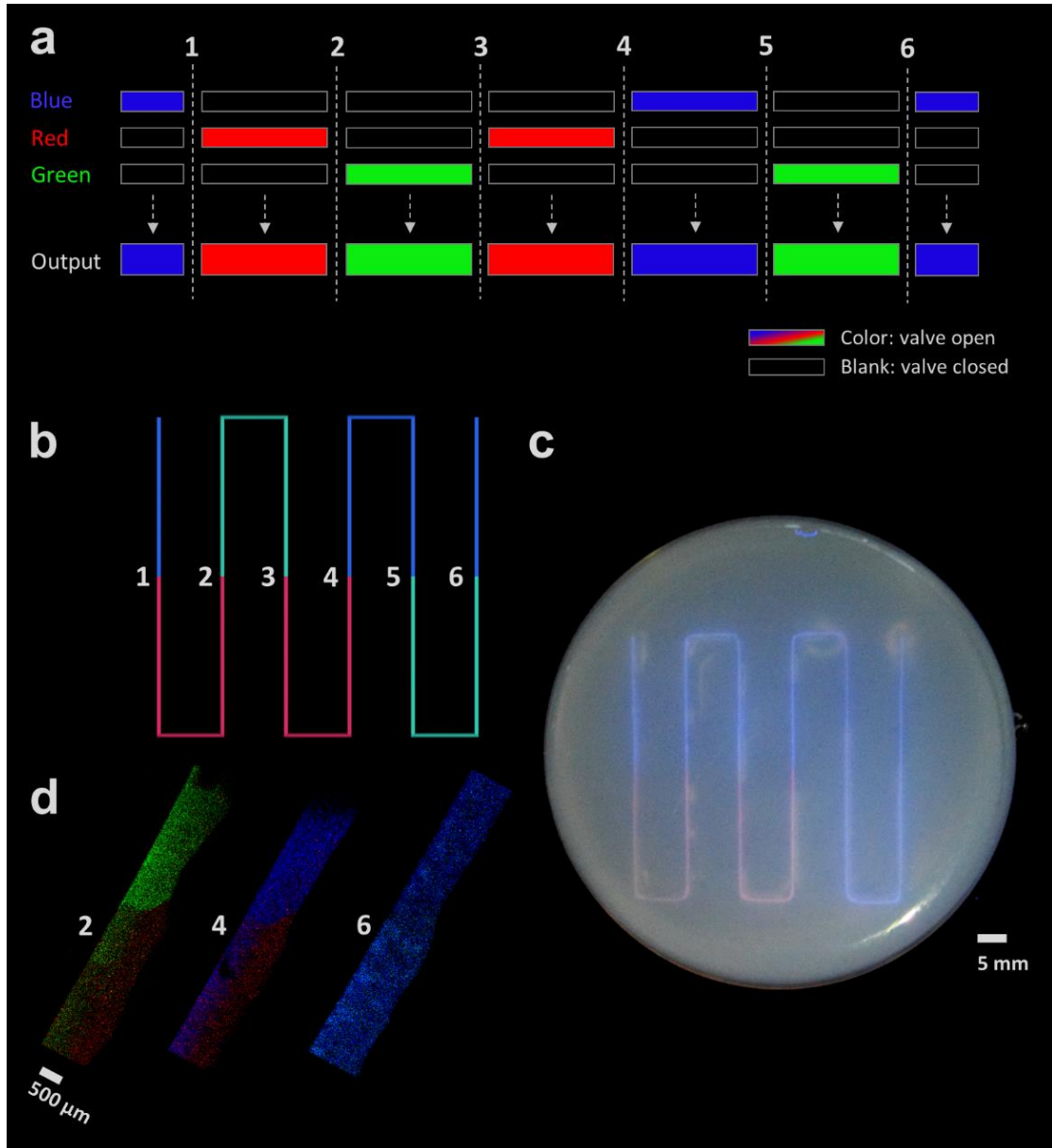


Figure 3.9 Investigation of transition regions. (a) Schematic of a code including transitions in between pressure-driven valves to evaluate hydrogel diffusion during transition. (b) Tool path planning of the continuous single stripe where transitions occur at 6 points. (c) Photograph of the continuous stripe that includes alternating extrusion of three different hydrogel solutions. (d) Confocal images of three parts of the continuous stripe where transitions occur between different fluorescent colors.

3.3.3. Multimaterial Printing of Complex-Shaped Structures Inside Support Bath

Following the optimization of extrusion parameters and investigation of pressure-driven valve transitions, embedded multimaterial printing studies were performed to evaluate printability of complex-shaped constructs with different material compositions.

Primarily, the initial letters of Sabanci University, letter S and letter U, were patterned inside the support bath (Figure 3.10). For the printing of these complex-shaped structures which include sharp turns and rapid position changes, blue and red fluorescent dyed hydrogels were extruded from the two channels of the microfluidic multimaterial printhead separately. While red fluorescent included hydrogel solution was deposited in outer two contours and blue fluorescent included hydrogel solution was deposited in inner two contours of the Letter S, deposition order was reversed for Letter U. Confocal microscope image clearly demonstrated the sequential deposition of the hydrogel solutions.

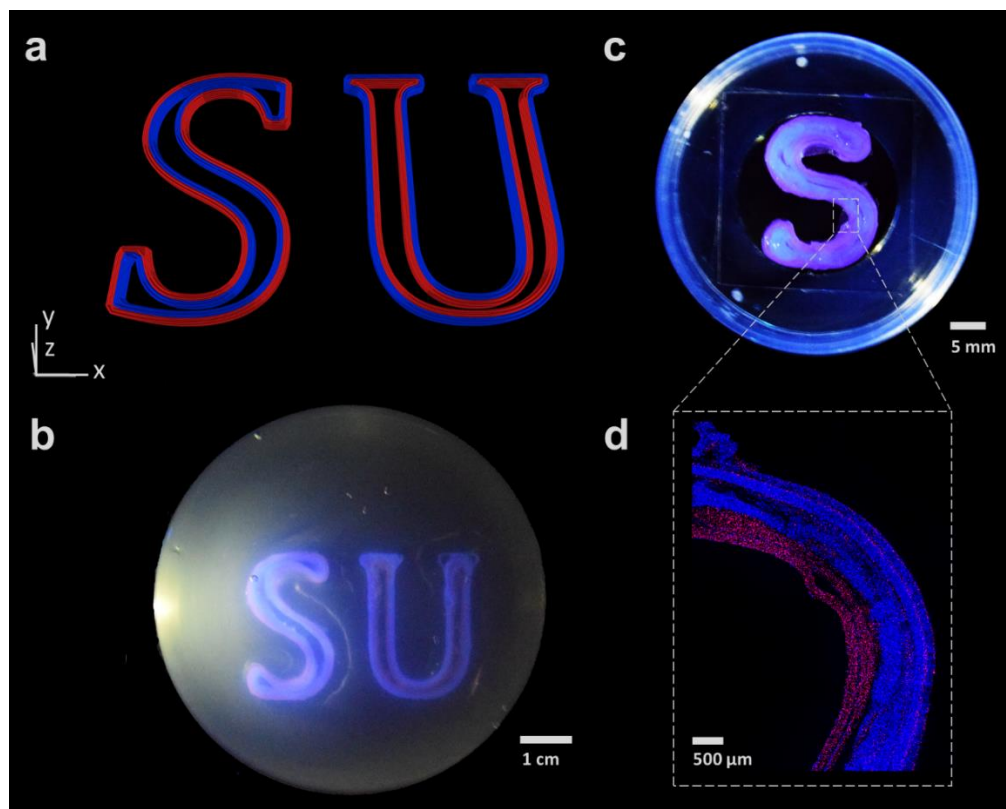


Figure 3.10 Embedded multimaterial printing of the initial letters of Sabanci University. (a) Tool path planning of the code which provides printing of structures with two

different material combinations. Photography of the printed structures (b) inside support bath and (c) after removal from the support bath. (d) Confocal image of the one part of the Letter S.

Following the successful printing of complex-shaped structures having two material compositions, embedded multimaterial printing with three fluorescently dyed hydrogel solutions was performed to prove capability of complex-shaped structures also with three material compositions (Figure 3.11). Tool path algorithm was planned in a way that six concentric contours of the four-layered cylindrical construct were patterned through the deposition of blue, red and green fluorescent dyed hydrogels in two outermost, three middle and one innermost contours, respectively. The same tool path planning was also employed for the biofabrication of aortic constructs. Printing the same structure previously without including the complexity of working with the living organisms ensured printing capability of the developed embedded multimaterial bioprinting platform for recapitulating the geometrical complexity of the native aortic tissues. In each of the four layers, six contours were patterned with three different hydrogels without encountering any valve transition issues.

3.1.Embedded Multimaterial Bioprinting of Vascular Constructs

This thesis work aims to recapitulate spatial heterogeneity, multicellular and multimaterial composition and hierarchical microarchitecture of native vascular tissues by developing an embedded multimaterial bioprinting platform for the biofabrication of vascular tissue substitutes. Sequential or simultaneous extrusion of multiple material combinations through the programmatic valve switching and patterning of complex-shaped structures with overhanging angles through the deposition into nanoclay-hydrogel support bath have enabled the fabrication of constructs with spatial heterogeneity and hierarchical microarchitecture. Capability of the developed embedded multimaterial bioprinting platform on this have been demonstrated through different optimization, valve interchangeability and embedded multimaterial printing experiments. Especially, multimaterial printing of a multi-layered cylindrical construct with six concentric contours in each layer evidenced the ability of the developed platform on mimicking hierarchical microarchitecture of native blood vessels.

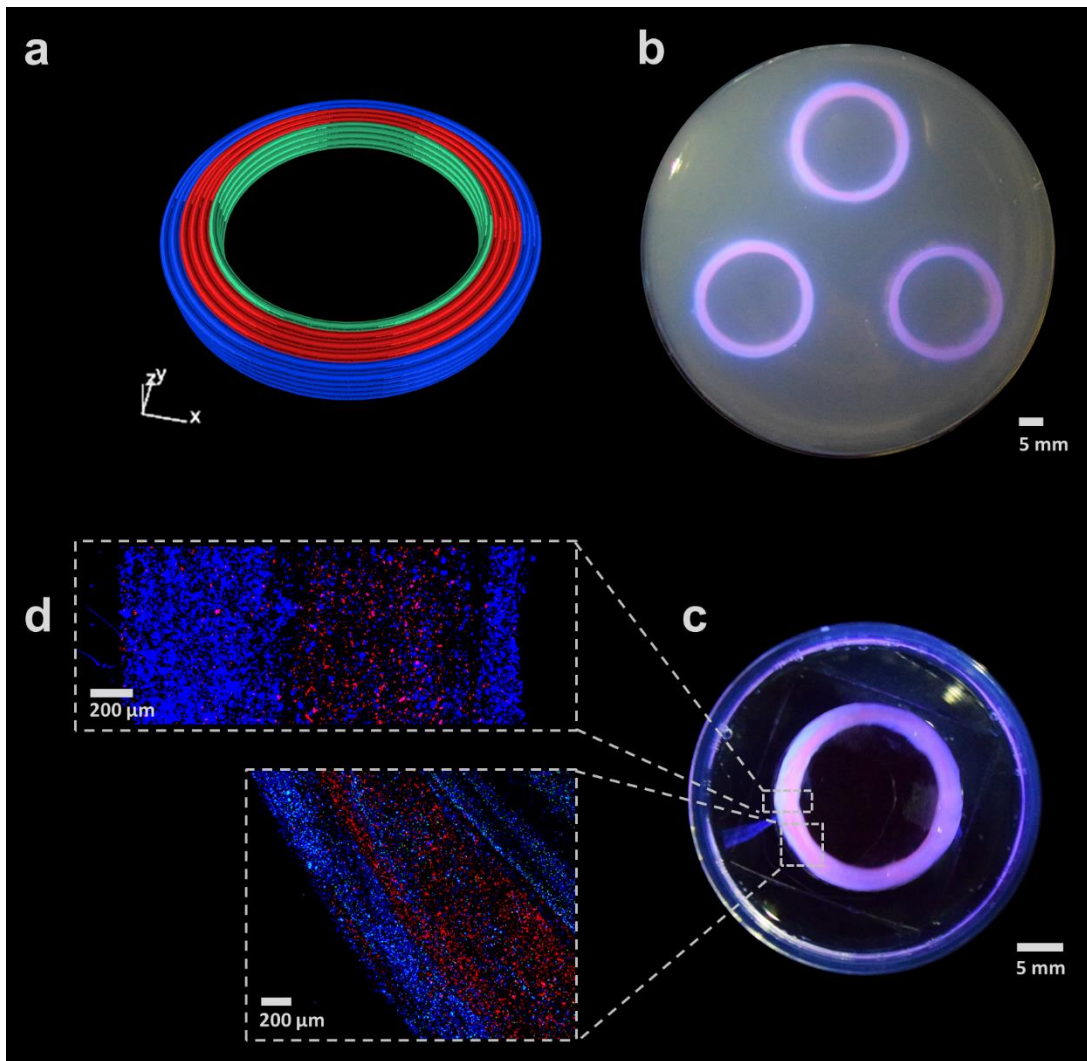


Figure 3.11 Embedded multimaterial printing of the four layered circular construct which includes three different material compositions. (a) Tool path planning of the code which provides printing of structures with three material combinations in different contours of each layer. Photography of the printed structures (b) inside support bath and (c) after removal from the support bath. (d) Confocal images of the two parts of the circular and concentric multilayered structure.

Extrusion of multiple type of cells existing in the native vascular tissues with a spatiotemporal control and continuation of their cellular viability are other parameters which needs to be investigated to demonstrate capability of the developed embedded multimaterial bioprinting platform on vascular tissue biofabrication. Even though their presence and thickness may vary depending on the type of vascular tissue, generally, blood vessels include three different type of layers: tunica intima comprised of endothelial

cells, tunica media comprised of smooth muscle cells and tunica adventitia which involve fibroblastic cells. These three different layers of the blood vessels bring different functionalities to the vascular tissue. In this regard, for mimicking multicellular and multimaterial composition of vascular tissues together with spatiotemporal heterogeneity, three different types of cells were sequentially extruded from three different channels of the developed microfluidic multimaterial printhead into the novel support bath (Figure 3.12). Viability of the cells encapsulated within the extruded bioinks were evaluated at Day 1, 4 and 7. All types of cells retained their viability throughout the seven days period and their overall viability was above 95% at all three time-points.

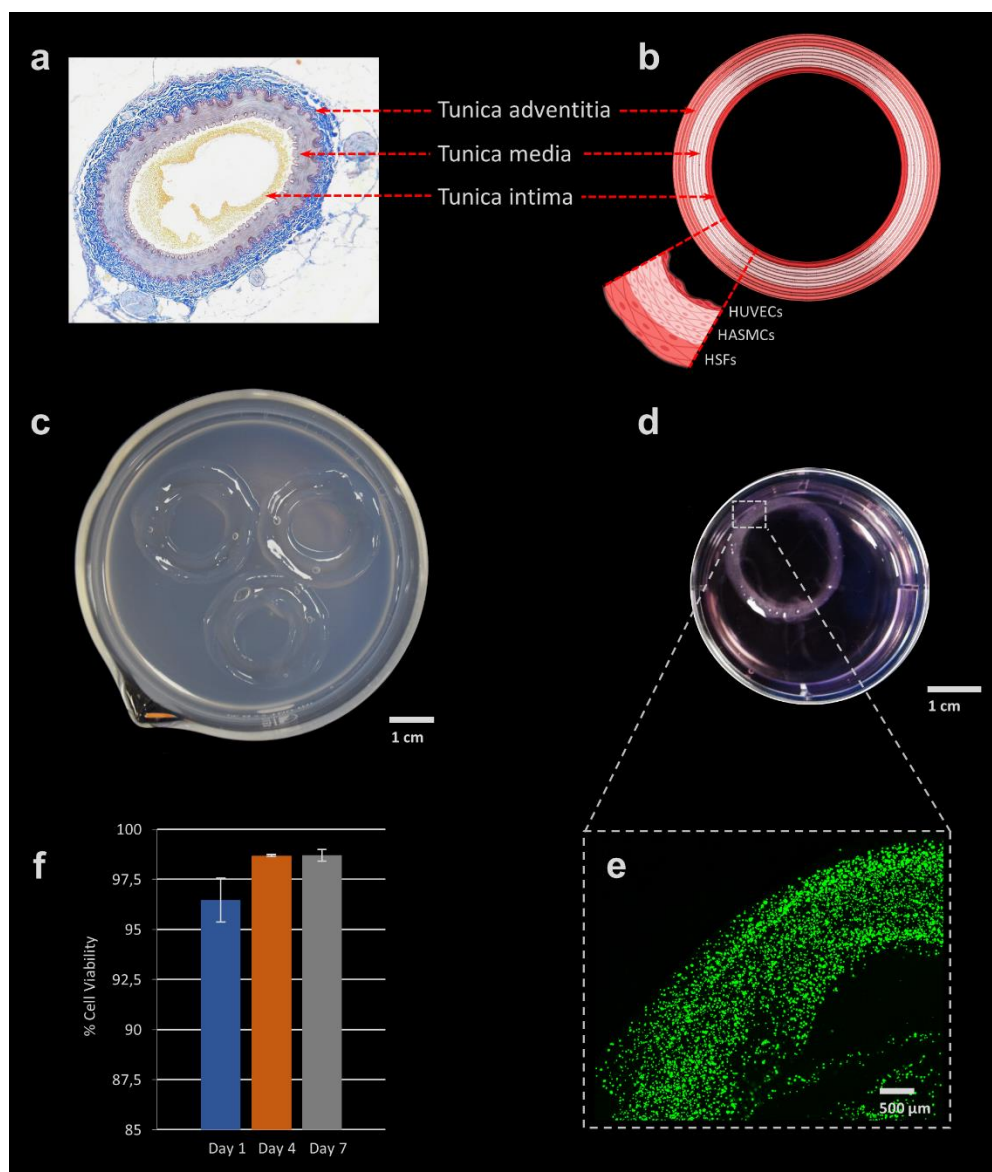


Figure 3.12 Embedded multimaterial bioprinting of three layers of the aortic construct incorporating six contours with bioink transitions in each layer. (a) Cross-sectional view

of the artery. (b) Top view of the aortic construct CAD model which includes concentric six contours: one contour, three contours and two contours resembling tunica intima, tunica media and tunica adventitia of the native aorta, respectively. Three different cell types were encapsulated within distinct bioink solutions. Photography of the bioprinted aortic constructs (c) inside support bath and (d) after removal from the support bath. (e) Confocal microscopy image of live and dead cells encapsulated within the biomanufactured aortic construct at Day 4. (f) Quantitative viability analysis of cells for Day 1, 4 and 7 after bioprinting.

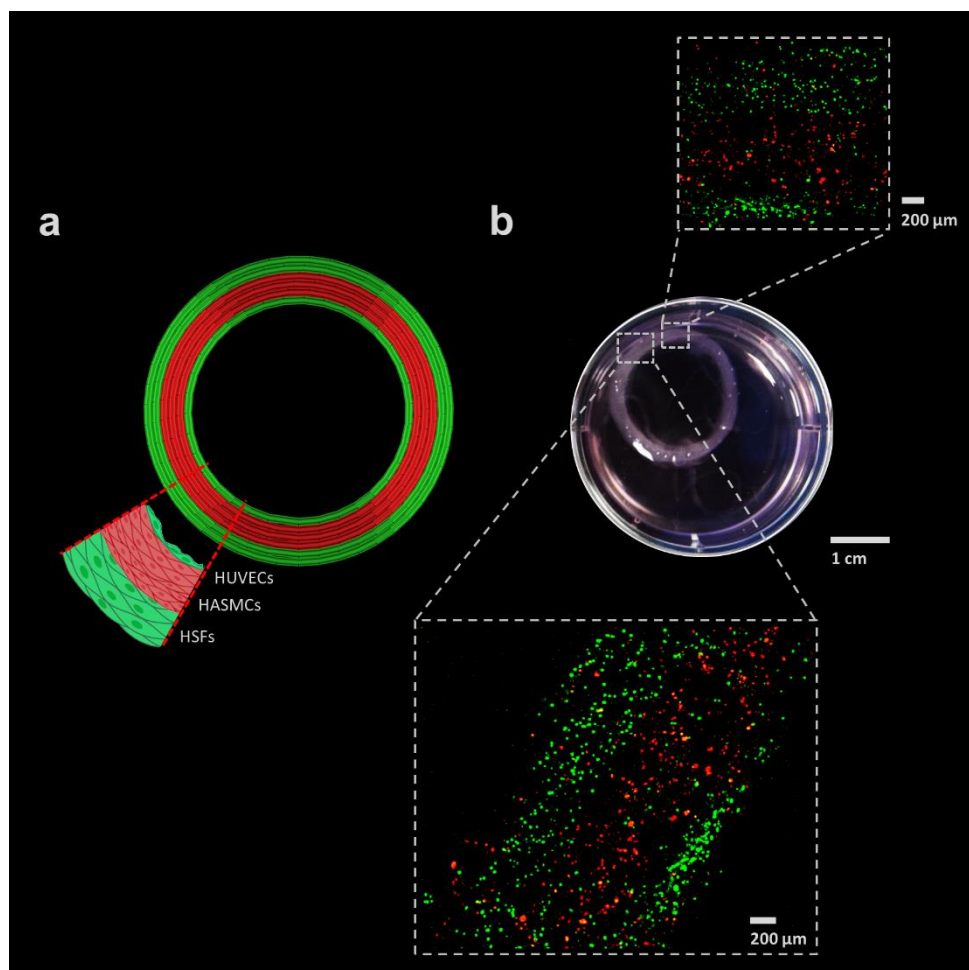


Figure 3.13 Demonstration of zonally stratified arrangement of the multimaterial bioprinted vascular constructs (a) Tool path planning of the aortic construct where HUVECs and HSFs were stained with green fluorescent tracker and HASMCs were stained with red fluorescent tracker. (b) Image of the bioprinted aortic construct together with confocal microscopy images of several regions

Following the investigation of biocompatibility of the developed embedded multimaterial bioprinting platform, zonally stratified arrangement of the biofabricated aortic constructs was also evaluated by incorporating green and red fluorescent dyes (Figure 3.13). Confocal images clearly demonstrate the arrangement of HUVECs in the innermost contour, HASMCs in the following three contours, and HSFs in the outermost two concentric contours which respectively mimics the arrangement of intimal, medial and adventitial layers of native vascular tissues. Diffusion was not observed in between the bioink solutions.

Multi-nozzle bioprinting platforms have been widely used for the biofabrication of constructs harboring multiple material combinations. However, these bioprinting platforms cause time delays due to printhead changeovers. The developed embedded multimaterial bioprinting platform, which possess multiple-channel microfluidic printhead, enables programmatic switching among different bioink formulations without encountering any time delays due to nozzle changeovers. Difference in the biofabrication time would be expressed through a multimaterial bioprinting scenario. A four-layered, 15 mm diameter cylindrical construct having six concentric contours in each layer is bioprinted within approximately 400 sec in the generated embedded multimaterial bioprinting platform. If the bioprinting platform was having a three-nozzles for extrusion, then 66 sec would be needed per each nozzle changeover, which makes 994 sec in total for that multimaterial construct. Together with reducing time delays happening as a result of printhead changeovers, the developed platform also prevents discontinuities and disruptions in the printing process. Sequentially or simultaneously extruded biological materials would be patterned continuously.

4. CONCLUSIONS AND FUTURE WORK

Bioprinting technology has demonstrated its potential for the biofabrication of artificial tissues and organs as it enables the generation of vascular or complex-shaped vascularized constructs in a spatially controlled manner. Recently developed multimaterial bioprinting approaches have further advanced the bioprinting technology over the course of fabricating anatomically correct, structurally and mechanically relevant and biologically functional structures, thanks to its capability to recapitulate multiscale microarchitecture of living tissues and organs including multiple cell types and ECM components. Multimaterial bioprinting approaches have incorporated spatial heterogeneity, multicellular and multimaterial composition and hierarchical microarchitecture into these structures by employing different strategies. Initially, multi-head multimaterial bioprinting approach was introduced, in which heterogeneous materials are dispensed from multiple printheads. Although this multimaterial bioprinting approach increased the degree of complexity in the fabricated tissue substitutes, the alignment of printheads affects precise patterning of bioinks and fabrication times increase, which led to the emergence of other multimaterial bioprinting approaches. Laser-based multimaterial bioprinting approaches have also been developed with capability of deposition in high resolutions, however scaling up and biocompatibility problems of the process needs to be resolved to be effectively used in tissue engineering. Coaxial multimaterial bioprinting and microfluidic multimaterial bioprinting approaches were developed as alternatives. While coaxial multimaterial bioprinting has been greatly welcomed for the biofabrication of tubular structures, incorporation of microfluidics technology into the multimaterial bioprinting has enhanced the control over the manipulation of the deposited fluidics with micron-level resolution. Moreover, in microfluidic multimaterial bioprinting, unlimited number of bioinks may be deposited with fast and smooth switching without any time delay.

Various multimaterial bioprinting approaches have been administered for approximating to the zonally stratified, heterocellular and hierarchically organized nature of vascular tissues. Among these approaches, coaxial multimaterial bioprinting has been extensively incorporated for the engineering of tubular constructs with distinct intimal, medial and adventitial layers as the core-shell arrangement of the printhead closely resembles the concentric structure of the blood vessels. Despite its capability for extruding meter-long vascular-like constructs, this approach exhibits limitations in the recapitulation of branched vascular tissues. However, microfluidic multimaterial bioprinting approaches, especially the ones that are combined with coaxial nozzles possess the capability of fully resembling the native vascular tissues and more study should be performed harboring microfluidic printheads. Further, integration of the approach with embedded bioprinting technique would also support the creation of freeform, multiscale vascular constructs.

In this thesis work, microfluidic-based multimaterial bioprinting platform combined with embedded bioprinting technique was developed, which have demonstrated its potential for the biofabrication of vascular tissues recapitulating both multicellular and multilayered hierarchical arrangement and complex geometrical shape of native vascular tissues. Multiple-channel microfluidic printhead designed in this work enabled the deposition of three different bioink formulations sequentially or simultaneously in a fully-automated and controlled manner. Bioink solutions were not mixed before deposition as they were delivered from and flowed through distinct microcapillary channels. Due to low mechanical strength, the printed hydrogels may not be strong enough to hold overhanging structures. In this context, extruded bioink formulations were patterned into a novel hydrogel-nanoclay support bath. Following the development of embedded multimaterial bioprinting platform incorporating the combination of microfluidic multimaterial printhead and in-gel printing technologies, CAD modeling and tool path planning of complex-shaped structures and vascular constructs were performed. Human abdominal aorta was biomodelled and then transformed into G-code through the generated tool path algorithm. Embedded multimaterial printing studies have demonstrated the capabilities of the developed platform on precise and controlled deposition of multiple materials with smooth valve transitions and on the generation of complex-shaped structures with high accuracy. Embedded multimaterial bioprinting studies has demonstrated the biofabrication of aortic vascular constructs with zonally

stratified, multicellular and concentric arrangement without damaging the viability of the various types of cells.

On the way of engineering of anatomically correct, structurally and mechanically relevant and biologically functional vascular constructs, the developed embedded multimaterial bioprinting platform would be improved in different aspects. In this study, alginate-GelMA blend bioink was employed in the biofabrication of all three different layers of vascular construct; however, different bioink formulations meeting the biological and mechanical needs of each vascular layers would be employed and loaded into hydrogel reservoirs. As hydrogel reservoirs are connected to separate dispensing pressure units, different feeding pressures required for the extrusion of different types of materials would be supplied. Printing speed would also be changed according to the type of biological material that will be extruded. Moreover, improvements would also be held on biomodelling and tool path planning of 3D bioprinting process. Most of the vascular constructs have branched and multi-scaled anatomies where presence and thickness of each vascular layers change spatiotemporally. Even though the multimaterial printing studies have confirmed the capabilities of embedded multimaterial bioprinting platform on the manufacturing of complex-shaped structures in different scales and geometries, bioprinting of branched and multi-scaled vascular-like constructs needs to be investigated. Another improvement on the biofabrication of vascular tissues would be realized through the integration of bioreactors into the biofabrication process to mimic dynamic conditions of the human body. Dynamic culture would promote viability and functionality of the cells encapsulated within the bioinks.

Building functional vascular networks within the created constructs has an enormous vitality for the engineering of physiologically-relevant artificial tissues and organs as vascular networks supply nutrients and oxygens to the cells, which is not achievable through diffusion into the engineered thick constructs above 150-200 μm distance. In this regard, various tissue engineering techniques have been employed but the generation of fully-functional vascularized tissues has remained as a grand challenge. Incorporation of multimaterial bioprinting has brought a different dimension and significantly advanced the field, however reconstruction of fully functional, multilayered and multiscale vascular networks within the engineered tissues have not been demonstrated yet and requires extensive research. The embedded multimaterial bioprinting platform developed in this

thesis may be employed for the biofabrication of vascularized tissues. Number of microchannels present in the multimaterial printhead would be increased and one or two types of bioinks would be extruded through the microchannels, while other microchannels are reserved for the delivery of targeted tissue-specific bioink formulations. By this means, vascularized tissue substitutes harboring multiple types of cells and ECM cues would be biofabricated.

BIBLIOGRAPHY

- Afghah, Ferdows, Mine Altunbek, Caner Dikyol, and Bahattin Koc. 2020. "Preparation and Characterization of Nanoclay-Hydrogel Composite Support-Bath for Bioprinting of Complex Structures." *Scientific Reports* 10 (1): 5257. <https://doi.org/10.1038/s41598-020-61606-x>.
- Ahearne, Mark. 2014. "Introduction to Cell – Hydrogel Mechanosensing." *Royal Society Interface* (2): 20130038. <https://doi.org/10.1098/rsfs.2013.0038>.
- Akkineni, Ashwini Rahul, Tilman Ahlfeld, Anja Lode, and Michael Gelinsky. 2016. "A Versatile Method for Combining Different Biopolymers in a Core/Shell Fashion by 3D Plotting to Achieve Mechanically Robust Constructs." *Biofabrication* 8 (4): 45001. <https://doi.org/10.1088/1758-5090/8/4/045001>.
- Antich, Cristina, Juan de Vicente, Gema Jiménez, Carlos Chocarro, Esmeralda Carrillo, Elvira Montañez, Patricia Gálvez-Martín, and Juan Antonio Marchal. 2020. "Bio-Inspired Hydrogel Composed of Hyaluronic Acid and Alginate as a Potential Bioink for 3D Bioprinting of Articular Cartilage Engineering Constructs." *Acta Biomaterialia* 106: 114–23. <https://doi.org/10.1016/j.actbio.2020.01.046>.
- Antoshin, A A, S N Churbanov, N V Minaev, Deying Zhang, Yuanyuan Zhang, A I Shpichka, and P S Timashev. 2019. "LIFT-Bioprinting, Is It Worth It?" *Bioprinting* 15: e00052. <https://doi.org/https://doi.org/10.1016/j.bprint.2019.e00052>.
- Attalla, R, C Ling, and P Selvaganapathy. 2016. "Fabrication and Characterization of Gels with Integrated Channels Using 3D Printing with Microfluidic Nozzle for Tissue Engineering Applications." *Biomedical Microdevices* 18 (1): 17. <https://doi.org/10.1007/s10544-016-0042-6>.
- Attalla, Rana, Erin Puersten, Nidhi Jain, and P. Selvaganapathy. 2018. "3D Bioprinting of Heterogeneous Bi- and Tri-Layered Hollow Channels within Gel Scaffolds Using Scalable Multi-Axial Microfluidic Extrusion Nozzle." *Biofabrication*. <https://doi.org/10.1016/j.cej.2007.09.011>.
- Au, Pek Ing, Siti Hassan, Jishan Liu, and Yee Kwong Leong. 2015. "Behaviour of Laponite Gels: Rheology, Ageing, PH Effect and Phase State in the Presence of Dispersant." *Chemical Engineering Research and Design* 101: 65–73. <https://doi.org/10.1016/j.cherd.2015.07.023>.
- Bakirci, E, B Toprakhisar, M C Zeybek, G O Ince, and B Koc. 2017. "Cell Sheet Based Bioink for 3D Bioprinting Applications." *Biofabrication* 9 (2): 24105. <https://doi.org/10.1088/1758-5090/aa764f>.
- Barron, J A, P Wu, H D Ladouceur, and B R Ringeisen. 2004. "Biological Laser Printing: A Novel Technique for Creating Heterogeneous 3-Dimensional Cell Patterns." *Biomedical Microdevices* 6 (2): 139–47. <https://doi.org/10.1023/B:BMMD.0000031751.67267.9f>.

- Beyer, S. T., A. Bsoul, A. Ahmadi, and K. Walus. 2013. "3D Alginate Constructs for Tissue Engineering Printed Using a Coaxial Flow Focusing Microfluidic Device." *2013 Transducers and Eurosensors XXVII: The 17th International Conference on Solid-State Sensors, Actuators and Microsystems, TRANSDUCERS and EUROSENSORS 2013*, no. June: 1206–9. <https://doi.org/10.1109/Transducers.2013.6626990>.
- Beyer, Simon Travis, Tamer Mohamed, and Konrad Walus. 2013. "A Microfluidics Based 3D Bioprinter with On-the-Fly Multimaterial Switching Capability." *17th International Conference on Miniaturized Systems for Chemistry and Life Sciences, MicroTAS 2013 1* (October): 176–78.
- Bhattacharjee, T., S. M. Zehnder, K. G. Rowe, S. Jain, R. M. Nixon, W. G. Sawyer, and T. E. Angelini. 2015. "Writing in the Granular Gel Medium." *Science Advances* 1 (8): e1500655–e1500655. <https://doi.org/10.1126/sciadv.1500655>.
- Boucenna, Imane, Laurent Royon, Pierre Colinart, Marie Alice Guedeau-Boudeville, and Ahmed Mouchid. 2010. "Structure and Thermorheology of Concentrated Pluronic Copolymer Micelles in the Presence of Laponite Particles." *Langmuir* 26 (18): 14430–36. <https://doi.org/10.1021/la102744c>.
- Bulcke, An I Van Den, Bogdan Bogdanov, Nadine De Rooze, Etienne H Schacht, Maria Cornelissen, and Hugo Berghmans. 2000. "Structural and Rheological Properties of Methacrylamide Modified Gelatin Hydrogels." *Biomacromolecules* 1 (1): 31–38. <https://doi.org/10.1021/bm990017d>.
- Burak, Jakub, Kamil P. Grela, Janusz Pluta, Bożena Karolewicz, and Dominik M. Marciniak. 2018. "Impact of Sterilisation Conditions on the Rheological Properties of Thermoresponsive Pluronic F-127-Based Gels for the Ophthalmic Use." *Acta Poloniae Pharmaceutica - Drug Research* 75 (2): 471–81.
- Burdick, Jason A, and Molly M Stevens. 2005. "Chapter 11 - Biomedical Hydrogels." In *Biomaterials, Artificial Organs and Tissue Engineering*, edited by Larry L Hench and Julian R B T - Biomaterials Jones Artificial Organs and Tissue Engineering, 107–15. Woodhead Publishing Series in Biomaterials. <https://doi.org/https://doi.org/10.1533/9781845690861.2.107>.
- Byambaa, Batzaya, Nasim Annabi, Kan Yue, Grissel Trujillo-de Santiago, Mario Moisés Alvarez, Weitao Jia, Mehdi Kazemzadeh-Narbat, Su Ryon Shin, Ali Tamayol, and Ali Khademhosseini. 2017. "Bioprinted Osteogenic and Vasculogenic Patterns for Engineering 3D Bone Tissue." *Advanced Healthcare Materials* 6 (16): 1700015. <https://doi.org/10.1002/adhm.201700015>.
- Campbell, Jennifer, Ian McGuinness, Holger Wirz, Andre Sharon, and Alexis F. Sauer-Budge. 2015. "Multimaterial and Multiscale Three-Dimensional Bioprinter." *Journal of Nanotechnology in Engineering and Medicine* 6 (2): 1–7. <https://doi.org/10.1115/1.4031230>.
- Campos, Daniela F.Duarte, Midhun A. Philip, Stefanie Gürzing, Christoph Melcher, Ying Ying Lin, Jan Schöneberg, Andreas Blaeser, Benjamin Theek, Horst Fischer, and Marcel Betsch. 2019. "Synchronized Dual Bioprinting of Bioinks and Biomaterial Inks as a Translational Strategy for Cartilage Tissue Engineering." *3D Printing and Additive Manufacturing* 6 (2): 63–71. <https://doi.org/10.1089/3dp.2018.0123>.

- Carrabba, Michele, and Paolo Madeddu. 2018. "Current Strategies for the Manufacture of Small Size Tissue Engineering Vascular Grafts." *Frontiers in Bioengineering and Biotechnology* 6 (APR): 1–12. <https://doi.org/10.3389/fbioe.2018.00041>.
- Castelletto, V., I. A. Ansari, and I. W. Hamley. 2003. "Influence of Added Clay Particles on the Structure and Rheology of a Hexagonal Phase Formed by an Amphiphilic Block Copolymer in Aqueous Solution." *Macromolecules* 36 (5): 1694–1700. <https://doi.org/10.1021/ma021396x>.
- Chan, Vincent, Pinar Zorlutuna, Jae Hyun Jeong, Hyunjoon Kong, and Rashid Bashir. 2010. "Three-Dimensional Photopatterning of Hydrogels Using Stereolithography for Long-Term Cell Encapsulation." *Lab on a Chip* 10 (16): 2062–70. <https://doi.org/10.1039/C004285D>.
- Chang, Chien Wen, Ariane Van Spreeuwel, Chao Zhang, and Shyni Varghese. 2010. "PEG/Clay Nanocomposite Hydrogel: A Mechanically Robust Tissue Engineering Scaffold." *Soft Matter* 6 (20): 5157–64. <https://doi.org/10.1039/c0sm00067a>.
- Choi, Jane Ru, Kar Wey Yong, Jean Yu Choi, and Alistair C Cowie. 2019. "Recent Advances in Photo-Crosslinkable Hydrogels for Biomedical Applications." *BioTechniques* 66 (1): 40–53. <https://doi.org/10.2144/btn-2018-0083>.
- Choi, Yeong-Jin, Young-Joon Jun, Dong Yeon Kim, Hee-Gyeong Yi, Su-Hun Chae, Junsu Kang, Juyong Lee, et al. 2019. "A 3D Cell Printed Muscle Construct with Tissue-Derived Bioink for the Treatment of Volumetric Muscle Loss." *Biomaterials* 206: 160–69. <https://doi.org/https://doi.org/10.1016/j.biomaterials.2019.03.036>.
- Coen, Matteo, Giulio Gabbiani, Marie-Luce Bochaton-Piallat, and Y Eugene Chen. 2011. "Myofibroblast-Mediated Adventitial Remodeling." *Arteriosclerosis, Thrombosis, and Vascular Biology* 31 (11): 2391–96. <https://doi.org/10.1161/ATVBAHA.111.231548>.
- Colosi, Cristina, Su Ryon Shin, Vijayan Manoharan, Solange Massa, Marco Costantini, Andrea Barbetta, Mehmet Remzi Dokmeci, Mariella Dentini, and Ali Khademhosseini. 2016. "Microfluidic Bioprinting of Heterogeneous 3D Tissue Constructs Using Low-Viscosity Bioink." *Advanced Materials* 28 (4): 677–84. <https://doi.org/10.1002/adma.201503310>.
- Compaan, Ashley M., Kaidong Song, and Yong Huang. 2019. "Gellan Fluid Gel as a Versatile Support Bath Material for Fluid Extrusion Bioprinting." Research-article. *ACS Applied Materials and Interfaces* 11: 5714–26. <https://doi.org/10.1021/acsami.8b13792>.
- Costantini, Marco, Stefano Testa, Pamela Mozetic, Andrea Barbetta, Claudia Fuoco, Ersilia Fornetti, Francesco Tamiro, et al. 2017. "Microfluidic-Enhanced 3D Bioprinting of Aligned Myoblast-Laden Hydrogels Leads to Functionally Organized Myofibers in Vitro and in Vivo." *Biomaterials* 131: 98–110. <https://doi.org/10.1016/j.biomaterials.2017.03.026>.
- Cui, Haitao, Wei Zhu, Yimin Huang, Chengyu Liu, Zu-Xi Yu, Margaret Nowicki, Shida Miao, et al. 2019. "In Vitro and in Vivo Evaluation of 3D Bioprinted Small-Diameter Vasculature with Smooth Muscle and Endothelium." *Biofabrication* 12 (1): 15004. <https://doi.org/10.1088/1758-5090/ab402c>.

- Cui, Haitao, Wei Zhu, Margaret Nowicki, Xuan Zhou, Ali Khademhosseini, and Lijie Grace Zhang. 2016. "Hierarchical Fabrication of Engineered Vascularized Bone Biphasic Constructs via Dual 3D Bioprinting: Integrating Regional Bioactive Factors into Architectural Design." *Advanced Healthcare Materials* 5 (17): 2174–81. <https://doi.org/10.1002/adhm.201600505>.
- Dai, Xingliang, Libiao Liu, Jia Ouyang, Xinda Li, Xinzhi Zhang, Qing Lan, and Tao Xu. 2017. "Coaxial 3D Bioprinting of Self-Assembled Multicellular Heterogeneous Tumor Fibers." *Scientific Reports* 7 (1): 1457. <https://doi.org/10.1038/s41598-017-01581-y>.
- Das, Sanskrita, Seok Won Kim, Yeong Jin Choi, Sooyeon Lee, Se Hwan Lee, Jeong Sik Kong, Hun Jun Park, Dong Woo Cho, and Jinah Jang. 2019. "Decellularized Extracellular Matrix Bioinks and the External Stimuli to Enhance Cardiac Tissue Development in Vitro." *Acta Biomaterialia* 95: 188–200. <https://doi.org/10.1016/j.actbio.2019.04.026>.
- Datta, Pallab, Bugra Ayan, and Ibrahim T. Ozbolat. 2017. "Bioprinting for Vascular and Vascularized Tissue Biofabrication." *Acta Biomaterialia* 51: 1–20. <https://doi.org/10.1016/j.actbio.2017.01.035>.
- Dávila, José Luis, and Marcos Akira D'Ávila. 2017. "Laponite as a Rheology Modifier of Alginate Solutions: Physical Gelation and Aging Evolution." *Carbohydrate Polymers* 157: 1–8. <https://doi.org/10.1016/j.carbpol.2016.09.057>.
- Dickman, Christopher T.D., Valerio Russo, Katherine Thain, Sheng Pan, Simon T. Beyer, Konrad Walus, Spiro Getsios, Tamer Mohamed, and Sam J. Wadsworth. 2020. "Functional Characterization of 3D Contractile Smooth Muscle Tissues Generated Using a Unique Microfluidic 3D Bioprinting Technology." *FASEB Journal* 34 (1): 1652–64. <https://doi.org/10.1096/fj.201901063RR>.
- Ding, Houzhu, and Robert Chang. 2018. "Printability Study of Bioprinted Tubular Structures Using Liquid Hydrogel Precursors in a Support Bath." *Applied Sciences* 8 (3): 403. <https://doi.org/10.3390/app8030403>.
- Distler, Thomas, Florian Ruther, Aldo R. Boccaccini, and Rainer Detsch. 2019. "Development of 3D Biofabricated Cell Laden Hydrogel Vessels and a Low-Cost Desktop Printed Perfusion Chamber for In Vitro Vessel Maturation." *Macromolecular Bioscience* 19 (9). <https://doi.org/10.1002/mabi.201900245>.
- Dolati, Farzaneh, Yin Yu, Yahui Zhang, Aribet M De Jesus, Edward A Sander, and Ibrahim T Ozbolat. 2014. "In Vitro Evaluation of Carbon-Nanotube-Reinforced Bioprintable Vascular Conduits." *Nanotechnology* 25 (14): 145101. <https://doi.org/10.1088/0957-4484/25/14/145101>.
- Dreher, Rachel, and Binil Starly. 2015. "Biofabrication of Multimaterial Three-Dimensional Constructs Embedded with Patterned Alginate Strands Encapsulating PC12 Neural Cell Lines." *Journal of Nanotechnology in Engineering and Medicine* 6 (2): 1–8. <https://doi.org/10.1115/1.4031173>.
- Duarte Campos, Daniela F., Andreas Blaeser, Michael Weber, Jörg Jäkel, Sabine Neuss, Wilhelm Jahnen-Dechent, and Horst Fischer. 2013. "Three-Dimensional Printing of Stem Cell-Laden Hydrogels Submerged in a Hydrophobic High-Density Fluid." *Biofabrication* 5 (1). <https://doi.org/10.1088/1758-5082/5/1/015003>.

- Dubbin, Karen, Anthony Tabet, and Sarah C. Heilshorn. 2017. “Quantitative Criteria to Benchmark New and Existing Bio-Inks for Cell Compatibility.” *Biofabrication* 9 (4). <https://doi.org/10.1088/1758-5090/aa869f>.
- Duchi, Serena, Carmine Onofrillo, Cathal D. O’Connell, Romane Blanchard, Cheryl Augustine, Anita F. Quigley, Robert M.I. Kapsa, et al. 2017. “Handheld Co-Axial Bioprinting: Application to in Situ Surgical Cartilage Repair.” *Scientific Reports* 7 (1): 1–12. <https://doi.org/10.1038/s41598-017-05699-x>.
- Duocastella, M., J.M. Fernandez-Pradas, J. Dominguez, P. Serra, and J.L. Morenza. 2008. “Printing Biological Solutions through Laser-Induced Forward Transfer.” *Applied Physics A*, 941–45. <https://doi.org/10.1007/s00339-008-4741-6>.
- Ehrbar, M., A. Sala, P. Lienemann, A. Ranga, K. Mosiewicz, A. Bittermann, S. C. Rizzi, F. E. Weber, and M. P. Lutolf. 2011. “Elucidating the Role of Matrix Stiffness in 3D Cell Migration and Remodeling.” *Biophysical Journal* 100 (2): 284–93. <https://doi.org/10.1016/j.bpj.2010.11.082>.
- Faulkner-Jones, Alan, Catherine Fyfe, Dirk-Jan Cornelissen, John Gardner, Jason King, Aidan Courtney, and Wenmiao Shu. 2015. “Bioprinting of Human Pluripotent Stem Cells and Their Directed Differentiation into Hepatocyte-like Cells for the Generation of Mini-Livers in 3D.” *Biofabrication* 7 (4): 44102. <https://doi.org/10.1088/1758-5090/7/4/044102>.
- Feng, Fan, Jiankang He, Jiabin Li, Mao Mao, and Dichen Li. 2019. “Multicomponent Bioprinting of Heterogeneous Hydrogel Constructs Based on Microfluidic Printheads.” *International Journal of Bioprinting* 5 (2): 39–48. <https://doi.org/10.18063/ijb.v5i2.202>.
- Gaebel, Ralf, Dario Furlani, Heiko Sorg, Bianca Polchow, Johannes Frank, Karen Bieback, Weiwei Wang, et al. 2011. “Cell Origin of Human Mesenchymal Stem Cells Determines a Different Healing Performance in Cardiac Regeneration.” *PLoS ONE* 6 (2). <https://doi.org/10.1371/journal.pone.0015652>.
- Gaebel, Ralf, Nan Ma, Jun Liu, Jianjun Guan, Lothar Koch, Christian Klopsch, Martin Gruene, et al. 2011. “Patterning Human Stem Cells and Endothelial Cells with Laser Printing for Cardiac Regeneration.” *Biomaterials* 32 (35): 9218–30. <https://doi.org/https://doi.org/10.1016/j.biomaterials.2011.08.071>.
- Gaharwar, Akhilesh K., Lauren M. Cross, Charles W. Peak, Karli Gold, James K. Carrow, Anna Brokesh, and Kanwar Abhay Singh. 2019. “2D Nanoclay for Biomedical Applications: Regenerative Medicine, Therapeutic Delivery, and Additive Manufacturing.” *Advanced Materials* 31 (23): 1–28. <https://doi.org/10.1002/adma.201900332>.
- Gaharwar, Akhilesh K., Patrick J. Schexnailder, Benjamin P. Kline, and Gudrun Schmidt. 2011. “Assessment of Using Laponite® Cross-Linked Poly(Ethylene Oxide) for Controlled Cell Adhesion and Mineralization.” *Acta Biomaterialia* 7 (2): 568–77. <https://doi.org/10.1016/j.actbio.2010.09.015>.
- Gao, Ge, Hyeok Kim, Byoung Soo Kim, Jeong Sik Kong, Jae Yeon Lee, Bong Woo Park, Suhun Chae, et al. 2019. “Tissue-Engineering of Vascular Grafts Containing Endothelium and Smooth-Muscle Using Triple-Coaxial Cell Printing.” *Applied Physics Reviews* 6 (4). <https://doi.org/10.1063/1.5099306>.

- Gao, Ge, Jun Hee Lee, Jinah Jang, Dong Han Lee, Jeong Sik Kong, Byoung Soo Kim, Yeong Jin Choi, et al. 2017. "Tissue Engineered Bio-Blood-Vessels Constructed Using a Tissue-Specific Bioink and 3D Coaxial Cell Printing Technique: A Novel Therapy for Ischemic Disease." *Advanced Functional Materials* 27 (33): 1–12. <https://doi.org/10.1002/adfm.201700798>.
- Gao, Ge, Ju Young Park, Byoung Soo Kim, Jinah Jang, and Dong Woo Cho. 2018. "Coaxial Cell Printing of Freestanding, Perfusable, and Functional In Vitro Vascular Models for Recapitulation of Native Vascular Endothelium Pathophysiology." *Advanced Healthcare Materials* 7 (23): 1–12. <https://doi.org/10.1002/adhm.201801102>.
- Gao, Qing, Yong He, Jian zhong Fu, An Liu, and Liang Ma. 2015. "Coaxial Nozzle-Assisted 3D Bioprinting with Built-in Microchannels for Nutrients Delivery." *Biomaterials* 61: 203–15. <https://doi.org/10.1016/j.biomaterials.2015.05.031>.
- Gao, Qing, Zhenjie Liu, Zhiwei Lin, Jingjiang Qiu, Yu Liu, An Liu, Yidong Wang, et al. 2017. "3D Bioprinting of Vessel-like Structures with Multilevel Fluidic Channels." *ACS Biomaterials Science and Engineering* 3 (3): 399–408. <https://doi.org/10.1021/acsbmaterials.6b00643>.
- Ghanizadeh Tabriz, Atabak, Christopher G Mills, John J Mullins, Jamie A Davies, and Wenmiao Shu. 2017. "Rapid Fabrication of Cell-Laden Alginate Hydrogel 3D Structures by Micro Dip-Coating." *Frontiers in Bioengineering and Biotechnology* 5: 13. <https://doi.org/10.3389/fbioe.2017.00013>.
- Grosskopf, Abigail K., Ryan L. Truby, Hyoungsoo Kim, Antonio Perazzo, Jennifer A. Lewis, and Howard A. Stone. 2018. "Viscoplastic Matrix Materials for Embedded 3D Printing." Research-article. *ACS Applied Materials and Interfaces* 10 (27): 23353–61. <https://doi.org/10.1021/acsaami.7b19818>.
- Gruene, Martin, Michael Pflaum, Christian Hess, Stefanos Diamantouros, Sabrina Schlie, Andrea Deiwick, Lothar Koch, et al. 2011. "Laser Printing of Three-Dimensional Multicellular Arrays for Studies of Cell-Cell and Cell-Environment Interactions." *Tissue Engineering - Part C: Methods* 17 (10): 973–82. <https://doi.org/10.1089/ten.tec.2011.0185>.
- Gudupati, Hemanth, Madhuri Dey, and Ibrahim Ozbolat. 2016. "A Comprehensive Review on Droplet-Based Bioprinting: Past, Present and Future." *Biomaterials*. <https://doi.org/10.1016/j.biomaterials.2016.06.012>.
- Guillotin, Bertrand, Agnès Souquet, Sylvain Catros, Martí Duocastella, Benjamin Pippenger, Séverine Bellance, Reine Bareille, et al. 2010. "Laser Assisted Bioprinting of Engineered Tissue with High Cell Density and Microscale Organization." *Biomaterials* 31 (28): 7250–56. <https://doi.org/10.1016/j.biomaterials.2010.05.055>.
- Halper, Jaroslava. 2018. "Basic Components of Vascular Connective Tissue and Extracellular Matrix." *Advances in Pharmacology (San Diego, Calif.)* 81: 95—127. <https://doi.org/10.1016/bs.apha.2017.08.012>.
- Han, Li-Hsin, Shalu Suri, Christine E Schmidt, and Shaochen Chen. 2010. "Fabrication of Three-Dimensional Scaffolds for Heterogeneous Tissue Engineering." *Biomedical Microdevices* 12 (4): 721–25. <https://doi.org/10.1007/s10544-010->

9425-2.

- Haraguchi, Kazutoshi, Robin Farnworth, Akira Ohbayashi, and Toru Takehisa. 2003. "Compositional Effects on Mechanical Properties of Nanocomposite Hydrogels Composed of Poly(N,N-Dimethylacrylamide) and Clay." *Macromolecules* 36 (15): 5732–41. <https://doi.org/10.1021/ma034366i>.
- Hardin, James O., Thomas J. Ober, Alexander D. Valentine, and Jennifer A. Lewis. 2015. "Microfluidic Printheads for Multimaterial 3D Printing of Viscoelastic Inks." *Advanced Materials* 27 (21): 3279–84. <https://doi.org/10.1002/adma.201500222>.
- Hasan, Anwarul, Arghya Paul, Adnan Memic, and Ali Khademhosseini. 2015. "A Multilayered Microfluidic Blood Vessel-like Structure." *Biomedical Microdevices* 17 (5): 88. <https://doi.org/10.1007/s10544-015-9993-2>.
- He, Jianyu, Junshi Shao, Xinda Li, Qing Huang, and Tao Xu. 2018. "Bioprinting of Coaxial Multicellular Structures for a 3D Co-Culture Model." *Bioprinting* 11: e00036. <https://doi.org/https://doi.org/10.1016/j.bprint.2018.e00036>.
- He, Qi, Wei Yu, Youjun Wu, and Chixing Zhou. 2012. "Shear Induced Phase Inversion of Dilute Smectic Liquid Crystal/Polymer Blends." *Soft Matter* 8 (10): 2992–3001. <https://doi.org/10.1039/c2sm06963f>.
- Heinrich, Marcel Alexander, Ruchi Bansal, Twan Lammers, Yu Shrike Zhang, Raymond Michel Schiffelers, and Jai Prakash. 2019. "3D-Bioprinted Mini-Brain: A Glioblastoma Model to Study Cellular Interactions and Therapeutics." *Advanced Materials* 31 (14): 1–9. <https://doi.org/10.1002/adma.201806590>.
- Higley, Christopher B., Christopher B. Rodell, and Jason A. Burdick. 2015. "Direct 3D Printing of Shear-Thinning Hydrogels into Self-Healing Hydrogels." *Advanced Materials* 27 (34): 5075–79. <https://doi.org/10.1002/adma.201501234>.
- Hinton, Thomas J., Andrew Hudson, Kira Pusch, Andrew Lee, and Adam W. Feinberg. 2016. "3D Printing PDMS Elastomer in a Hydrophilic Support Bath via Freeform Reversible Embedding." *ACS Biomaterials Science and Engineering* 2 (10): 1781–86. <https://doi.org/10.1021/acsbiomaterials.6b00170>.
- Hinton, Thomas J., Quentin Jallerat, Rachelle N. Palchesko, Joon Hyung Park, Martin S. Grodzicki, Hao Jan Shue, Mohamed H. Ramadan, Andrew R. Hudson, and Adam W. Feinberg. 2015. "Three-Dimensional Printing of Complex Biological Structures by Freeform Reversible Embedding of Suspended Hydrogels." *Science Advances* 1 (9). <https://doi.org/10.1126/sciadv.1500758>.
- Hoch, Eva, Christian Schuh, Thomas Hirth, Günter E M Tovar, and Kirsten Borchers. 2012. "Stiff Gelatin Hydrogels Can Be Photo-Chemically Synthesized from Low Viscous Gelatin Solutions Using Molecularly Functionalized Gelatin with a High Degree of Methacrylation." *Journal of Materials Science: Materials in Medicine* 23 (11): 2607–17. <https://doi.org/10.1007/s10856-012-4731-2>.
- Holland, Ian, Jack Logan, Jiezhong Shi, Christopher McCormick, Dongsheng Liu, and Wenmiao Shu. 2018. "3D Biofabrication for Tubular Tissue Engineering." *Bio-Design and Manufacturing* 1 (2): 89–100. <https://doi.org/10.1007/s42242-018-0013-2>.

- Holzappel, Gerhard A, Gerhard Sommer, Martin Auer, Peter Regitnig, and Ray W Ogden. 2007. "Layer-Specific 3D Residual Deformations of Human Aortas with Non-Atherosclerotic Intimal Thickening." *Annals of Biomedical Engineering* 35 (4): 530–45. <https://doi.org/10.1007/s10439-006-9252-z>.
- Hölzl, Katja, Shengmao Lin, Liesbeth Tytgat, Sandra Van Vlierberghe, Linxia Gu, and Aleksandr Ovsianikov. 2016. "Bioink Properties before, during and after 3D Bioprinting." *Biofabrication* 8 (3). <https://doi.org/10.1088/1758-5090/8/3/032002>.
- Hong, Soyong, Ji Seon Kim, Boyoung Jung, Chonghyun Won, and Changmo Hwang. 2019. "Coaxial Bioprinting of Cell-Laden Vascular Constructs Using a Gelatin-Tyramine Bioink." *Biomaterials Science* 7 (11): 4578–87. <https://doi.org/10.1039/c8bm00618k>.
- Howard A. Barnes. 2000. *A Handbook of Elementary Rheology*. The University of Wales Institute of Non-Newtonian Fluid Mechanics.
- Idaszek, Joanna, Marco Costantini, Tommy A. Karlsen, Jakub Jaroszewicz, Cristina Colosi, Stefano Testa, Ersilia Fornetti, et al. 2019. "3D Bioprinting of Hydrogel Constructs with Cell and Material Gradients for the Regeneration of Full-Thickness Chondral Defect Using a Microfluidic Printing Head." *Biofabrication* 11 (4). <https://doi.org/10.1088/1758-5090/ab2622>.
- Jang, Eui Hwa, Jung-Hwan Kim, Jun Hee Lee, Dae-Hyun Kim, and Young-Nam Youn. 2020. "Enhanced Biocompatibility of Multi-Layered, 3D Bio-Printed Artificial Vessels Composed of Autologous Mesenchymal Stem Cells." *MDPI Polymers*. <https://doi.org/10.32388/6cpxbl>.
- Jatav, Shweta, and Yogesh M. Joshi. 2014. "Chemical Stability of Laponite in Aqueous Media." *Applied Clay Science* 97–98: 72–77. <https://doi.org/10.1016/j.clay.2014.06.004>.
- Jeon, Oju, Yu Bin Lee, Hyoen Jeong, Sang Jin Lee, Derrick Wells, and Eben Alsberg. 2019. "Individual Cell-Only Bioink and Photocurable Supporting Medium for 3D Printing and Generation of Engineered Tissues with Complex Geometries." *Materials Horizons*. <https://doi.org/10.1039/c9mh00375d>.
- Jeong, Hun Jin, Hyoryung Nam, Jinah Jang, and Seung Jae Lee. 2020. "3D Bioprinting Strategies for the Regeneration of Functional Tubular Tissues and Organs." *Bioengineering* 7 (2): 1–24. <https://doi.org/10.3390/bioengineering7020032>.
- Jia, Weitao, P Selcan Gungor-Ozkerim, Yu Shrike Zhang, Kan Yue, Kai Zhu, Wanjun Liu, Qingment Pi, et al. 2016. "Direct 3D Bioprinting of Perfusable Vascular Constructs Using a Blend Bioink." *Biomaterials* 106 (November): 58–68. <https://doi.org/10.1016/j.biomaterials.2016.07.038>.
- Jiang, Jun, Chunhua Li, Jack Lombardi, Ralph H. Colby, Basil Rigas, Miriam H. Rafailovich, and Jonathan C. Sokolov. 2008. "The Effect of Physiologically Relevant Additives on the Rheological Properties of Concentrated Pluronic Copolymer Gels." *Polymer* 49 (16): 3561–67. <https://doi.org/10.1016/j.polymer.2008.05.038>.
- Jin, Yifei, Wenxuan Chai, and Yong Huang. 2017. "Printability Study of Hydrogel Solution Extrusion in Nanoclay Yield-Stress Bath during Printing-Then-Gelation Biofabrication." *Materials Science and Engineering C* 80: 313–25.

- <https://doi.org/10.1016/j.msec.2017.05.144>.
- . 2018. “Fabrication of Stand-Alone Cell-Laden Collagen Vascular Network Scaffolds Using Fugitive Pattern-Based Printing-Then-Casting Approach.” Research-article. *ACS Applied Materials and Interfaces* 10 (34): 28361–71. <https://doi.org/10.1021/acsami.8b09177>.
- Jin, Yifei, Ashley Compaan, Tapomoy Bhattacharjee, and Yong Huang. 2016. “Granular Gel Support-Enabled Extrusion of Three-Dimensional Alginate and Cellular Structures.” *Biofabrication* 8 (2). <https://doi.org/10.1088/1758-5090/8/2/025016>.
- Jin, Yifei, Ashley Compaan, Wenxuan Chai, and Yong Huang. 2017. “Functional Nanoclay Suspension for Printing-Then-Solidification of Liquid Materials.” *ACS Applied Materials and Interfaces* 9 (23): 20057–66. <https://doi.org/10.1021/acsami.7b02398>.
- Jin, Yifei, Yangyang Shen, Jun Yin, Jin Qian, and Yong Huang. 2018. “Nanoclay-Based Self-Supporting Responsive Nanocomposite Hydrogels for Printing Applications.” *ACS Applied Materials and Interfaces* 10 (12): 10461–70. <https://doi.org/10.1021/acsami.8b00806>.
- Kang, Donggu, Geunseon Ahn, Donghwan Kim, Hyun-Wook Kang, Seokhwan Yun, Won-Soo Yun, Jin-Hyung Shim, and Songwan Jin. 2018. “Pre-Set Extrusion Bioprinting for Multiscale Heterogeneous Tissue Structure Fabrication.” *Biofabrication* 10 (3): 35008. <https://doi.org/10.1088/1758-5090/aac70b>.
- Kang, Donggu, Gysik Hong, Seongmin An, Ilho Jang, Won-Soo Yun, Jin-Hyung Shim, and Songwan Jin. 2020. “Bioprinting of Multiscaled Hepatic Lobules within a Highly Vascularized Construct.” *Small* 16 (13): 1905505. <https://doi.org/10.1002/smll.201905505>.
- Kang, Edward, Yoon Young Choi, Su-Kyoung Chae, Jin-Hee Moon, Joon-Young Chang, and Sang-Hoon Lee. 2012. “Microfluidic Spinning of Flat Alginate Fibers with Grooves for Cell-Aligning Scaffolds.” *Advanced Materials* 24 (31): 4271–77. <https://doi.org/10.1002/adma.201201232>.
- Kang, Hyun-Wook, Sang Jin Lee, In Kap Ko, Carlos Kengla, James J Yoo, and Anthony Atala. 2016. “A 3D Bioprinting System to Produce Human-Scale Tissue Constructs with Structural Integrity.” *Nature Biotechnology* 34 (3): 312–19. <https://doi.org/10.1038/nbt.3413>.
- Kang, Hyun Wook, Sang Jin Lee, In Kap Ko, Carlos Kengla, James J. Yoo, and Anthony Atala. 2016. “A 3D Bioprinting System to Produce Human-Scale Tissue Constructs with Structural Integrity.” *Nature Biotechnology* 34 (3): 312–19. <https://doi.org/10.1038/nbt.3413>.
- Khani, Navid, Ali Nadernezhad, Paulo Bartolo, and Bahattin Koc. 2017. “Hierarchical and Spatial Modeling and Bio-Additive Manufacturing of Multi-Material Constructs.” *CIRP Annals* 66 (1): 229–32. <https://doi.org/10.1016/j.cirp.2017.04.132>.
- Kim, Byoung Soo, Ge Gao, Jae Yun Kim, and Dong-Woo Cho. 2019. “3D Cell Printing of Perfusable Vascularized Human Skin Equivalent Composed of Epidermis, Dermis, and Hypodermis for Better Structural Recapitulation of Native Skin.”

- Advanced Healthcare Materials* 8 (7): 1801019.
<https://doi.org/10.1002/adhm.201801019>.
- Kim, Byoung Soo, Yang Woo Kwon, Jeong Sik Kong, Gyu Tae Park, Ge Gao, Wonil Han, Moon Bum Kim, Hyungseok Lee, Jae Ho Kim, and Dong Woo Cho. 2018. “3D Cell Printing of in Vitro Stabilized Skin Model and in Vivo Pre-Vascularized Skin Patch Using Tissue-Specific Extracellular Matrix Bioink: A Step towards Advanced Skin Tissue Engineering.” *Biomaterials* 168: 38–53.
<https://doi.org/10.1016/j.biomaterials.2018.03.040>.
- Kim, Byoung Soo, Jung-Seob Lee, Ge Gao, Dong-Woo Cho, Nieves Cubo, Marta Garcia, and Juan F Del Cañizo. 2017. “Direct 3D Cell-Printing of Human Skin with Functional Transwell System 3D Bioprinting of Functional Human Skin: Production and in Vivo Analysis.” *Biofabrication* 9 (2): 1–12.
<https://doi.org/10.1088/1758-5090/aa71c8>.
- Kim, WonJin, and GeunHyung Kim. 2018. “Intestinal Villi Model with Blood Capillaries Fabricated Using Collagen-Based Bioink and Dual-Cell-Printing Process.” *ACS Applied Materials & Interfaces* 10 (48): 41185–96.
<https://doi.org/10.1021/acsami.8b17410>.
- Koch, Lothar, Andrea Deiwick, Sabrina Schlie, Stefanie Michael, Martin Gruene, Vincent Coger, Daniela Zychlinski, et al. 2012. “Skin Tissue Generation by Laser Cell Printing.” *Biotechnology and Bioengineering* 109 (7): 1855–63.
<https://doi.org/10.1002/bit.24455>.
- Koch, Lothar, Stefanie Kuhn, Heiko Sorg, Martin Gruene, Sabrina Schlie, Ralf Gaebel, Bianca Polchow, et al. 2009. “Laser Printing of Skin Cells and Human Stem Cells.” *Tissue Engineering Part C: Methods* 16 (5): 847–54.
<https://doi.org/10.1089/ten.tec.2009.0397>.
- Kolesky, David B, Kimberly A Homan, Mark A Skylar-Scott, and Jennifer A Lewis. 2016. “Three-Dimensional Bioprinting of Thick Vascularized Tissues.” *Proceedings of the National Academy of Sciences* 113 (12): 3179 LP – 3184.
<https://doi.org/10.1073/pnas.1521342113>.
- Kolesky, David B, Ryan L Truby, A Sydney Gladman, Travis A Busbee, Kimberly A Homan, and Jennifer A Lewis. 2014. “3D Bioprinting of Vascularized, Heterogeneous Cell-Laden Tissue Constructs.” *Advanced Materials* 26 (19): 3124–30. <https://doi.org/10.1002/adma.201305506>.
- Krishnamoorthy, Srikumar, Behnam Noorani, and Changxue Xu. 2019. “Effects of Encapsulated Cells on the Physical–Mechanical Properties and Microstructure of Gelatin Methacrylate Hydrogels.” *International Journal of Molecular Sciences* 20 (20). <https://doi.org/10.3390/ijms20205061>.
- Kucukgul, Can, S. Burce Ozler, Ilyas Inci, Ezgi Karakas, Ster Irmak, Devrim Gozuacik, Alpay Taralp, and Bahattin Koc. 2015. “3D Bioprinting of Biomimetic Aortic Vascular Constructs with Self-Supporting Cells.” *Biotechnology and Bioengineering* 112 (4): 811–21. <https://doi.org/10.1002/bit.25493>.
- Kumar, Hitendra, and Keekyoung Kim. 2020. “Stereolithography 3D Bioprinting.” In *3D Bioprinting: Principles and Protocols*, edited by Jeremy M Crook, 93–108. New York, NY: Springer US. https://doi.org/10.1007/978-1-0716-0520-2_6.

- Kumar, Vivek A, Jeffrey M Caves, Carolyn A Haller, Erbin Dai, Liying Liu, Stephanie Grainger, and Elliot L Chaikof. 2013. "Acellular Vascular Grafts Generated from Collagen and Elastin Analogs." *Acta Biomaterialia* 9 (9): 8067–74. <https://doi.org/https://doi.org/10.1016/j.actbio.2013.05.024>.
- L'heureux, Nicolas, Stéphanie Pâquet, Raymond Labbé, Lucie Germain, and François A Auger. 1998. "A Completely Biological Tissue-Engineered Human Blood Vessel." *The FASEB Journal* 12 (1): 47–56. <https://doi.org/10.1096/fasebj.12.1.47>.
- Laxton, Peter B., and John C. Berg. 2006. "Relating Clay Yield Stress to Colloidal Parameters." *Journal of Colloid and Interface Science* 296 (2): 749–55. <https://doi.org/10.1016/j.jcis.2005.09.061>.
- Lee, A., A. R. Hudson, D. J. Shiwarski, J. W. Tashman, T. J. Hinton, S. Yerneni, J. M. Bliley, P. G. Campbell, and A. W. Feinberg. 2019. "3D Bioprinting of Collagen to Rebuild Components of the Human Heart." *Science* 365 (6452): 482–87. <https://doi.org/10.1126/science.aav9051>.
- Lee, Bo Ram, Kwang Ho Lee, Edward Kang, Dong-Sik Kim, and Sang-Hoon Lee. 2011. "Microfluidic Wet Spinning of Chitosan-Alginate Microfibers and Encapsulation of HepG2 Cells in Fibers." *Biomicrofluidics* 5 (2): 22208. <https://doi.org/10.1063/1.3576903>.
- Lee, Hyungseok, and Dong-woo Cho. 2016. "One-Step Fabrication of an Organ-on-a-Chip with Spatial Heterogeneity Using a 3D Bioprinting Technology." *Lab on a Chip*. <https://doi.org/10.1039/C6LC00450D>.
- Lee, Kang Woog, Dae-Hyun Kim, Jun Hee Lee, and Young-Nam Youn. 2018. "The Effect of Pulsatile Flow on BMSC-Derived Endothelial-Like Cells in a Small-Sized Artificial Vessel Made by 3-Dimensional Bioprinting." Edited by Dong-Soo Lee. *Stem Cells International* 2018: 7823830. <https://doi.org/10.1155/2018/7823830>.
- Lee, Vivian K, Diana Y Kim, Haygan Ngo, Young Lee, Lan Seo, Seung-Schik Yoo, Peter A Vincent, and Guohao Dai. 2014. "Creating Perfused Functional Vascular Channels Using 3D Bio-Printing Technology." *Biomaterials* 35 (28): 8092–8102. <https://doi.org/https://doi.org/10.1016/j.biomaterials.2014.05.083>.
- Lee, Vivian K, Alison M Lanzi, Haygan Ngo, Seung-Schik Yoo, Peter A Vincent, and Guohao Dai. 2014. "Generation of Multi-Scale Vascular Network System Within 3D Hydrogel Using 3D Bio-Printing Technology." *Cellular and Molecular Bioengineering* 7 (3): 460–72. <https://doi.org/10.1007/s12195-014-0340-0>.
- Leijten, Jeroen, Jungmok Seo, Kan Yue, Grissel Trujillo-de Santiago, Ali Tamayol, Guillermo U. Ruiz-Esparza, Su Ryon Shin, et al. 2017. "Spatially and Temporally Controlled Hydrogels for Tissue Engineering." *Materials Science and Engineering R: Reports* 119 (September): 1–35. <https://doi.org/10.1016/j.mser.2017.07.001>.
- Levato, Riccardo, Tomasz Jungst, Ruben G. Scheuring, Torsten Blunk, Juergen Groll, and Jos Malda. 2020. "REFERENCE From Shape to Function: The Next Step in Bioprinting." *Advanced Materials* 32 (12). <https://doi.org/10.1002/adma.201906423>.
- Li, Chuang, Alan Faulkner-Jones, Alison R Dun, Juan Jin, Ping Chen, Yongzheng Xing, Zhongqiang Yang, et al. 2015. "Rapid Formation of a Supramolecular

- Polypeptide–DNA Hydrogel for In Situ Three-Dimensional Multilayer Bioprinting.” *Angewandte Chemie International Edition* 54 (13): 3957–61. <https://doi.org/10.1002/anie.201411383>.
- Li, Shengjie, Zhuo Xiong, Xiaohong Wang, Yongnian Yan, Haixia Liu, and Renji Zhang. 2009. “Direct Fabrication of a Hybrid Cell/Hydrogel Construct by a Double-Nozzle Assembling Technology.” *Journal of Bioactive and Compatible Polymers* 24 (3): 249–65. <https://doi.org/10.1177/0883911509104094>.
- Liu, Wanjun, Yu Shrike Zhang, Marcel A Heinrich, Fabio De Ferrari, Hae Lin Jang, Syeda Mahwish Bakht, Mario Moisés Alvarez, et al. 2017. “Rapid Continuous Multimaterial Extrusion Bioprinting.” *Advanced Materials* 29 (3): 1604630. <https://doi.org/10.1002/adma.201604630>.
- Liu, Wanjun, Zhe Zhong, Ning Hu, Yixiao Zhou, Lucia Maggio, Amir K Miri, Alessio Fragasso, Xiangyu Jin, Ali Khademhosseini, and Yu Shrike Zhang. 2018. “Coaxial Extrusion Bioprinting of 3D Microfibrous Constructs with Cell-Favorable Gelatin Methacryloyl Microenvironments.” *Biofabrication* 10 (2): 24102. <https://doi.org/10.1088/1758-5090/aa9d44>.
- Liu, Xiao, Sarah Sophia D. Carter, Max Jurie Renes, Juewan Kim, Darling Macarena Rojas-Canales, Daniella Penko, Cameron Angus, et al. 2019. “Development of a Coaxial 3D Printing Platform for Biofabrication of Implantable Islet-Containing Constructs.” *Advanced Healthcare Materials* 8 (7): 1–12. <https://doi.org/10.1002/adhm.201801181>.
- Loessner, Daniela, Christoph Meinert, Elke Kaemmerer, Laure C Martine, Kan Yue, Peter A Levett, Travis J Klein, Ferry P W Melchels, Ali Khademhosseini, and Dietmar W Hutmacher. 2016. “Functionalization, Preparation and Use of Cell-Laden Gelatin Methacryloyl–Based Hydrogels as Modular Tissue Culture Platforms.” *Nature Protocols* 11 (4): 727–46. <https://doi.org/10.1038/nprot.2016.037>.
- Lu, Peter J., Jacinta C. Conrad, Hans M. Wyss, Andrew B. Schofield, and David A. Weitz. 2006. “Fluids of Clusters in Attractive Colloids.” *Physical Review Letters* 96 (2): 1–4. <https://doi.org/10.1103/PhysRevLett.96.028306>.
- Lu, Yi, Gazell Mapili, Gerry Suhali, Shaochen Chen, and Krishnendu Roy. 2006. “A Digital Micro-Mirror Device-Based System for the Microfabrication of Complex, Spatially Patterned Tissue Engineering Scaffolds.” *Journal of Biomedical Materials Research Part A* 77A (2): 396–405. <https://doi.org/10.1002/jbm.a.30601>.
- Luo, Yongxiang, Anja Lode, and Michael Gelinsky. 2013. “Direct Plotting of Three-Dimensional Hollow Fiber Scaffolds Based on Concentrated Alginate Pastes for Tissue Engineering.” *Advanced Healthcare Materials* 2 (6): 777–83. <https://doi.org/10.1002/adhm.201200303>.
- Ma, Jingyun, Yachen Wang, and Jing Liu. 2018. “Bioprinting of 3D Tissues/Organs Combined with Microfluidics.” *RSC Advances* 8 (39): 21712–27. <https://doi.org/10.1039/c8ra03022g>.
- Ma, Xuanyi, Xin Qu, Wei Zhu, Yi Shuan Li, Suli Yuan, Hong Zhang, Justin Liu, et al. 2016. “Deterministically Patterned Biomimetic Human iPSC-Derived Hepatic Model via Rapid 3D Bioprinting.” *Proceedings of the National Academy of Sciences* 113 (12): 3207–12. <https://doi.org/10.1073/pnas.1518811113>.

- Sciences of the United States of America* 113 (8): 2206–11.
<https://doi.org/10.1073/pnas.1524510113>.
- Maiullari, Fabio, Marco Costantini, Marika Milan, Valentina Pace, Maila Chirivì, Silvia Maiullari, Alberto Rainer, et al. 2018. “A Multi-Cellular 3D Bioprinting Approach for Vascularized Heart Tissue Engineering Based on HUVECs and iPSC-Derived Cardiomyocytes.” *Scientific Reports* 8 (1): 1–15. <https://doi.org/10.1038/s41598-018-31848-x>.
- Mandrycky, Christian, Zongjie Wang, Keekyoung Kim, and Deok-Ho Kim. 2016. “3D Bioprinting for Engineering Complex Tissues.” *Biotechnology Advances* 34 (4): 422–34. <https://doi.org/https://doi.org/10.1016/j.biotechadv.2015.12.011>.
- Matsuzaki, Yuichi, Kelly John, Toshihiro Shoji, and Toshiharu Shinoka. 2019. “Bioprinting Vasculature: Materials, Cells and Emergent Techniques.” *Applied Sciences* 9 (7). <https://doi.org/10.3390/app9071274>.
- McCormack, Andrew, Christopher B Highley, Nicholas R Leslie, and Ferry P.W. Melchels. 2020. “3D Printing in Suspension Baths: Keeping the Promises of Bioprinting Afloat.” *Trends in Biotechnology*. Elsevier Ltd. <https://doi.org/10.1016/j.tibtech.2019.12.020>.
- Merceron, Tyler K., Morgan Burt, Young Joon Seol, Hyun Wook Kang, Sang Jin Lee, James J. Yoo, and Anthony Atala. 2015. “A 3D Bioprinted Complex Structure for Engineering the Muscle-Tendon Unit.” *Biofabrication* 7 (3): 35003. <https://doi.org/10.1088/1758-5090/7/3/035003>.
- Mezger, Thomas G. 2006. “The Rheology Handbook (2nd Ed.).” *Vincentz*.
- Miri, Amir K., Akbar Khalilpour, Berivan Cecen, Sushila Maharjan, Su Ryon Shin, and Ali Khademhosseini. 2019. “Multiscale Bioprinting of Vascularized Models.” *Biomaterials* 198: 204–16. <https://doi.org/10.1016/j.biomaterials.2018.08.006>.
- Miri, Amir K., Daniel Nieto, Luis Iglesias, Hossein Goodarzi Hosseinabadi, Sushila Maharjan, Guillermo U. Ruiz-Esparza, Parastoo Khoshakhlagh, et al. 2018. “Microfluidics-Enabled Multimaterial Maskless Stereolithographic Bioprinting.” *Advanced Materials* 30 (27). <https://doi.org/10.1002/adma.201800242>.
- Mitsuhashi, Nobutaka, Kaori Fujieda, Takuro Tamura, Shoko Kawamoto, Toshihisa Takagi, and Kousaku Okubo. 2008. “BodyParts3D: 3D Structure Database for Anatomical Concepts.” *Nucleic Acids Research* 37 (suppl_1): D782–85. <https://doi.org/10.1093/nar/gkn613>.
- Mota, Carlos, Sandra Camarero-Espinosa, Matthew B Baker, Paul Wieringa, and Lorenzo Moroni. 2020. “Bioprinting: From Tissue and Organ Development to in Vitro Models.” *Chemical Reviews*, May. <https://doi.org/10.1021/acs.chemrev.9b00789>.
- Murphy, Sean V., and Anthony Atala. 2014. “3D Bioprinting of Tissues and Organs.” *Nature Biotechnology* 32 (8): 773–85. <https://doi.org/10.1038/nbt.2958>.
- Nadernezhad, Ali, Ozum S. Caliskan, Fuat Topuz, Ferdows Afghah, Batu Erman, and Bahattin Koc. 2019. “Nanocomposite Bioinks Based on Agarose and 2D Nanosilicates with Tunable Flow Properties and Bioactivity for 3D Bioprinting.” Research-article. *ACS Applied Bio Materials* 2 (2): 796–806.

- <https://doi.org/10.1021/acsabm.8b00665>.
- Negro, Andrea, Thibaud Cherbuin, and Matthias P. Lutolf. 2018. "3D Inkjet Printing of Complex, Cell-Laden Hydrogel Structures." *Scientific Reports* 8 (1): 1–9. <https://doi.org/10.1038/s41598-018-35504-2>.
- Nelson, Andrew, and Terence Cosgrove. 2004. "Dynamic Light Scattering Studies of Poly(Ethylene Oxide) Adsorbed on Laponite: Layer Conformation and Its Effect on Particle Stability." *Langmuir* 20 (24): 10382–88. <https://doi.org/10.1021/la049323p>.
- . 2005. "Small-Angle Neutron Scattering Study of Adsorbed Pluronic Tri-Block Copolymers on Laponite." *Langmuir* 21 (20): 9176–82. <https://doi.org/10.1021/la050680p>.
- Nemeno-Guanzon, Judee Grace, Soojung Lee, Johan Robert Berg, Yong Hwa Jo, Jee Eun Yeo, Bo Mi Nam, Yong-Gon Koh, and Jeong Ik Lee. 2012. "Trends in Tissue Engineering for Blood Vessels." Edited by Brynn Levy. *Journal of Biomedicine and Biotechnology* 2012: 956345. <https://doi.org/10.1155/2012/956345>.
- Noor, Nadav, Assaf Shapira, Reuven Edri, Idan Gal, Lior Wertheim, and Tal Dvir. 2019. "3D Printing of Personalized Thick and Perfusable Cardiac Patches and Hearts." *Advanced Science* 6 (11): 1900344. <https://doi.org/10.1002/advs.201900344>.
- Norotte, Cyrille, Francois S. Marga, Laura E. Niklason, and Gabor Forgacs. 2009. "Scaffold-Free Vascular Tissue Engineering Using Bioprinting." *Biomaterials* 30 (30): 5910–17. <https://doi.org/10.1016/j.biomaterials.2009.06.034>.
- O'Connell, Cathal D, Claudia Di Bella, Fletcher Thompson, Cheryl Augustine, Stephen Beirne, Rhys Cornock, Christopher J Richards, et al. 2016. "Development of the Biopen: A Handheld Device for Surgical Printing of Adipose Stem Cells at a Chondral Wound Site." *Biofabrication* 8 (1): 15019. <https://doi.org/10.1088/1758-5090/8/1/015019>.
- Ober, Thomas J, Daniele Foresti, and Jennifer A Lewis. 2015. "Active Mixing of Complex Fluids at the Microscale." *Proceedings of the National Academy of Sciences* 112 (40): 12293 LP – 12298. <https://doi.org/10.1073/pnas.1509224112>.
- Onoe, Hiroaki, Teru Okitsu, Akane Itou, Midori Kato-Negishi, Riho Gojo, Daisuke Kiriya, Koji Sato, et al. 2013. "Metre-Long Cell-Laden Microfibres Exhibit Tissue Morphologies and Functions." *Nature Materials* 12 (6): 584–90. <https://doi.org/10.1038/nmat3606>.
- Othman, Rebeen, Gavin E Morris, Disheet A Shah, Stephen Hall, Graham Hall, Keith Wells, Kevin M Shakesheff, and James E Dixon. 2015. "An Automated Fabrication Strategy to Create Patterned Tubular Architectures at Cell and Tissue Scales." *Biofabrication* 7 (2): 25003. <https://doi.org/10.1088/1758-5090/7/2/025003>.
- Othon, Christina M, Xingjia Wu, Juanita J Anders, and Bradley R Ringeisen. 2008. "Single-Cell Printing to Form Three-Dimensional Lines of Olfactory Ensheathing Cells." *Biomedical Materials* 3 (3): 34101. <https://doi.org/10.1088/1748-6041/3/3/034101>.

- Ozbolat, Ibrahim T., Howard Chen, and Yin Yu. 2014. "Development of 'Multi-Arm Bioprinter' for Hybrid Biofabrication of Tissue Engineering Constructs." *Robotics and Computer-Integrated Manufacturing* 30 (3): 295–304. <https://doi.org/10.1016/j.rcim.2013.10.005>.
- Ozbolat, Ibrahim T., and Monika Hospodiuk. 2016. "Current Advances and Future Perspectives in Extrusion-Based Bioprinting." *Biomaterials* 76: 321–43. <https://doi.org/10.1016/j.biomaterials.2015.10.076>.
- Ozler, Saime Burce, Ezgi Bakirci, Can Kucukgul, and Bahattin Koc. 2017. "Three-Dimensional Direct Cell Bioprinting for Tissue Engineering." *Journal of Biomedical Materials Research Part B: Applied Biomaterials* 105 (8): 2530–44. <https://doi.org/10.1002/jbm.b.33768>.
- Pashneh-Tala, Samand, Sheila MacNeil, and Frederik Claeyssens. 2016. "The Tissue-Engineered Vascular Graft-Past, Present, and Future." *Tissue Engineering. Part B, Reviews* 22 (1): 68–100. <https://doi.org/10.1089/ten.teb.2015.0100>.
- Peak, Charles W., Jean Stein, Karli A. Gold, and Akhilesh K. Gaharwar. 2018. "Nanoengineered Colloidal Inks for 3D Bioprinting." *Langmuir* 34 (3): 917–25. <https://doi.org/10.1021/acs.langmuir.7b02540>.
- Pek-Ing, Au, and Leong Yee-Kwong. 2015. "Surface Chemistry and Rheology of Laponite Dispersions - Zeta Potential, Yield Stress, Ageing, Fractal Dimension and Pyrophosphate." *Applied Clay Science* 107: 36–45. <https://doi.org/10.1016/j.clay.2015.01.033>.
- Pereira, Rúben F, and Paulo J Bártolo. 2015. "3D Photo-Fabrication for Tissue Engineering and Drug Delivery." *Engineering* 1 (1): 90–112. <https://doi.org/https://doi.org/10.15302/J-ENG-2015015>.
- Pi, Qingmeng, Sushila Maharjan, Xiang Yan, Xiao Liu, Bijay Singh, Anne Metje van Genderen, Felipe Robledo-Padilla, et al. 2018. "Digitally Tunable Microfluidic Bioprinting of Multilayered Cannular Tissues." *Advanced Materials* 30 (43): 1–10. <https://doi.org/10.1002/adma.201706913>.
- Pugsley, M K, and R Tabrizchi. 2000. "The Vascular System. An Overview of Structure and Function." *Journal of Pharmacological and Toxicological Methods* 44 (2): 333–340. [https://doi.org/10.1016/s1056-8719\(00\)00125-8](https://doi.org/10.1016/s1056-8719(00)00125-8).
- Qin, Lian, Zhou Linian, Li Xiao, Mao Wei, and Li Dichen. 2020. "Perfusive and Osmotic Capabilities of 3D Printed Hollow Tube for Fabricating Large-Scaled Muscle Scaffold." *Rapid Prototyping Journal* 26 (1): 1–10. <https://doi.org/10.1108/RPJ-08-2017-0152>.
- Rocca, Marco, Alessio Fragasso, Wanjun Liu, Marcel A. Heinrich, and Yu Shrike Zhang. 2018. "Embedded Multimaterial Extrusion Bioprinting." *SLAS Technology* 23 (2): 154–63. <https://doi.org/10.1177/2472630317742071>.
- Rose, Jonas C, and Laura De Laporte. 2018. "Hierarchical Design of Tissue Regenerative Constructs." *Advanced Healthcare Materials* 7 (6): 1701067. <https://doi.org/10.1002/adhm.201701067>.
- Ruiz-Cantu, Laura, Andrew Gleadall, Callum Faris, Joel Segal, Kevin Shakesheff, and Jing Yang. 2020. "Multi-Material 3D Bioprinting of Porous Constructs for

- Cartilage Regeneration.” *Materials Science and Engineering C* 109: 110578. <https://doi.org/10.1016/j.msec.2019.110578>.
- Ruther, F., T. Distler, A. R. Boccaccini, and R. Detsch. 2019. “Biofabrication of Vessel-like Structures with Alginate Di-Aldehyde—Gelatin (ADA-GEL) Bioink.” *Journal of Materials Science: Materials in Medicine* 30 (1). <https://doi.org/10.1007/s10856-018-6205-7>.
- Saeidi, Nima, Edward A Sander, and Jeffrey W Ruberti. 2009. “Dynamic Shear-Influenced Collagen Self-Assembly.” *Biomaterials* 30 (34): 6581–92. <https://doi.org/https://doi.org/10.1016/j.biomaterials.2009.07.070>.
- Sakai, Shinji, Kohei Ueda, Enkhtuul Gantumur, Masahito Taya, and Makoto Nakamura. 2018. “Drop-On-Drop Multimaterial 3D Bioprinting Realized by Peroxidase-Mediated Cross-Linking.” *Macromolecular Rapid Communications* 39 (3): 1–6. <https://doi.org/10.1002/marc.201700534>.
- Sakairi, N., M. Kobayashi, and Y. Adachi. 2005. “Effects of Salt Concentration on the Yield Stress of Sodium Montmorillonite Suspension.” *Journal of Colloid and Interface Science* 283 (1): 245–50. <https://doi.org/10.1016/j.jcis.2004.08.181>.
- Schöneberg, Jan, Federica De Lorenzi, Benjamin Theek, Andreas Blaeser, Dirk Rommel, Alexander J.C. Kuehne, Fabian Kießling, and Horst Fischer. 2018. “Engineering Biofunctional in Vitro Vessel Models Using a Multilayer Bioprinting Technique.” *Scientific Reports* 8 (1): 1–13. <https://doi.org/10.1038/s41598-018-28715-0>.
- Schulze-Bauer, Christian A J, Christian Mörth, and Gerhard A Holzapfel. 2003. “Passive Biaxial Mechanical Response of Aged Human Iliac Arteries.” *Journal of Biomechanical Engineering* 125 (3): 395–406. <https://doi.org/10.1115/1.1574331>.
- Schutte, Stacey C, Zhenzhen Chen, Kelvin G M Brockbank, and Robert M Nerem. 2010. “Cyclic Strain Improves Strength and Function of a Collagen-Based Tissue-Engineered Vascular Media.” *Tissue Engineering Part A* 16 (10): 3149–57. <https://doi.org/10.1089/ten.tea.2010.0009>.
- Seifarth, Volker, Joachim O Grosse, Matthias Gossmann, Heinz Peter Janke, Patrick Arndt, Sabine Koch, Matthias Epple, Gerhard M Artmann, and Aysegül Temiz Artmann. 2017. “Mechanical Induction of Bi-Directional Orientation of Primary Porcine Bladder Smooth Muscle Cells in Tubular Fibrin-Poly(Vinylidene Fluoride) Scaffolds for Ureteral and Urethral Repair Using Cyclic and Focal Balloon Catheter Stimulation.” *Journal of Biomaterials Applications* 32 (3): 321–330. <https://doi.org/10.1177/0885328217723178>.
- Serex, Ludovic, Arnaud Bertsch, and Philippe Renaud. 2018. “Microfluidics: A New Layer of Control for Extrusion-Based 3D Printing.” *Micromachines* 9 (2). <https://doi.org/10.3390/mi9020086>.
- Shanjani, Y, C C Pan, L Elomaa, and Y Yang. 2015. “A Novel Bioprinting Method and System for Forming Hybrid Tissue Engineering Constructs.” *Biofabrication* 7 (4): 45008. <https://doi.org/10.1088/1758-5090/7/4/045008>.
- Shao, Lei, Qing Gao, Chaoqi Xie, Jianzhong Fu, Meixiang Xiang, and Yong He. 2020. “Directly Coaxial 3D Bioprinting of Large-Scale Vascularized Tissue Constructs.” *Biofabrication* 12 (3): 35014. <https://doi.org/10.1088/1758-5090/ab7e76>.

- Sharma, Ruchi, Imke P.M. Smits, Laura De La Vega, Christopher Lee, and Stephanie M. Willerth. 2020. "3D Bioprinting Pluripotent Stem Cell Derived Neural Tissues Using a Novel Fibrin Bioink Containing Drug Releasing Microspheres." *Frontiers in Bioengineering and Biotechnology* 8 (February): 1–12. <https://doi.org/10.3389/fbioe.2020.00057>.
- Sheikhi, Amir, Samson Afewerki, Rahmi Oklu, Akhilesh K. Gaharwar, and Ali Khademhosseini. 2018. "Effect of Ionic Strength on Shear-Thinning Nanoclay-Polymer Composite Hydrogels." *Biomaterials Science* 6 (8): 2073–83. <https://doi.org/10.1039/c8bm00469b>.
- Singh, Mahima, and Sriramakamal Jonnalagadda. 2020. "Advances in Bioprinting Using Additive Manufacturing." *European Journal of Pharmaceutical Sciences* 143: 105167. <https://doi.org/https://doi.org/10.1016/j.ejps.2019.105167>.
- Singh, Narendra K, Wonil Han, Sun Ah Nam, Jin Won Kim, Jae Yun Kim, Yong Kyun Kim, and Dong-Woo Cho. 2020. "Three-Dimensional Cell-Printing of Advanced Renal Tubular Tissue Analogue." *Biomaterials* 232: 119734. <https://doi.org/https://doi.org/10.1016/j.biomaterials.2019.119734>.
- Skardal, Aleksander, Sean V Murphy, Mahesh Devarasetty, Ivy Mead, Hyun-Wook Kang, Young-Joon Seol, Yu Shrike Zhang, et al. 2017. "Multi-Tissue Interactions in an Integrated Three-Tissue Organ-on-a-Chip Platform." *Scientific Reports* 7 (1): 8837. <https://doi.org/10.1038/s41598-017-08879-x>.
- Soman, Pranav, Peter H Chung, A Ping Zhang, and Shaochen Chen. 2013. "Digital Microfabrication of User-Defined 3D Microstructures in Cell-Laden Hydrogels." *Biotechnology and Bioengineering* 110 (11): 3038–47. <https://doi.org/10.1002/bit.24957>.
- Song, Jie Liang, Xin Ye Fu, Ali Raza, Nai An Shen, Ya Qi Xue, Hua Jie Wang, and Jin Ye Wang. 2020. "Enhancement of Mechanical Strength of TCP-Alginate Based Bioprinted Constructs." *Journal of the Mechanical Behavior of Biomedical Materials* 103 (March 2019): 103533. <https://doi.org/10.1016/j.jmbbm.2019.103533>.
- Song, Seung Joon, Jaesoon Choi, Yong Doo Park, Soyoung Hong, Jung Joo Lee, Chi Bum Ahn, Hyuk Choi, and Kyung Sun. 2011. "Sodium Alginate Hydrogel-Based Bioprinting Using a Novel Multinozzle Bioprinting System." *Artificial Organs* 35 (11): 1132–36. <https://doi.org/10.1111/j.1525-1594.2011.01377.x>.
- Sorkio, Anni, Lothar Koch, Laura Koivusalo, Andrea Deiwick, Susanna Miettinen, Boris Chichkov, and Heli Skottman. 2018. "Human Stem Cell Based Corneal Tissue Mimicking Structures Using Laser-Assisted 3D Bioprinting and Functional Bioinks." *Biomaterials* 171: 57–71. <https://doi.org/https://doi.org/10.1016/j.biomaterials.2018.04.034>.
- Stock, Ulrich A, and Joseph P Vacanti. 2001. "Tissue Engineering: Current State and Prospects." *Annual Review of Medicine* 52 (1): 443–51. <https://doi.org/10.1146/annurev.med.52.1.443>.
- Sun, Kunshan, and Srinivasa R. Raghavan. 2010. "Thermogelling Aqueous Fluids Containing Low Concentrations of Pluronic F127 and Laponite Nanoparticles." *Langmuir* 26 (11): 8015–20. <https://doi.org/10.1021/la904907b>.

- Sun, Ye, Yongqing You, Wenbo Jiang, Zanjin Zhai, and Kerong Dai. 2019. "3D-Bioprinting a Genetically Inspired Cartilage Scaffold with GDF5-Conjugated BMSC-Laden Hydrogel and Polymer for Cartilage Repair." *Theranostics* 9 (23): 6949–61. <https://doi.org/10.7150/thno.38061>.
- Suzanne, M., and H. Steller. 2013. "Shaping Organisms with Apoptosis." *Cell Death and Differentiation* 20 (5): 669–75. <https://doi.org/10.1038/cdd.2013.11>.
- Syedain, Zeeshan H, Lee A Meier, Jason W Bjork, Ann Lee, and Robert T Tranquillo. 2011. "Implantable Arterial Grafts from Human Fibroblasts and Fibrin Using a Multi-Graft Pulsed Flow-Stretch Bioreactor with Noninvasive Strength Monitoring." *Biomaterials* 32 (3): 714–22. <https://doi.org/https://doi.org/10.1016/j.biomaterials.2010.09.019>.
- Tan, Edgar Yong Sheng, and Wai Yee Yeong. 2015. "Concentric Bioprinting of Alginate-Based Tubular Constructs Using Multi-Nozzle Extrusion-Based Technique." *International Journal of Bioprinting* 1 (1).
- Tan, Yu, Dylan J Richards, Thomas C Trusk, Richard P Visconti, Michael J Yost, Mark S Kindy, Christopher J Drake, William Scott Argraves, Roger R Markwald, and Ying Mei. 2014. "3D Printing Facilitated Scaffold-Free Tissue Unit Fabrication." *Biofabrication* 6 (2): 1–16. <https://doi.org/10.1088/1758-5082/6/2/024111>.
- Tomás, Helena, Carla S. Alves, and João Rodrigues. 2018. "Laponite®: A Key Nanoplatfrom for Biomedical Applications?" *Nanomedicine: Nanotechnology, Biology, and Medicine*. <https://doi.org/10.1016/j.nano.2017.04.016>.
- Tomasina, Clarissa, Tristan Bodet, Carlos Mota, Lorenzo Moroni, and Sandra Camarero-espinoza. 2018. "Bioprinting Vasculature: Materials, Cells and Emergent Techniques." *Materials* 12 (17): 2701. <https://doi.org/10.3390/ma12172701>.
- Topuz, Fuat, Ali Nadernezhad, Ozum S. Caliskan, Yusuf Z. Menciloglu, and Bahattin Koc. 2018. "Nanosilicate Embedded Agarose Hydrogels with Improved Bioactivity." *Carbohydrate Polymers* 201: 105–12. <https://doi.org/10.1016/j.carbpol.2018.08.032>.
- Wang, Xuanzhi, Xinda Li, Xingliang Dai, Xinzhi Zhang, Jing Zhang, Tao Xu, and Qing Lan. 2018. "Coaxial Extrusion Bioprinted Shell-Core Hydrogel Microfibers Mimic Glioma Microenvironment and Enhance the Drug Resistance of Cancer Cells." *Colloids and Surfaces B: Biointerfaces* 171: 291–99. <https://doi.org/https://doi.org/10.1016/j.colsurfb.2018.07.042>.
- Wang, Yongkang, Xiaobo Huang, Yi Shen, Ruiqiang Hang, Xiangyu Zhang, Yueyue Wang, Xiaohong Yao, and Bin Tang. 2019. "Direct Writing Alginate Bioink inside Pre-Polymers of Hydrogels to Create Patterned Vascular Networks." *Journal of Materials Science* 54 (10): 7883–92. <https://doi.org/10.1007/s10853-019-03447-2>.
- Wang, Zhan, Sang Jin Lee, Heng-jie Cheng, James J Yoo, and Anthony Atala. 2018. "3D Bioprinted Functional and Contractile Cardiac Tissue Constructs." *Acta Biomaterialia*, no. February: 48–56. <https://doi.org/10.1016/j.actbio.2018.02.007>.
- Wilkens, Camila A, Christopher J Rivet, Tamara L Akentjew, Julian Alverio, Maroun Khoury, and Juan Pablo Acevedo. 2016. "Layer-by-Layer Approach for a Uniformed Fabrication of a Cell Patterned Vessel-like Construct." *Biofabrication* 9

- (1): 15001. <https://doi.org/10.1088/1758-5090/9/1/015001>.
- Wu, Chia Jung, Akhilesh K. Gaharwar, Burke K. Chan, and Gudrun Schmidt. 2011. “Mechanically Tough Pluronic F127/Laponite Nanocomposite Hydrogels from Covalently and Physically Cross-Linked Networks.” *Macromolecules* 44 (20): 8215–24. <https://doi.org/10.1021/ma200562k>.
- Wu, Chia Jung, and Gudrun Schmidt. 2009. “Thermosensitive and Dissolution Properties in Nanocomposite Polymer Hydrogels.” *Macromolecular Rapid Communications* 30 (17): 1492–97. <https://doi.org/10.1002/marc.200900163>.
- Wu, P K, and B R Ringeisen. 2010. “Development of Human Umbilical Vein Endothelial Cell (HUVEC) and Human Umbilical Vein Smooth Muscle Cell (HUVMC) Branch / Stem Structures on Hydrogel Layers via Biological Laser Printing (BioLP).” *Biofabrication* 014111. <https://doi.org/10.1088/1758-5082/2/1/014111>.
- Yang, Kai, Zhiwei Liu, Jun Wang, and Wei Yu. 2018. “Stress Bifurcation in Large Amplitude Oscillatory Shear of Yield Stress Fluids.” *Journal of Rheology* 62 (1): 89–106. <https://doi.org/10.1122/1.4986062>.
- Yang, Shuai, Hao Tang, Chunmei Feng, Jianping Shi, and Jiquan Yang. 2020. “The Research on Multi-Material 3D Vascularized Network Integrated Printing Technology.” *Micromachines* 11 (3): 1–13. <https://doi.org/10.3390/mi11030237>.
- Yeo, Myung Gu, Ji Seon Lee, Wook Chun, and Geun Hyung Kim. 2016. “An Innovative Collagen-Based Cell-Printing Method for Obtaining Human Adipose Stem Cell-Laden Structures Consisting of Core-Sheath Structures for Tissue Engineering.” *Biomacromolecules* 17 (4): 1365–75. <https://doi.org/10.1021/acs.biomac.5b01764>.
- Yi, Hee-Gyeong, Young Hun Jeong, Yona Kim, Yeong-Jin Choi, Hyo Eun Moon, Sung Hye Park, Kyung Shin Kang, et al. 2019. “A Bioprinted Human-Glioblastoma-on-a-Chip for the Identification of Patient-Specific Responses to Chemoradiotherapy.” *Nature Biomedical Engineering* 3 (7): 509–19. <https://doi.org/10.1038/s41551-019-0363-x>.
- Yoon, Hee Jeong, Su Ryon Shin, Jae Min Cha, Soo-Hong Lee, Jin-Hoi Kim, Jeong Tae Do, Hyuk Song, and Hojae Bae. 2016. “Cold Water Fish Gelatin Methacryloyl Hydrogel for Tissue Engineering Application.” *PLOS ONE* 11 (10): e0163902. <https://doi.org/10.1371/journal.pone.0163902>.
- Yu, Yin, Yahui Zhang, James A. Martin, and Ibrahim T. Ozbolat. 2013a. “Evaluation of Cell Viability and Functionality in Vessel-like Bioprintable Cell-Laden Tubular Channels.” *Journal of Biomechanical Engineering* 135 (9): 1–9. <https://doi.org/10.1115/1.4024575>.
- Yu, Yin, Yahui Zhang, James A Martin, and Ibrahim T Ozbolat. 2013b. “Evaluation of Cell Viability and Functionality in Vessel-like Bioprintable Cell-Laden Tubular Channels.” *Journal of Biomechanical Engineering* 135 (9): 91011. <https://doi.org/10.1115/1.4024575>.
- Yun, Byeong Gon, Se Hwan Lee, Jung Ho Jeon, Seok Won Kim, Chan Kwon Jung, Gyeongsin Park, Su Young Kim, et al. 2019. *Accelerated Bone Regeneration via Three-Dimensional Cell-Printed Constructs Containing Human Nasal Turbinate-*

- Derived Stem Cells as a Clinically Applicable Therapy. ACS Biomaterials Science and Engineering*. Vol. 5. <https://doi.org/10.1021/acsbiomaterials.9b01356>.
- Zhang, Bin, Qian Xue, Han yi Hu, Meng fei Yu, Lei Gao, Yi chen Luo, Yang Li, et al. 2019. "Integrated 3D Bioprinting-Based Geometry-Control Strategy for Fabricating Corneal Substitutes." *Journal of Zhejiang University: Science B* 20 (12): 945–59. <https://doi.org/10.1631/jzus.B1900190>.
- Zhang, Yahui, Yin Yu, Adil Akkouch, Amer Dababneh, Farzaneh Dolati, and Ibrahim T Ozbolat. 2015. "In Vitro Study of Directly Bioprinted Perfusable Vasculature Conduits." *Biomaterials Science* 23 (1): 1–7. <https://doi.org/10.1038/jid.2014.371>.
- Zhang, Zhengyi, Yifei Jin, Jun Yin, Changxue Xu, Ruitong Xiong, Kyle Christensen, Bradley R. Ringeisen, Douglas B. Chrisey, and Yong Huang. 2018. "Evaluation of Bioink Printability for Bioprinting Applications." *Applied Physics Reviews* 5 (4). <https://doi.org/10.1063/1.5053979>.
- Zheng, Fuyin, Fanfan Fu, Yao Cheng, Chunyan Wang, Yuanjin Zhao, and Zhongze Gu. 2016. "Organ-on-a-Chip Systems: Microengineering to Biomimic Living Systems." *Small* 12 (17): 2253–82. <https://doi.org/10.1002/sml.201503208>.
- Zhou, You, Shenglong Liao, Xinglei Tao, Xiao Qi Xu, Quan Hong, Di Wu, and Yapei Wang. 2018. "Spider-Inspired Multicomponent 3d Printing Technique for next-Generation Complex Biofabrication." *ACS Applied Bio Materials* 1 (2): 502–10. <https://doi.org/10.1021/acsabm.8b00230>.
- Zhu, Wei, Haitao Cui, Benchaa Boualam, Fahed Masood, Erin Flynn, Raj D. Rao, Zhi Yong Zhang, and Lijie Grace Zhang. 2018. "3D Bioprinting Mesenchymal Stem Cell-Laden Construct with Core-Shell Nanospheres for Cartilage Tissue Engineering." *Nanotechnology* 29 (18). <https://doi.org/10.1088/1361-6528/aaafa1>.
- Zhu, Wei, Jinxing Li, Yew J Leong, Isaac Rozen, Xin Qu, Renfeng Dong, Zhiguang Wu, et al. 2015. "3D-Printed Artificial Microfish." *Advanced Materials* 27 (30): 4411–17. <https://doi.org/10.1002/adma.201501372>.
- Zhu, Wei, Xin Qu, Jie Zhu, Xuanyi Ma, Sherrina Patel, Justin Liu, Pengrui Wang, et al. 2017. "Direct 3D Bioprinting of Prevascularized Tissue Constructs with Complex Microarchitecture." *Biomaterials* 124: 106–15. <https://doi.org/https://doi.org/10.1016/j.biomaterials.2017.01.042>.
- Zimmermann, Ralf, Christoph Hentschel, Felix Schrön, Denise Moedder, Teresa Büttner, Passant Atallah, Thomas Wegener, et al. 2019. "High Resolution Bioprinting of Multi-Component Hydrogels." *Biofabrication* 11 (4). <https://doi.org/10.1088/1758-5090/ab2aa1>.